Catalytic activity and kinetic studies for the hydrodesulphurisation of thiophene.

Hernandez, Jose

Award date:
1983

Awarding institution:
University of Bath

CATALYTIC ACTIVITY AND KINETIC STUDIES FOR THE HYDRODESULPHURISATION OF THIOPHENE

submitted by José Hernandez

for the degree of Ph.D

of the University of Bath,

1983

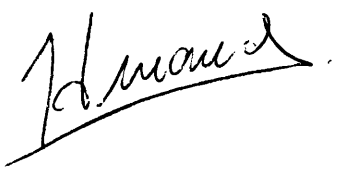

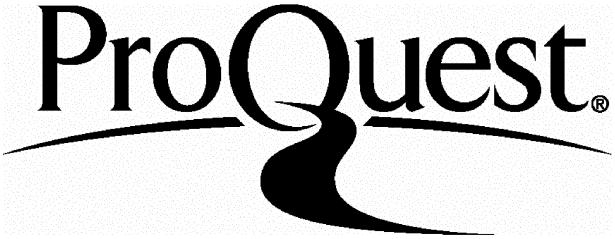

ACKNOWLEDGEMENTS

I would like to express my sincere gratitude to Professor W.J. Thomas for his excellent guidance, continued encouragement and valuable suggestions throughout the period of this research work.

I would also like to thank Dr. M. Bhaduri for his invaluable assistance and helpful discussions.

My thanks are due to Mr. E. Minshall of the School of Chemistry, for permission to use the e.s.r. and reflectance spectrometers.

I am grateful to the postgraduate students of the School of Chemical Engineering for their informal discussions and also for creating a very pleasant atmosphere in which to work.

The help of the technical support staff is gratefully acknowledged. Their assistance during the course of this work is much appreciated.

Provision of the catalyst free of charge from Universal Matthey Limited is gratefully acknowledged.

Acknowledgement is also due to FONINVES for the financial support without which it would have been impossible to carry out my studies.

Thanks are due to Mrs. Paula Keilthy, for carefully typing the thesis.

Finally, but my no means least, I should like to express my indebtedness to my wife Anita, for her patience and support throughout this project. The thesis is dedicated to her.

SUMMARY

The dissertation describes a study of the catalytic hydrodesulphurisation (hds) reaction over a series of lithium added cobalt-molybdate catalysts supported on γ-alumina. Attempts have been made to interpret the change in catalytic activity in terms of the results of physico-chemical studies on a series of different catalyst preparations. Studies on the kinetics of hds of thiophene were also undertaken on two catalysts having different atomic ratios of lithium and cobalt (Li/Co = 0.0; Li/Co = 1.63).

A continuous flow tubular fixed-bed microcatalytic reactor at 400° C and atmospheric pressure was employed to study catalytic activities. It was found that small lithium additions to the cobalt-molybdate catalyst increased the catalytic activity. Results also indicated that lithium addition to the hds catalyst affects the isomerisation of but-1-ene which occurs simultaneously with hydrogenolysis.

Various characterisation techniques were also applied to the lithium series of catalysts. Among them, physisorption and electron spin resonance (e.s.r.) spectroscopic studies were found to be the most useful. Characterisation by physisorption indicated that, for catalysts with low lithium content (Li/Co $\leq$ 6.53), the surface area and the pore structure were not significantly altered. However, for catalysts with higher lithium contents the surface area decreased sharply. The results of e.s.r. studies indicated that lithium addition to the cobalt-molybdate catalyst affects the reducibility of molybdenum and a correlation was observed between the catalytic activity and the reducibility.

The chemical kinetics of hds of thiophene were also studied in a tubular differential reactor at atmospheric pressure and in the temperature range 260-320° C. The hds of thiophene was found to be less than first order with respect to thiophene, while both thiophene and hydrogen sulphide were found to have an inhibiting effect on the thiophene hds conversion.

Empirical power function, Langmuir-Hinshelwood (LH) and Eley-Rideal (ER) type of kinetic models were used to correlate the data on thiophene hydrogenolysis. Although the empirical power function analysis did not yield a unique rate expression which describes the experimental data, nevertheless two alternative rate expressions of the LH type were found, which describe the experimental data with reasonable precision.

CONTENTS

NOMENCLATURE

In the following list of nomenclature, the units are given in fundamental dimensions of mass (M), length (L), time (T), energy (E) and temperature (θ) where appropriate.

a_i	molar concentration of species i	mol L^{-3}
A_i	peak area of species i	L^2
A	thickness	L
b_i	estimated parameter i	
c	constant in BET equation	
C	percentage composition	
d	length	L
E	transition energy	E
E	activation energy	E mol^{-1}
f_i	response factor of species i	
F_i	molar flowrate of species i	mol T^{-1}
F	volumetric flowrate	L^3T^{-1}
g	spectroscopic splitting factor	
h	Planck's constant	ML^2T^{-1}
H	enthalpy	E mol^{-1}
H	magnetic field strength	gauss
k	reaction rate constant	
K	equilibrium constant	
K_i	adsorption equilibrium constant of i	
m_s	quantum number	

n	order of diffraction	
n_i	order of reaction with respect to species i	
N_o	Avogadro's number	mol^{-1}
p	pressure	$M\ L^{-1}T^{-2}$
P_s	saturation pressure	$M\ L^{-1}T^{-2}$
P_i	partial pressure of i	$M\ L^{-1}T^{-2}$
r	reaction rate per unit mass	$mol\ T^{-1}\ M^{-1}$
r_c	pore radius	L
r	radius	L
R	percent reflectance	
R	gas constant	$E\ mol^{-1}\ \theta^{-1}$
s	surface area per unit mass	$L^2\ M^{-1}$
S	active site	
S	entropy	$E\ mol^{-1}\ \theta^{-1}$
t	thickness of adsorbed gas layer	L
T	temperature	θ
V	volume	L^3
V_p	pore volume	L^3
V_m	volume of a monolayer	L^3
W	mass of catalyst	M
X	conversion of thiophene	
X_i	independent variables	
y	dependent variable	

Greek letters

α	area covered by N_2 molecule	L^2
β_i	parameter values	
β	Bohr magneton	E $gauss^{-1}$
θ	angle of diffraction	
θ_i	fractional coverage of species i	
θ_s	fraction of vacant site	
λ	wavelength	L
ν	frequency of radiation	T^{-1}
σ	surface tension	$M\ T^{-2}$

CHAPTER 1

I N T R O D U C T I O N

1.1 The Hydrodesulphurisation Reaction and its Importance

The hydrodesulphurisation (hds) reaction embodies the elimination of sulphur from organic molecules by reaction with hydrogen over metal sulphide catalysts. This reaction has been known since the beginning of the century. However, the industrial process became economically feasible only after the installation of hydroreforming plants, where vast quantities of hydrogen were produced as a by-product.

The hds reaction has been extensively reviewed by several authors.[1-3] McKinley[1] pointed out some important reasons why petroleum fractions should be desulphurised: reduction of corrosion during refining and handling; odour improvement; improvement of petroleum properties (colour, stability, octane number, resistance to gum formation). Nowadays other important reasons, such as protection of air quality, protection of the catalyst used in reforming, and production of clean fuels from shale oils and coal have increased the need for hds processes.

The relative amounts and the variety of sulphur compounds changes with differing types of crude oil, even with the different treatment given to a particular crude oil. Typical sulphur-containing organic compounds which can be generally found in practice are shown in Table 1.1.

1.2 The Hydrodesulphurisation (hds) Reaction

The hds reaction is a destructive hydrogenation (hydrogenolysis) in which the sulphur compound is transformed to hydrocarbon and hydrogen sulphide. The general reaction is shown below:

Compound Class	Structure
Thiols	RSH
Sulphides	RSR'
Disulphides	RSSR'
Thiophenes	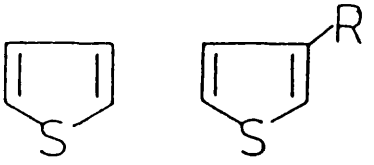
Benzothiophenes	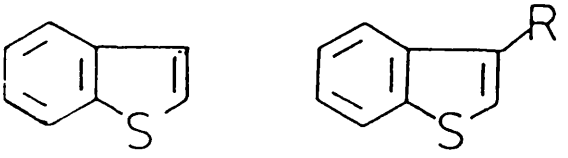
Dibenzothiophenes	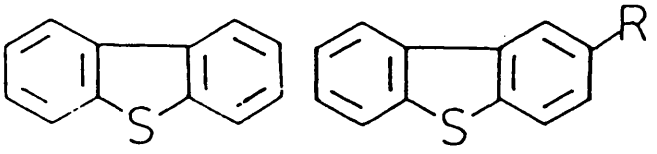
Benzonaphthothiophenes	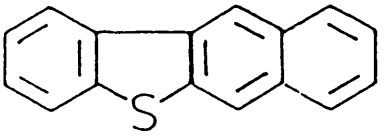
Benzodibenzothiophenes	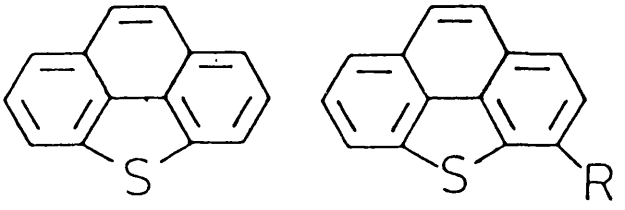

Table 1.1 Some sulphur compounds in petroleum

$$\text{Sulphur compound} + H_2 \longrightarrow \text{Hydrocarbon} + H_2S \qquad (1.1)$$

Hydrocarbon reactions other than reaction (1.1) may also take place within the wide working range of temperature and pressures used. Such other reactions, for example, are hydrocracking and isomerisation. Coking and hydrometallisation of organometallic compounds could also occur during the hds reaction. Both reactions lead to deactivation of the catalyst, but hydrometallisation, unlike coking, leads to permanent damage of the catalyst (making regeneration impossible or difficult), this being the main problem in the hds of heavy oils.

Finally, the relative importance of all these various reactions is different. The catalytic activity observed and the state of the catalyst during operation might be explained in terms of the effect of each of the above reactions.

(1) Thermodynamics of the hds reaction

Hydrogenation reactions of sulphur-containing compounds are all thermodynamically favourable, as shown by McKinley, who applied thermodynamic data[1] to derive information concerning some typical hydrogenation reactions which might occur under hds conditions. McKinley used the data to calculate the equilibrium constant for the following reactions:

$$\text{Sulphur compound} + H_2 \rightleftharpoons \text{Saturated hydrocarbon} + H_2S \qquad (1.2)$$

$$\text{Sulphur compound} \rightleftharpoons \text{Unsaturated hydrocarbon} + H_2S \qquad (1.3)$$

$$\text{Open chain sulphide} \rightleftharpoons \text{Thiol} + \text{Olefin} \qquad (1.4)$$

$$\text{Thiol sulphide} \rightleftharpoons \text{Open chain sulphide} + H_2S \qquad (1.5)$$

$$\text{Open chain sulphide} + H_2 \rightleftharpoons \text{Thiol} \qquad (1.6)$$

Figures 1.1a and b show the plot of the logarithm of the equilibrium constants against reciprocal absolute temperature (1/T), for some typical examples of reactions (1.2) and (1.3) and Table 1.2 gives the heat of reaction of some hydrogenation reactions. The values of log Keq for the reduction of sulphur compounds to saturated hydrocarbons are highly positive over the temperature range 298-800 K. It can also be seen from Figure 1.1b that the decomposition of sulphur compounds to yield unsaturated hydrocarbons is not favoured below 610 K, while at about 900 K the reactions approach completion.

Reaction	$\Delta H^{\circ}_{700\,K}$ k cal/mole
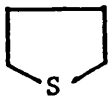 + $2H_2$ ⟶ n-C_4H_{10} + H_2S	-28.73
 + $4H_2$ ⟶ n-C_4H_{10} + H_2S	-66.98
$C_6H_{12} + H_2$ ⟶ n-C_6H_{14}	-31.10
$C_2H_5SH + H_2$ ⟶ $C_2H_6 + H_2S$	-16.77

Table 1.2 Heats of hydrogenation reactions

There seems to be no thermodynamic limitation to the reaction of hydrogen with thiols, sulphides, disulphides and thiophenes to produce saturated hydrocarbons and hydrogen sulphide. These indications are generally confirmed in practice. Cope and Farkas[4] and Hoog[5] worked on the hydrogenation of thiols to produce saturated hydrocarbons over a variety of catalysts.

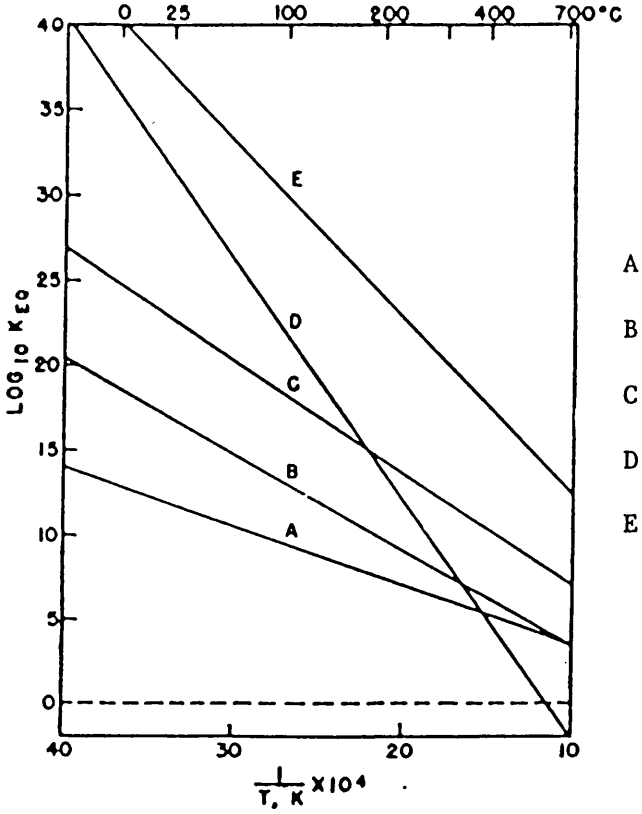

A, ethanethiol to ethane

B, thiacyclohexane to *n*-pentane

C, 2-thiabutane to methane + ethane

D, thiophene to *n*-butane

E, 3,4-dithiahexane to ethane

Figure 1.1a Reduction of sulphur-containing compounds with hydrogen to saturated hydrocarbons and hydrogen sulphide.

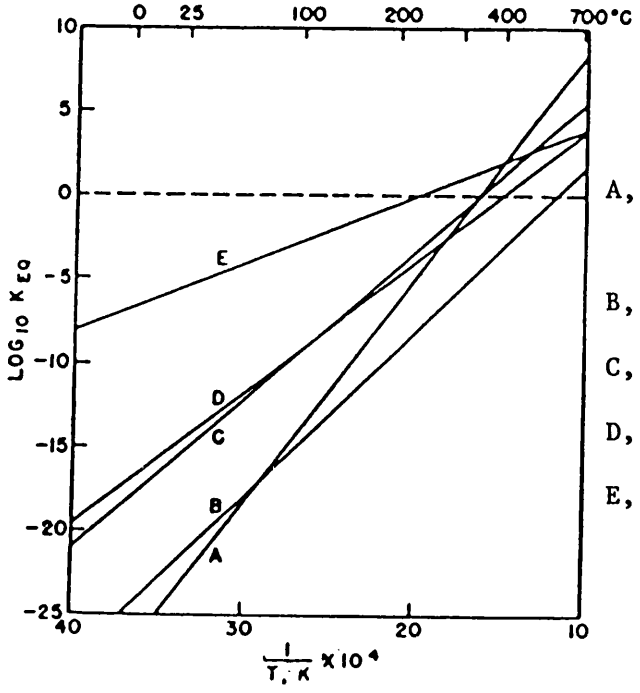

A, 3,4-dithiahexene to ethylene + acetylene

B, thiacyclohexane to 1-pentyne

C, 3-thiapentane to ethylene

D, thiacyclohexane to 1,4-pentadiene

E, 2-propanethiol to propylene

Figure 1.1b Decomposition of sulphur compounds to unsaturated hydrocarbons and hydrogen sulphide.

(2) Mechanism and kinetics of the hds reaction

Thiophenic derivatives are more difficult to desulphurise than other sulphur compounds. It has been reported[5,6] that heavy oil fractions and residues from oil stocks contain a considerable amount of complex thiophenic compounds. The simplest of these thiophenic sulphur compounds is thiophene itself, which is chosen as a model compound for investigation. In recent years, attention has been given to systematic studies of the mechanism and kinetics of hydrogenolysis of thiophene. Some of the studies have been reviewed and are summarised below.

(i) Mechanism of thiophene hydrogenolysis

Important aspects such as:

a) nature of the adsorption of thiphene,

b) identification of catalytic intermediates,

c) hydrogenation of unsaturated hydrocarbon, and

d) type of hydrogen chemisorption

were the starting points of various investigations towards a better understanding of the hds mechanism. From these studies a series of mechanisms for the hds of thiophene has been proposed.

Cawley and Hall[7] studied thiophene hydrogenolysis over an unspecified catalyst and found tetrahydrothiophene as an intermediate in the reaction. Their experimental conditions were 550-727 K and (1-10) x 10^6 Pa. Later Griffith *et al.*[8] found no tetrahydrothiophene in the products when working with nickel sulphide and molybdenum sulphide in the temperature range 473-773 K and atmospheric pressure. They suggested that the presence of tetrahydrothiophene in Cowley's work was due to the catalyst not being fully

sulphided. They proposed a reaction mechanism (see Figure 1.2a) based on a two point adsorption of thiophene and a partial hydrogenation of the thiophenic ring before C-S bond cleavage.

Butadiene was first observed in the reaction products by Komarewsky and Knaggs[9] by studying the reaction over a vanadium oxide catalyst supported on alumina at 673 K. On this basis, they suggested that the C-S bond cleavage was the first step, rather than the hydrogenation of the ring. A two-point adsorption for thiophene is involved. They proposed a reaction mechanism as shown in Figure 1.2b.

Amberg[10] reviewed some of the work (which he and his co-workers had carried out) in which thiophene and methylthiophenes were used as model compounds over several hds catalyst. The reactions were carried out in excess hydrogen at atmospheric pressure in the temperature range 440-670 K. They suggested that, at least at atmospheric pressure, the C-S bond cleavage takes precedence over ring hydrogenation, yielding butadiene as an initial product. This view supports the work of Komarewsky and Knaggs.[9] They also claimed that at least two types of catalytic sites are operative,[11-16] the bulk of hydrogenolysis taking place at the weak (Lewis) acid site, while the olefin hydrogenation occurs at the other type of sites (strong Lewis acid).

Adsorption studies of both reactants and products were carried out by Owen and Amberg.[11] Thiophene adsorption was strongly temperature dependent, having a temperature coefficient of 9.5 k cal/mole. Hydrogen sulphide adsorbed quickly and desorbed at a rate proportional to the coverage. Relatively weakly bound, or free hydrogen appeared to be reactive, but adsorbed hydrogen was thought to modify the adsorption of

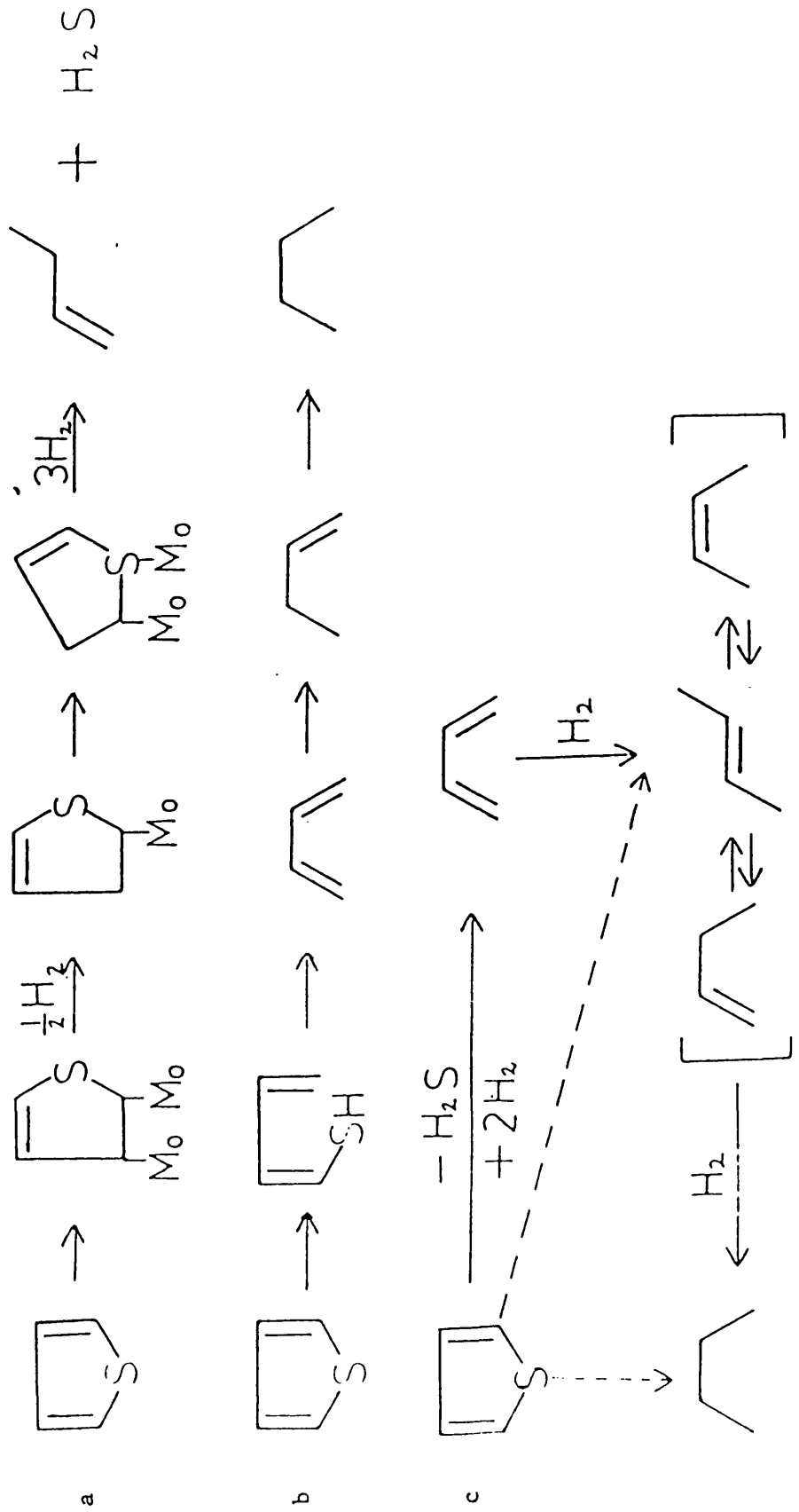

Figure 1.2 Proposed mechanisms of the hds reaction: a, by Griffith *et al.*;[8] b, by Komarewsky and Knaggs;[9] c, by Owen and Amberg.[11]

thiophene and butene. Adsorbed H_2S had an appreciable effect on the rate of desulphurisation. Olefins were weakly adsorbed and had only a small effect on desulphurisation. Figure 1.2c shows the reaction scheme proposed by Owen and Amberg.

Kolboe[17] studied the rate of hydrodesulphurisation of thiophene, tetrahydrothiophene and *n*-butanethiol over MoS_2, CoO_3-MoO_3/Al_2O_3, and Cr_2O_3 catalysts at 561 K and atmospheric pressure. He observed that the amount of butadiene formed in hydrodesulphurisation of tetrahydrothiophene exceeded that arising from the hds of thiophene. Hence it was suggested that the reaction involving thiophene did not occur by hydrodesulphurisation at all, but rather by a dehydrodesulphurisation route whereby H_2S was removed by β elimination (intramolecular dehydrodesulphurisation). Figure 1.3a shows Kolboe's mechanism. Deuterium tracer experiments by Mikovsky, Silvestry and Heinemann[18] provided support for Kolboe's mechanism.

Lipsch and Schuit[19] developed a one point adsorption mechanism for thiophene desulphurisation. They explained the hydrogen transfer process in the hydrogenolysis of thiophene by a MoO_3 catalyst. They described the mechanism as follows:

(a) Thiophene is adsorbed on an anion vacancy formed by previous reduction of the MoO_3 catalyst.

(b) One hydrogen atom is transferred from an adjacent -OH group to the adsorbed thiophene and one C-S bond is broken.

(c) A second hydrogen atom is transferred by breaking the other C-S bond.

(d) 1,3-Butadiene desorbs and then is hydrogenated, on the same or a different site. Figure 1.3b depicts

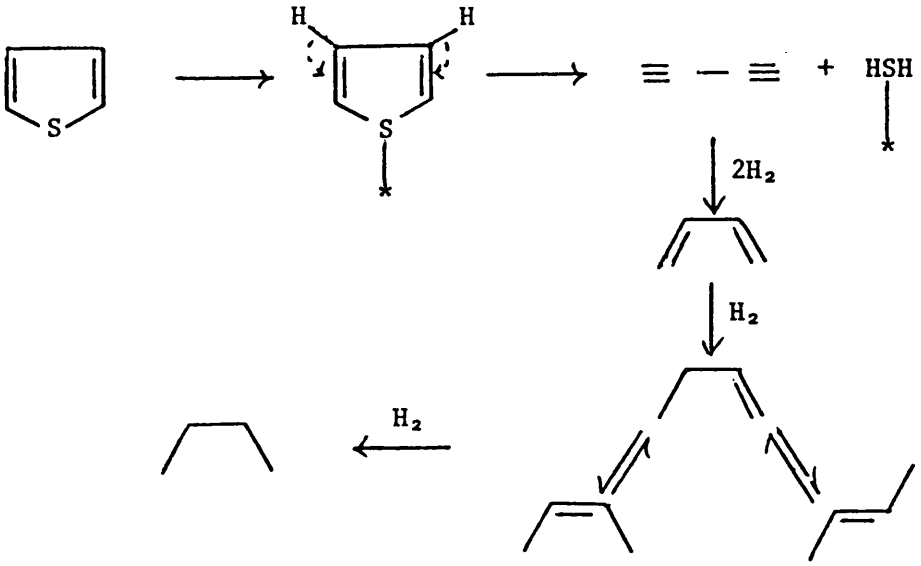

a The reaction mechanism by Kolboe[17]

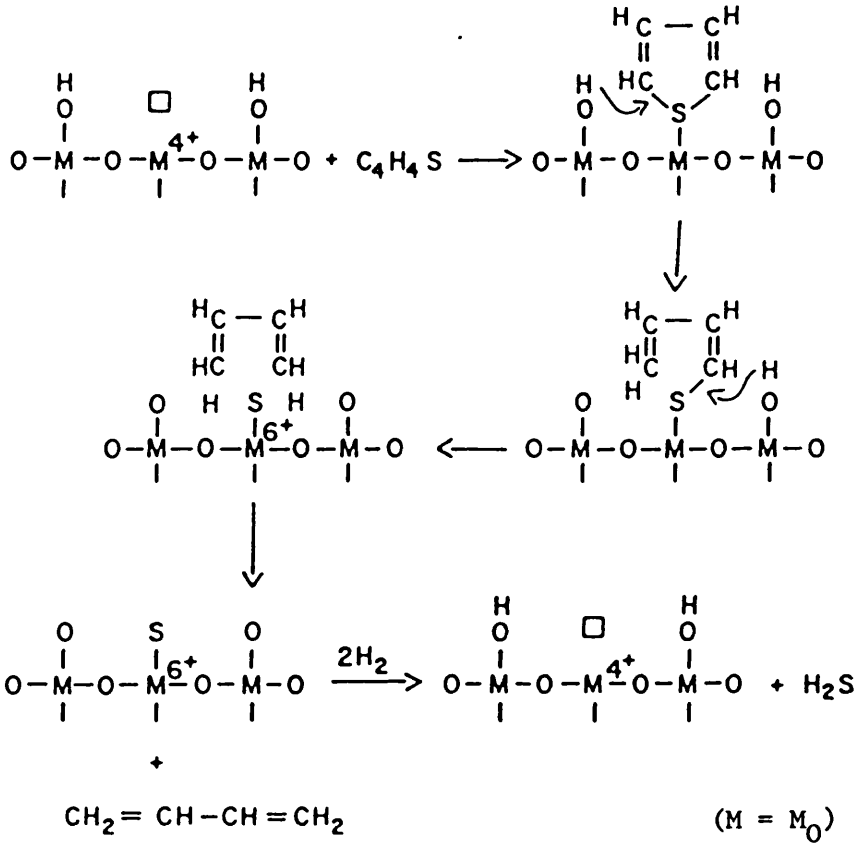

b The reaction mechanism by Lipsch *et al.*[19]

Figure 1.3

a scheme of this mechanism.

This work is consistent with Komarewsky and Knaggs,[9] and Amberg and co-workers[11-16] who proposed that the C-S bond cleavage occurs before ring hydrogenation.

Studies of H_2-D_2 exchange and thiophene hydrogenolysis by Smith *et al.*[20] over γ-alumina, MoO_3/γ-Al_2O_3, and CoO-MoO_3/γ-Al_2O_3 catalysts suggested that adsorption of thiophene occurs *via* the heteroatom due to the predomiant α-exchange of deuterium on molybdenum-containing catalysts. α-Exchange was correlated with desulphurisation, while multiple exchange was correlated with hydrogenation. They also suggested that π-complex formation is important in multiple exchange and the role of cobalt may be to facilitate surface hydrogen mobility and thereby decreasing coke formation.

The idea of hydrogenation of the thiophene ring prior to C-S bond cleavage has been put forward by several investigators. Kieran and Kemball[21] studied deuterium exchange and hydrogenolysis of thiophene over unsupported MoS_2 catalysts. They indicated that hydrogenation could precede C-S bond breakage in hds. Zdrazil,[22] and Kraus and Zdrazil[23] also supported this idea. They claimed that on the basis of the aromaticity of thiophene, direct hydrogenolysis seemed highly improbable.

Recently, Zdrazil *et al.*[24] studied, in the presence of several catalysts, the selectivity of the saturated intermediate, dihydrobenzothiophene formed during benzothiophene hydrodesulphurisation.

This model sulphur compound was chosen because the amount of hydrogenated intermediate was sufficient to make a more reliable measurement. However, the result of this study was also applicable to the mechanism of the hds of thiophene. They used the concept of bifunctional catalysis[25] to explain the reaction sequences. They suggested that the reaction proceeded by hydrogenation of the thiophene ring (hydrogenation function) followed by C-S bond rupture (acid function of the catalyst) with the formation of unsaturated C=C bonds which are subsequently hydrogenated (hydrogenation function). These sequences do not assume the existence of a hydrogenolysis step. They also suggested, by comparing unpromoted and promoted catalysts, that promoters decrease the kinetic stability of saturated intermediates. The proposed mechanism is shown in Figure 1.4a.

The above series of papers indicate that the heteroatom of the thiophenic molecule interacts with the anion vacancy of the metal catalyst. According to Kwart, Schuit and Gates,[26] these mechanisms fail to explain the effect of steric hindrance observed in practice for substituted compounds. They proposed a multipoint adsorption mechanism of the hds of thiophene where the C=C interacts with a Mo cation and the sulphur atom of the reactant interacts with a 'sulphur' ion on the surface. The mechanism proposed also accounts for the observed deuterium exchange and hydrodesulphurisation reactions. A schematic diagram of the reaction mechanism is shown in Figure 1.4b.

To summarise this review of mechanistic studies of thiophene hds, it is clear that some controversial points still exist about the true nature of the mechanism. These are:

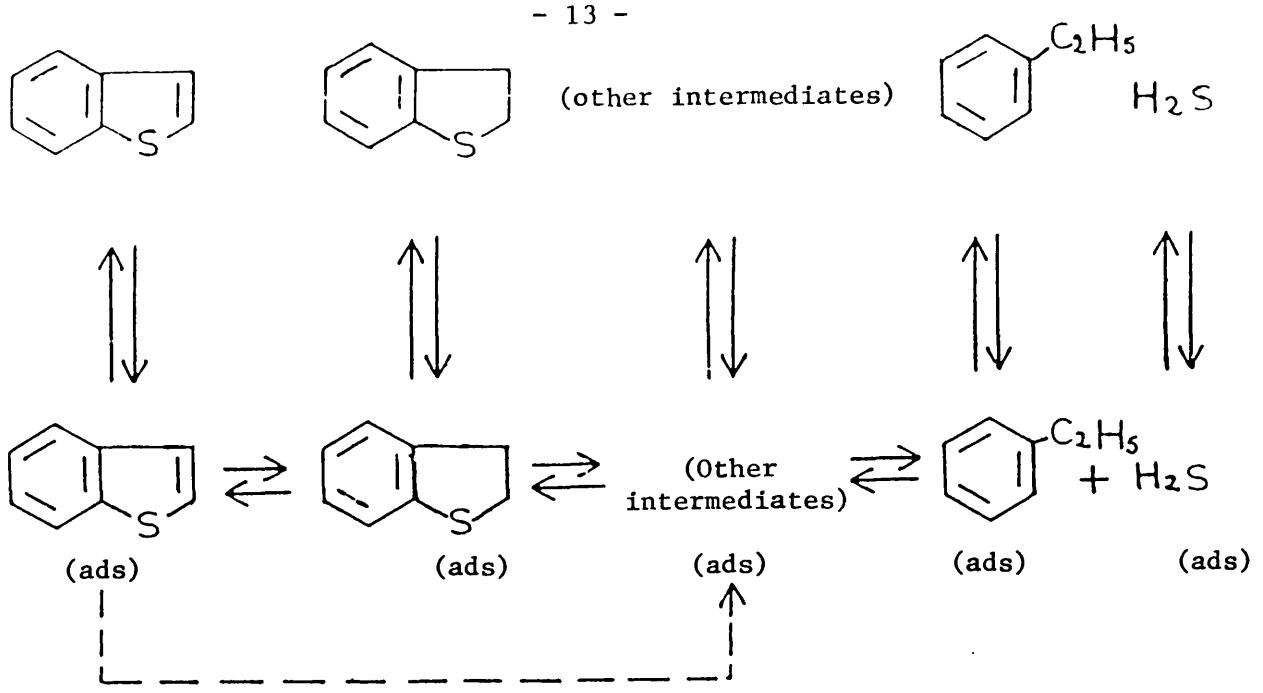

a Reduction sequence by Zdrazil *et al.*[24]

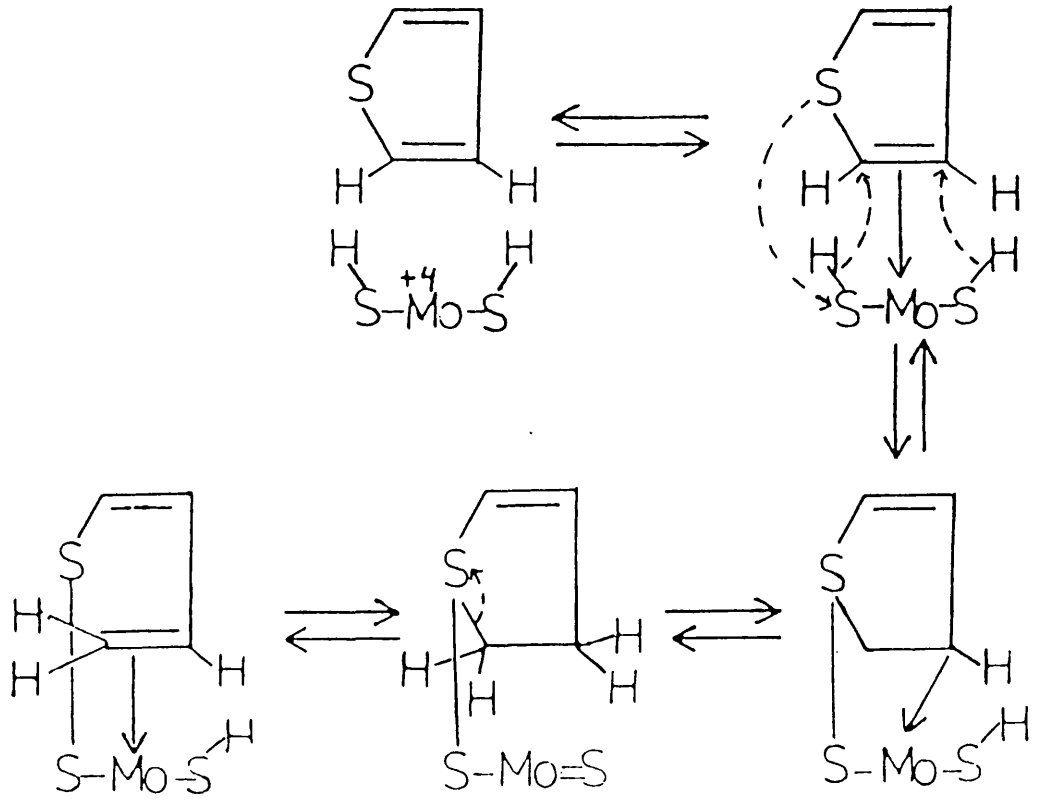

b Reduction mechanism by Kwart *et al.*[26]

Figure 1.4

1) It is not clear whether the adsorption of thiophene occurs *via* the heteroatom or whether other points of attachment are also involved.

2) The nature of interaction of thiophene with the catalyst surface is not unequivocal. It may occur (a) through the S atom or (b) through the C=C atoms.

3) The sequence of reaction steps in hds may involve any of the following alternatives:

   (a) hydrogenation of thiophene, followed by hydrogenolysis plus hydrogenation of the unsaturated hydrocarbon;

   (b) hydrogenolysis of the thiophenic ring, followed by hydrogenation of the unsaturated hydrocarbon; or

   (c) hydrogenation of the thiophenic ring, rupture of the C-S bond, followed by hydrogenation of the unsaturated compound.

(ii) Kinetics of thiophene hydrodesulphurisation

A wide range of experimental conditions and catalysts prepared in different ways have been used in order to obtain information about the reaction kinetics of thiophene hds. Table 1.3 shows a summary of some of the work done on thiophene hydrogenolysis, specifying the catalysts and conditions used for the reactions. In general, reaction orders are in the range 0-1 with respect to both thiophene and hydrogen. Sometimes these reaction orders vary with temperature. It can also be seen that the values of the apparent activation energy vary over the range 3.4-25 k cal/mole.

The kinetic modelling of the rate for thiophene hydrodesulphurisation has been examined by several workers.[32-36] The proposed rate expressions are based mainly on Langmuir-Hinshelwood (L-H) type correlations, assuming the surface reaction as a rate limiting step. A summary of the rate

	Experimental Condition		Order of Reaction		Activation Energy	Remarks	Ref.
	T (° C)	p (atm)	Hydrogen	Thiophene	k cal/mole		
$CoS-MoO_3$	200	1	≈0	<1	-	Thiophene order less than 1 might be due to inhibition by reaction product	27
Ni_3S_2	200-500	1	-	≈1	1	Reaction order varied with temperature	8
MoO_2-MoS_2				0.2-0.6			
$CoO\ MoO_3/Al_2O_3$	325-428	1	1	0	4.2	Reaction order for thiophene was assumed to be zero	28
$CoO\ MoO_3/Al_2O_3$	250-370	1-17	0.5	1	10.5	For other sulphur compounds hydrogen reaction order varied 0.3-0.5	29
$Co_3O_4MoO_3/Al_2O_3$	350-425	1	1	1	3.4	Thiophene order of reaction assumed to be first	30
$CoO\ MoO_3/Al_2O_3$	290-425	1	1	0.8	6.7	-	31

Table 1.3 Summary of some work on the kinetics of thiophene

expressions is presented in Table 1.4.

The experimental data contained in the survey presented in Table 1.4 were obtained using different types of reactors. These types of reactor include a static reactor,[33] a differential reactor with external recirculation,[34] a differential reactor with internal recirculation,[35] and a tubular differential reactor.[36] The first three reactors do not permit an examination of the separate effect of thiophene and hydrogen sulphide on the rate of reaction. To report the plot of the rate data collected as a function of one of these two variables may sometimes be misleading. For example, the investigation of Van Looy and Limido[33] and that of Satterfield and Roberts[34] indicated the presence of a maximum of the rate of reaction with respect to thiophene partial pressure. The selection of their kinetic model was based on this observation. However, the maximum in the rate of reaction may have been caused by a simultaneous variation of thiophene and hydrogen sulphide partial pressure, as it is well known that hydrogen sulphide can affect the rate of reaction when present in significant amounts.[11-37] In these reported investiations it was always present and its amount was not held constant. Furthermore, Lee and Butt[36] investigated a larger range of thiophene partial pressure than that of Satterfield and Roberts.[34] No maximum in the rate was observed even though, in their experiments, hydrogen sulphide was always present and in variable amounts. This indicates that the rate data reported may be affected by simultaneous effects of thiophene and hydrogen sulphide concentration. Their proposed kinetic model (see Table 1.4) is a combination of L-H models with an empirical temperature dependent constant to take into account the contribution of the strongly adsorbed hydrogen with increasing temperature.

CATALYST	EXPERIMENTAL CONDITIONS T (°C)	P (ATM)	KINETIC MODELS	HEAT OF ADSORPTION AND ACTIVATION ENERGY (KCAL/MOL) $\triangle H_h$	$\triangle H_t$	$\triangle H_s$	E	REF.
			ELEY RIDEAL MECHANISM (ER)					
$CoOMoO_3/Al_2O_3$	300-375	16	$r = \frac{Ka_h a_t}{(1 + K_s a_s)}$	-	-	-	≃7	32
Cr_2O_3/CARBON	319-448	1	$r = \frac{KK_tK_hP_tP_h}{(1 + K_tP_t + K_hP_h)^2}$	-8	-17	-	25	33
$CoOMoO_3/Al_2O_3$	235-265	1	$r = \frac{KP_tP_h}{(1 + K_tP_t + K_sP_s)^n}$ $n = 1$	-	-18	-12	9	34
			$n = 2$	-	-24	-13	3.7	
$CoOMoO_3/Al_2O_3$	250-350	1	$r = \frac{KP_tP_t}{(1 + K_tP_t + K_sP_s)^2}$	-	-	-	10-12	35
$CoOMoO_3/Al_2O_3$	250-313	1	$r = \frac{KP_tP_h}{(1 + K_tP_t + K_sP_s)^m} \frac{1}{(1 + K_hP_h)^n}$ $m = 2$ $n = 0$	-	-12.2	-20.6	11.9	36
			$r = \frac{KP_tP_h}{(1 + K_tP_t + K_sP_s)} \left[\frac{1}{1 + K_hP_h} + K'\right]$	-53.6	-13.9	-29.6	12/9	

TABLE 1.4 LANGMUIR HINSHELWOOD HOUGEN WATSON (LH-HW) KINETIC EXPRESSION FOR THIOPHENE HYDROGENOLYSIS

A tubular differential reactor was used by Morooka and Hamrin[35] in their kinetic studies. This reactor allowed the separate study of the effects of thiophene and hydrogen sulphide on the rate of reaction. However, they covered only a narrow range of thiophene partial pressure ($\lesssim$40 mmHg) and only three values of partial pressure of hydrogen sulphide were studied. On this basis their proposed model was similar to that of Satterfield and Roberts (see Table 1.4).

1.3 The Catalyst

Studies on the composition and structure of hds catalysts have been carried out and frequently reviewed by many workers.[1-3,38-44] Generally, commercial hds catalysts contain metal oxides of Group 6B (Mo, W) and metal oxides of Group 8 (Co, Ni), the latter acting as promoters. Due to its very low hydrocracking property, γ-alumina has been commonly used as a support for the hds catalyst. The most common commercial catalyst is the so-called 'cobalt-molybdate' represented usually by $CoO-MoO_3/\gamma-Al_2O_3$. The metal content of the cobalt-molybdate catalysts varies from 3-5 weight % in cobalt and 7-12 weight % in molybdenum. This cobalt-molybdate catalyst is highly active and selective towards the hds reaction. The composition of the cobalt-molydate catalyst is usually given in terms of CoO and MoO_3 content. However, Mitchell[38] pointed out that the composition of the catlyst given in this way could be misleading as those oxides are probably not present as such on the catalyst.

Most studies on cobalt-molybdate catalysts have covered three broad areas, as follows:

(1) Identification of chemical species present in the catalyst

Richardson[45] investigated in detail the nature of the components in a fresh catalyst by using a magnetic susceptibility technique. He found that the catalyst consisted of Al_2O_3 and $CoAl_2O_4$, both inactive for hds reactions. On the other hand, CoO, MoO_3 and $CoMoO_4$ presented a moderate activity. The same author[45] found that a mixture of Co and Mo oxides (whose complex structure was not precisely determined) was highly active. During thiophene hds, CoO sulphided to Co_9S_8; $CoMoO_4$ sulphided to a mixture of Co_9S_8 and either MoOS or a mixture of MoO_2 and MoS_2; MoO_3 sulphided completely to MoS_2. Richardson concluded that the true catalyst was MoS_2 promoted with cobalt. On the other hand, Ashley and Mitchell[46] found that cobalt-molybdate catalysts were not present as CoO, Co_3O_4, or $CoMoO_4$. Molybdenum and cobalt were found in tetrahedral co-ordination with oxide ions. However, octahedral and five-co-ordinated cobalt were also found.

A detailed study of the cobalt-molybdate catalyst was carried out by Lipsch and Schuit[19] using several physical characterisation techniques. The catalyst contained 4% CoO and 12.3% MoO_3, supported on γ-alumina. It was found that molybdenum is octahedrally surrounded by oxygen and is essentially MoO_3, whereas the cobalt is distributed through the bulk of the alumina as $CoAl_2O_4$. Mitchell and Trifiro[47] reported that molybdenum and cobalt are associated in catalysts with the presence of linked MoO_4 tetrahedra and CoO_6 hexahedra. They also questioned the assumption of ion vacancies, proposed by Lipsch and Schuit, as it was found that the bridging oxygen is replaced in preference to terminal oxide in the sulphidation reaction of a binuclear

oxomolybdenum(V). Recently Giordano *et al.*[48] examined a MoO_3 catalyst supported on alumina by means of reflectance spectroscopy and e.s.r. techniques. It was found that the nature of the surface structure is affected by molybdenum concentration and conditions of reduction.

In general, CoO and MoO_3 are precursors of the true active species which are known to be sulphides of Co-Mo obtained either by presulphidation using a mixture of $H_2S + H_2$, or by the effect of the sulphur compound plus hydrogen during hds reaction.

(2) Studies of the catalytic activity as a function of the Co:Mo atomic ratio

It is well known that the cobalt in the cobalt-molybdate catalyst is acting as a promotor (*i.e.*, enhances the catalytic activity of the MoO_3/Al_2O_3 when added in specified amounts). These two phases, when present on their own, are relatively inactive for desulphurisation.

The cobalt/molybdenum ratio is one of the most important features of these catalysts. A list of several studies on the effect of Co:Mo ratios is given below:

Co:Mo for maximum activity	Ref.	
0.3	Beuther *et al.*	49
1.0	Mann	50
0.75	Andrew	51
0.18	Richardson	45
0.25	Ahuja *et al.*	52
no maximum found	Hargreave and Ross	53

It has been pointed out by Massoth[41] that the discrepancy in results of studies on Co-Mo catalysts may be due to the differences in catalyst preparation (addition of active phases, calcination temperature, pretreatment, support used). In addition to Co, De Beer *et al.*[54] also used other metals such as Zn, Ni, Mn, as promoters for molybdenum catalysts. They found that for each of these metal promoters, including cobalt, the activity increases for metal to molybdenum ratios less than 0.3. The promoting effect of these metals was in the order Co > Zn > Ni > Mn.

The role of cobalt as a promoter is still not well understood. Massoth[41] summarised several theories on the effect of cobalt contained within a molybdenum catalyst and they are given briefly below:

a) Cobalt enhances the Mo dispersion in the support and hence increases the molybdenum monolayer area.

b) Cobalt enhances the extent of molybdenum reduction on which the catalytic activity is thought to be dependent.

c) Cobalt occupies a very specific site in MoS_2 crystallites (assumption for the intercalation model), engendering formation of Mo^{3+}, which is the active site for hds reaction.

d) Cobalt enhances the activity of molybdenum catalysts at the phase boundary between MoS_2 and Co_9S_8 (synergy model).

e) Cobalt may affect the adsorption-desorption properties or the intrinsic activity of vacancies present in the catalyst and hence affects the specific kinetics of reaction.

f) Cobalt increases the hydrogenating ability. This prevents coke formation and subsequent deactivation-

g) Cobalt hinders formation of relatively inactive conglomerates of MoS_2 crystallites.

(3) Modification of the cobalt-molybdate catalysts

Many investigations have been carried out in order to improve hds catalysts (activity and/or life), in particular the cobalt-molybdate catalyst, by modifying the support,[58] or by adding a third metal component (known as an activator).[57] Most of the literature concerning the modification of hds catalysts is found in patents, as reviewed by Ranney[55] and Mitchell.[56] However, not many works had been published which attempt to elucidate the effects of these additives on the catalytic system. Martinez and Mitchell[57] studied a series of zinc and magnesium containing $CoO-MoO_3/Al_2O_3$ catalysts by using pulse and flow techniques at atmospheric pressure and at 623 K, in order to elucidate the role of Mg and Zn as additives. It was found that for an additive to cobalt ratio of 0.25, magnesium decreased both thiophene conversion and butane/butene ratio, whereas zinc increased both. They also extended their studies in order to understand the effect of increasing amounts of magnesium and zinc on hds activity, product distribution and isomerisation. A correlation was found between the effect of additive and the structure and also on catalytic properties.

Ratnasamy *et al.*[58] found from thermo-gravimetric (TG) studies that the presence of sodium on the alumina support affects the reducibility of cobalt and molybdenum. In the absence of sodium, cobalt inhibits

the reduction of MoO_3/Al_2O_3. However, in the presence of sodium, cobalt accelerates the reduction process. The author postulated that in the presence of sodium, most of the cobalt occurs in the form of Co_3O_4, which, upon reduction, forms the metal. The hds activity for a series of Co-Mo catalysts with and without sodium was measured and plotted against their specific reducibility (α_{sp}) determined by the TG method. The authors observed a correlation between the reducibility of the catalysts and their hds activity which shows a maximum at a certain value of α_{sp}. Catalysts containing little or no sodium had a low α_{sp} value, as well as a low catalytic activity. The results were explained by proposing a model based on the idea of the existence of molybdenum in various phases and its interaction with support and cobalt.

The effect of sodium on the cobalt-molybdate systems was also studied by Lycourghiotis and co-workers.[59,60] Cobalt and molybdenum dispersion were observed by using several physical characterisation techniques. They found that, for the catalysts with low cobalt content, the dispersion of cobalt increases when the sodium content increases, and the transformation of Co_3O_4 into $CoAl_2O_4$ was noted. On the other hand, for catalysts with a higher cobalt content, no change was observed throughout the sodium composition range studied. Molybdenum dispersion was independent of sodium content up to 3.6% Na, but it decreased above this content. No attempt was made to measure the catalytic activity of these catalysts.

Kelly and Ternan[61] used alkali metal promoters in $CoO-MoO_3/Al_2O_3$ catalysts in order to investigate the effect of promoter on coke deposition during hydrocracking of athabasca bitumen. The experimental work was carried out at 13.9 MPa and at 450° C. It was found:

a) The surface area for a Li promoted catalyst showed a maximum. However, for a Na and K promoted catalyst it decreased continuously with increasing alkali metal content.

b) The conversion for pitch, oxygen, sulphur and nitrogen improved for small additions of Li, passing through a maximum. In general, however, the conversion decreases with Na or K.

c) The variation of H_2/carbon ratio in the liquid product was similar to the variation in conversion data (maximum for Li-containing catalyst, whereas there was continous decrease for Na or K promoted catalysts).

d) Coke deposition for the Li catalyst passed through a minimum, while for the Na and K catalysts there was a continuous decrease.

These results were explained in terms of the effect of promoter on the electronic properties of the catalyst.

1.4 Objectives of the Present Investigation

The objectives of the present studies can be broadly divided into two sections: (1) catalytic activity studies and (2) reaction kinetic studies.

(1) Catalytic activity studies

Addition of a second promoter on a standard cobalt-molybdate catalyst has been practised by several workers.[55,57,61] Such promoters generally belong to alkali and alkali-metal groups, since these metals are known to decrease coke deposition and therefore may lead to an increase in the life-span of a catalyst. There is also evidence that these metals influence the catalytic properties of the cobalt-molybdate in favour of sulphur removal.[57,58,61] However, not many investigations have been undertaken in order to elucidate the effect of those additives on the catalyst structure and hence on the activity.

The first objective of the present investigation, therefore, is to study the effect of lithium as a second promoter on a standard $CoO-MoO_3/Al_2O_3$ catalyst. A number of physical characterisation techniques, together with catalytic activity measurements, are employed to seek a correlation (if there is any) between the structure property and the activity of the catalyst. The reaction to be studied is thiophene hds, which involves the desulphurisation reaction, together with hydrogenation and isomerisation of hydrocarbons.

(2) Reaction kinetic studies

The second objective of this investigation is to study the kinetics of thiophene hds in order to find out if the addition of lithium as a second promoter changes the kinetics of the hds reaction [with respect to the unpromoted (commercial) catalyst].

The kinetic studies are investigated by means of a differential reactor, whereby one can obtain information about the effect of individual components (reactants and products) on the rate of reaction. Special attention is paid to a detailed investigation of the inhibiting effect of hydrogen sulphide. Earlier workers[33,37] carried out limited studies in this direction. Use of an integral reactor or a differential reactor with recycling (external or internal) does not provide sufficient information to understand the effect of individual components on the rate of reaction.

The kinetic data available from the present study is then analysed and an attempt made to find a suitable model for the rate of the thiophene hydrogenolysis reaction, utilising LH-HW rate expressions. In modelling the kinetic rate expression, the information provided by the mechanistic studies of the hds reaction (as has been mentioned previously) is also taken into consideration.

CHAPTER 2

E X P E R I M E N T A L

2.1 Catalytic Measurement and Kinetic Studies

(1) Introduction

This section describes several experimental techniques which have been used throughout this research, and can be divided into two broad categories:

(a) Catalytic activity measurement

A series of lithium containing cobalt-molybdenum catalysts was prepared and tested for activity in respect of thiophene hydrodesulphurisation. The objective of the study was to understand the influence of lithium content on thiophnene desulphurisation and other reactions such as isomerisation and hydrogenation, occurring simultaneously with hds.

The activity measurements were carried out in a microcatalytic flow reactor which has been extensively employed by other workers when rapid catalyst screening and evaluation are demanded.[62,63]

(b) Kinetic measurements

During the second part of this research, studies of the kinetics of the hydrodesulphurisation reaction were carried out using two catalyst samples, namely:

(i) Pure Co-Mo/γ-Al_2O_3

(ii) 0.25% Li on Co-Mo/γ-Al_2O_3 (Li/Co = 1.63)

A stainless steel microreactor was used [see section 2.1(3)(i)] and the range of conditions was as follows:

Temperature:	260-320° C
Thiophene pressure:	11-101 mmHg
Hydrogen sulphide pressure:	18-154 mmHg
Hydrogen pressure:	505-749 mmHg

Once the experimental kinetic data were obtained, attempts to find a suitable model for the thiophene hydrogenolysis reaction were made by using several discrimination techniques (see Chapter 4).

(2) Catalyst preparation

The commercial Co-Mo/γ-Al_2O_3 catalyst was provided by Universal-Matthey as an extrudate. This was crushed and sieved in order to obtain particles between 30-60 mesh size (250-500 μm) and this portion was dried for 24 h at 150° C.

Using a pore filling technique,[64] the water pore volume of the CoO-MoO_3/γ-Al_2O_3 catalyst was found to be 0.71 ± 0.05 l kg^{-1}. Lithium was added to the catalyst by impregnating Co-Mo/γ-Al_2O_3 with an aqueous solution of $LiNO_3$ (BDH Analar grade) using an impregnation technique.[64] For this purpose a solution of lithium nitrate of the required concentration in a volume just sufficient to fill the pores was added dropwise on to 20 g of commercial Co-Mo catalyst up to incipient wetness. Several samples with increasing lithium content (up to 2 wt % Li) were prepared in this way. The catalysts were dried in air at 120° C for 6 h and then calcined in air at 650° C for 16 h. Chemical compositions (nominal) of the lithium-containing catalyst prepared are given in Table 2.1.

% Li (wt %)	% Co (wt %)	% Mo (wt %)	Li:Co ratio	Li:Mo ratio
0.00	1.30	11.65	0.00	0.00
0.10	1.30	11.64	0.65	0.12
0.25	1.30	11.62	1.63	0.30
0.50	1.29	11.59	3.26	0.59
0.75	1.29	11.56	4.89	0.89
1.00	1.29	11.53	6.52	1.19
1.30	1.28	11.50	8.48	1.54
1.50	1.28	11.47	9.78	1.78
1.75	1.27	11.44	11.43	2.08
2.00	1.27	11.42	13.06	2.37

Table 2.1 Chemical composition of the lithium promoted $CoO-MoO_3/\gamma-Al_2O_3$ catalysts

(3) Experimental

A diagram of the experimental apparatus used is shown in Figure 2.1. The few changes made for either activity measurements or kinetic measurements will be mentioned in the appropriate section.

(i) Catalytic reactor

a) Preheater - This consisted of a section of tubing 12" long and $\frac{1}{4}$" external diameter, packed with a rolled stainless steel wire mesh to improve the mixing of the reactants and heat exchange to the gas phase. The preheater section finished just above the catalyst bed.

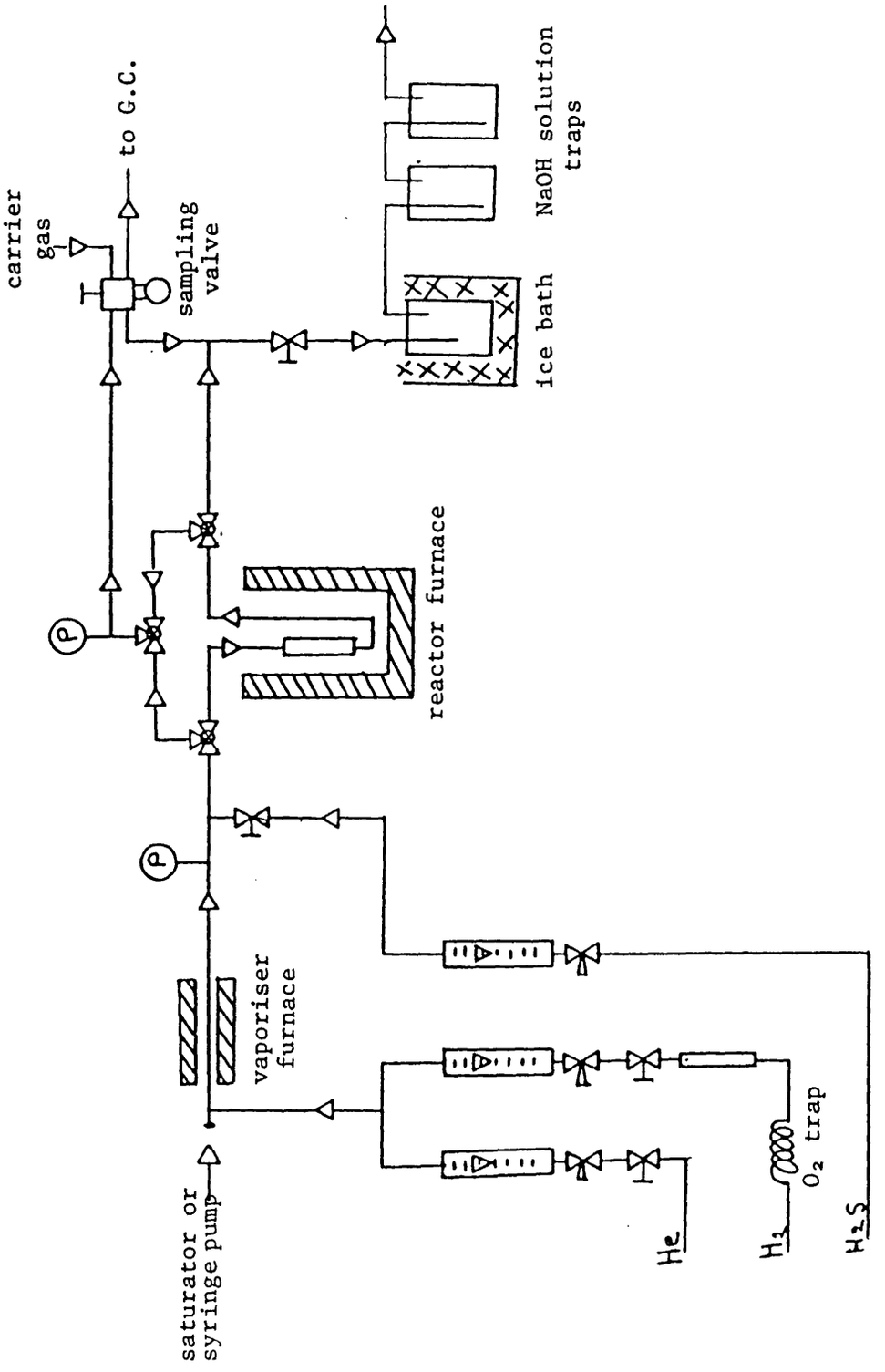

Figure 2.1 Diagram of the experimental apparatus

b) Reactor - Two types of reactor were used. Diagrams of these are shown in Figure 2.2. One type was for catalytic activity measurements and the other was for reaction kinetic measurements. The reactor for catalytic activity measurements was made of glass (Pyrex), 7" long and 18 mm internal diameter, having a thermocouple well (for temperature measurement) axially held at the top of the reactor by a captive seal nut in addition to a glass appendix of 13 cm long and 3 mm diameter for further physical characterisations of the catalyst *in situ*. The catalyst was supported on a sintered glass disc (grade 1) of 18 mm diameter. The reactor was connected to the main system by a captive seal reducing union 5/16"to $\frac{1}{4}$".

The reactor for kinetic measurements was a 6" long and $\frac{1}{4}$" diameter tube mounted vertically. A swagelok $\frac{1}{4}$" 'T' fitting, was mounted on the top of the reactor to handle the inlet of gases at one side and to support the thermocouple axially in the reactor at the other side. The catalyst was supported inside the reactor by piston-like glass wool which, in turn, was held in place by stainless steel rolled gauze.

All parts of the preheating section and the reactor were made of 316 stainless steel, except for the thermocouple sheaths, which were 321 stainless steel. When a syringe pump was installed to inject the thiophene feed a vaporiser chamber was required. This was made of 316 stainless steel tubing (6" long and $\frac{1}{4}$" diameter) packed with glass beads. At one end of the tube an injection port was fitted for thiophene delivery and for hydrogen supply.

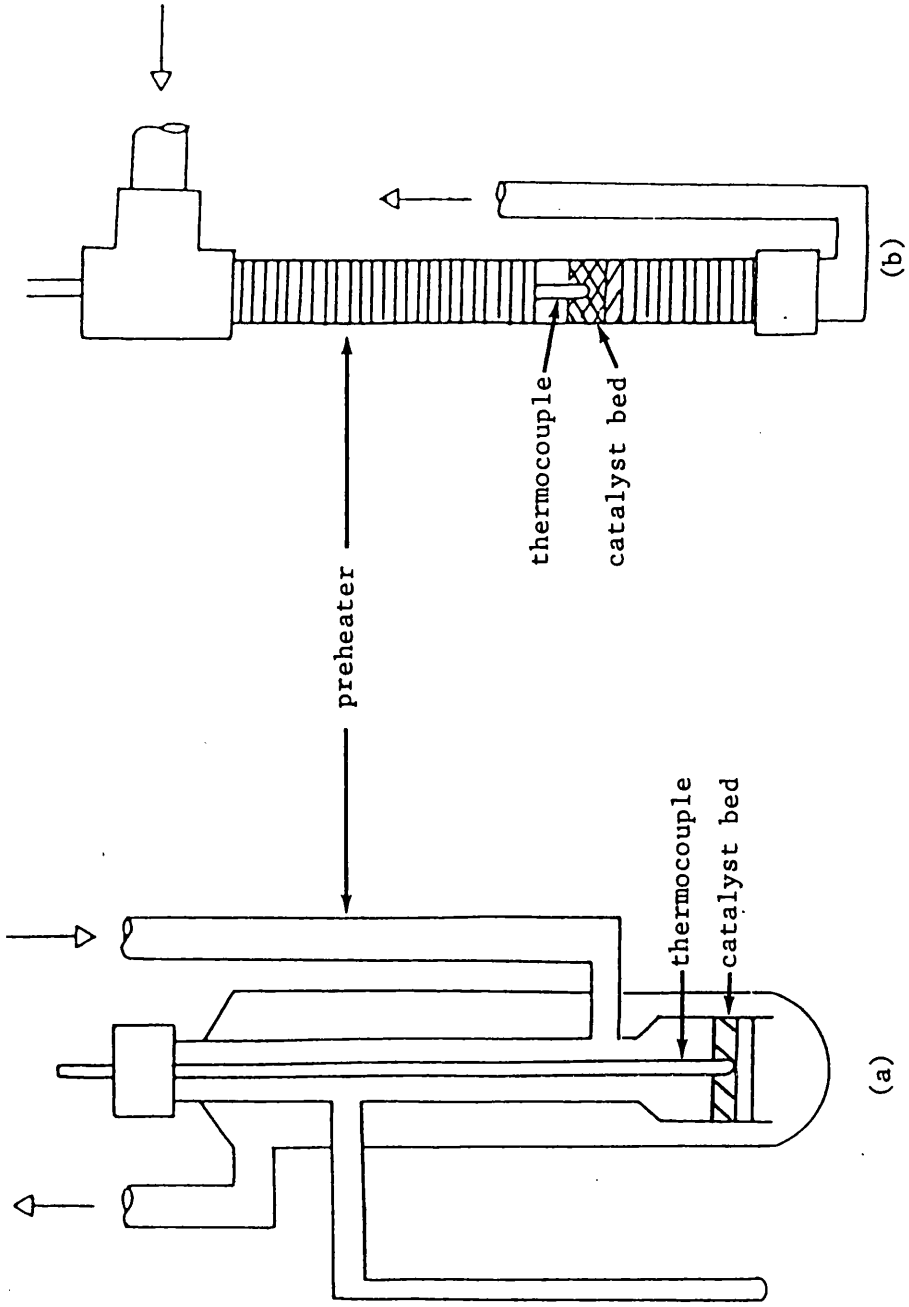

Figure 2.2 Diagram of different types of reactur used: (a) catalytic actitivy studies;
(b) reaction kinetic studies

c) Catalysts - For the catalytic activity tests the reactor loading was based on the percentage of lithium on the catalyst. The charge for the sample with 0.0% lithium was 0.5000 g. For the rest of the lithium series, the amount of sample was taken in such a way that the weight of $CoO-MoO_3/\gamma Al_2O_3$ in each case remained constant (0.5000 g), while the percentage of lithium on the catalyst gradually increased from 0.1 to 2 wt %. The amount of catalyst taken in each case was determined according to the following relation:

$$W = Wo \left(\frac{100}{100 - C}\right) \qquad (2.1)$$

where Wo = amount of catalyst with 0% Li (0.5000 g) and C = lithium composition (wt - %).

(ii) Temperature control and measurement

The heating and control of the temperature in the system was achieved by the following means:

a) Reactor and vaporiser furnaces - The reactor furnace was built using a ceramic tube (9" long and 1½" inside diameter) wound with a low resistancd wire and heavily insulated by means of glass wool. The furnace temperature (up to 500° C) was controlled by a P.I.D. temperature controller (Eurotherm, model 020-091-03). It was possible to maintain the temperature within ± 1° C of the required temperature. The vaporising chamber was housed in a furnace built in the same way as the reactor furnace, but its temperature was controlled by a P.D. temperature controller (Pye, model mini) which maintained the temperature to within ± 4° C.

b) Preheating section - The preheater tube was wound with an insulated heating cord ($\frac{1}{4}$" diameter). The heating leads were connected to a Zenith variable voltage transformer (model V3HM) which, in turn, was supplied with 240 volts line voltage.

c) Sampling line and exhaust line - These lines were wound with a well insulated heating tape ($\frac{1}{2}$" cross section). The power supply for the heating tape was controlled by a second Zenith variable voltage transformer (model V3HM). Temperature measurements were recorded at three places in the reaction system. The first thermocouple was located in the preheating section, the second in the catalytic bed (placed axially within the reactor) and the third was located in the sampling loop. The leads from all three thermocouples were connected to a rotary switch which, in turn, was connected to a digital temperature indicator (Eurotherm, model 140-03). All the thermocouples were Chromel-Alumel, protected with a 321 stainless steeel sheath. The temperature in the three sections of equipment could be adjusted independently. For all the runs temperature in the preheater was adjusted to that of the reaction temperature.

(iii)Gas flow system

a) Hydrogen feed system - High purity hydrogen (Air Products Ltd., 99.99%) was fed from a cylinder equipped with a two-stage pressure regulator (B.O.C. M150) into an oxygen-trap containing 50 g of a proprietary catalyst capable of converting traces of oxygen into water. The gas was then passed through 18" long by $\frac{3}{4}$" diameter copper tubing packed with 13 X molecular sieve to adsorb water from the hydrogen

stream. The sieve was activated periodically by heating at 400° C for about 12 h. The flow rate of hydrogen was adjusted by a calibrated rotameter (G.E.C. Marconi, series 1100) which contained a built-in micrometer valve. Final adjustment of the flow rate was achieved by using a bubble-flow-meter at the exit of the system. The hydrogen, after leaving the rotameter, entered the reactor system either at the inlet of the saturator (containing thiophene) or at the thiophene injection port in the vaporiser. Nylon and copper tubing, together with brass fittings, were used for the hydrogen line.

b) Hydrogen sulphide feed system - Hydrogen sulphide of 99.6% purity (supplied by B,D.H.) was fed from a cylinder equipped with a single stage pressure regulator (Brook, model 8601). The gas flow was controlled by a calibrated rotameter (G.E.C. Marconi, series 1100) with a built-in micrometer valve. An on-off valve was fitted downstream from the rotameter to isolate the main stream when there was no flow of hydrogen sulphide. For the hydrogen feed system, the final adjustment of the hydrogen sulphide flow was made by using a bubble-flow-meter at the exit of the gas system. All materials used in the hydrogen sulphide line were made of 316 stainless steel.

(iv) Thiophene delivery system

a) With saturator in line - For the measurement of the activity of the lithium series catalyst, a saturator was used for feeding thiophene vapour into the reactor. The saturator was a 500 ml glass bottle fitted with a sparger consisting of a sintered glass filter mainly to give a

good distribution of the incoming hydrogen gas. At the top of the saturator a by-pass made of glass tubing with a three way P.T.F.E. valve was fitted, so that the hydrogen flow rate could be adjusted before the gas entered the saturator.

The saturator was immersed in a water bath maintained at a constant temperature (300 ± 0.5 K) to achieve a constant feed of thiophene vapour (F_t = 6.3 ml/min at t = 22° C and 1 atm) in the hydrogen steam. Care was taken to maintain the bath temperature constant because the saturation of hydrogen stream depends on thiophene vapour pressure which, in turn, is highly dependent on temperature. The temperature in the bath was controlled by a Fi monitor keeping the temperature within ± 0.5° C. The saturator was connected to the reactor system using stainless steel straight unions ($\frac{1}{4}$" to $\frac{1}{4}$").

b) With syringe pump in line - Thiophene was fed into a vaporising chamber by a syringe pump (Schuco, model B) which consists of a synchronous motor that drives a screw with an attached metal plate. The plate is butted against the plunger of a hypodermic syringe containing thiophene and the motion of the travelling screw pushes the plunger into the barrel of the syringe. The delivery flow rate depended on the following: (1) dimension of the syringe used, (2) the path of the screw, and (3) the frequencies of the synchronous motor used. All these are related by a formula given by the supplier:

$$F = \frac{R \times V \times 2.54}{20 \times L} \qquad (2.2)$$

F = Flow rate in cm^3 per min,

R = Motor speed in revs per min,

V = Total volume of the syringe in cm^3, and

L = Distance between indicated total volume marks on syringe in cm.

The constants 20 and 2.54 are involved because the precision screw thread used to drive the syringe piston has 20 turns per 2.54 cm.

The pump was calibrated by filling the syringe with water. The liquid thiophene flow rate varied from 0.8 to 4.58 ml/h. The discharge line was 5" long by 1/16" diameter stainless steel needle which was connected to the injection port of the vaporising chamber where thiophene vapour was mixed with hydrogen. Thiophene (99 + %, Aldrich gold label) was used as supplied.

(v) Analytical section

a) Analysis of the products - The analytical section consisted of a gas chromatograph (Pye Unicam, series 204) provided with a thermal conductivity detector and a chart recorder (Bryans, model 27000) using a chart speed of 1 cm/min. The areas under the peaks were measured using an integrator unit (Venture, Mark II). The peak area was proportional to the concentration of each component present in the sample analysed. Figure 2.3 shows a diagram of the analytical section.

For the catalytic activity measurement a double column analysis system was used due to the difference in the boiling points of the

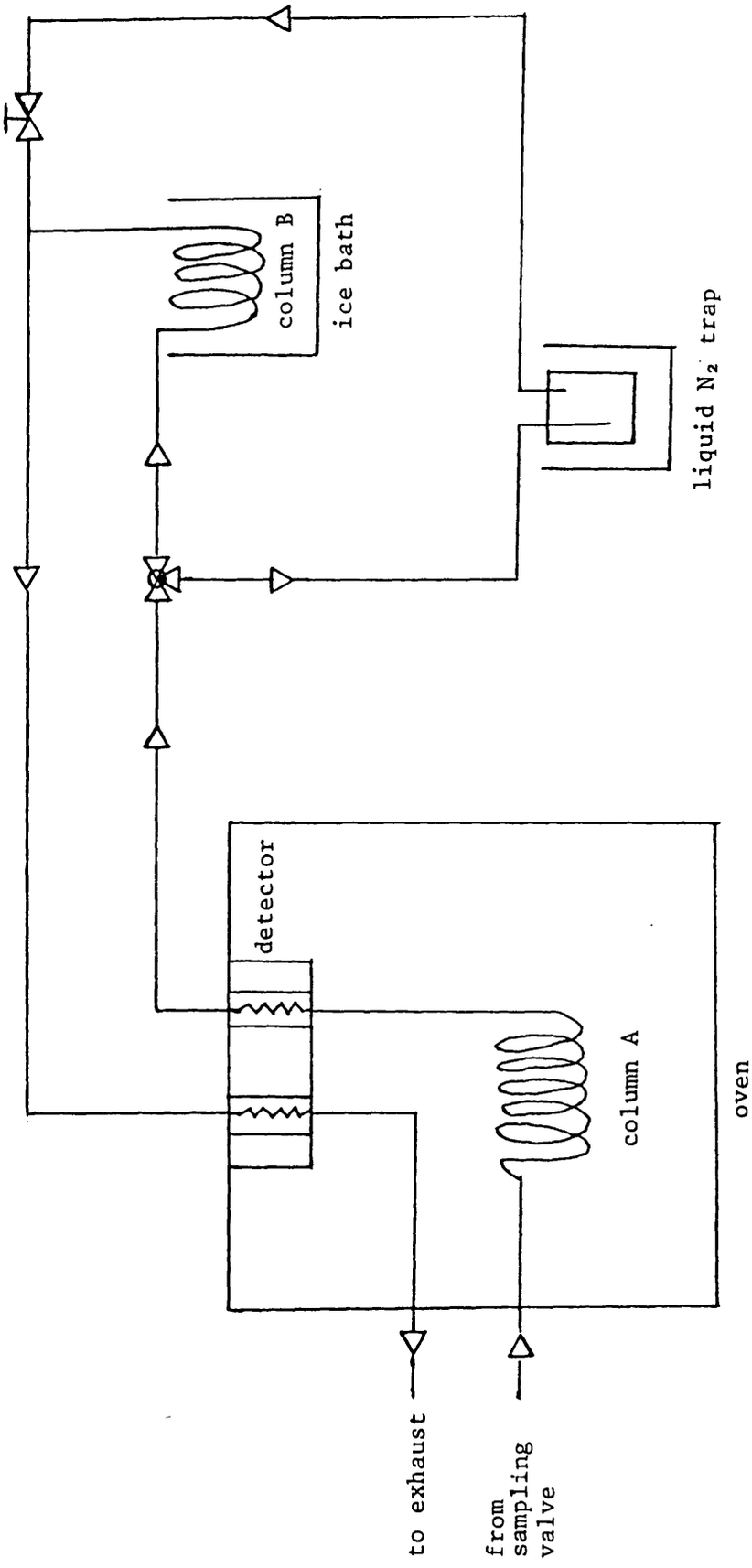

Figure 2.3 Diagram of the analytical apparatus

products. The first column was a glass one, 7' long, ¼" overall diameter, 4 mm id, packed with 25% squalane on diatomite S-ANW, 80-100 mesh. This was used to separate the mixture of light hydrocarbons and thiophene. The second column was stainless steel, 20' long, ¼" overall diameter, packed with a 20% mixture of 2:1 dimethyl sulphonate to hexamethyl phosphoramide supported on chromosorb p, 30-60 mesh. This was used to resolve the mixture of C_4 products.

The dual column analysis was operated as follows: The gas sample was collected by a sampling valve (Pye Unicam, 204) fitted with a 10 ml gas sampling loop. The sample was injected into column 'A' (fitted inside the oven which was maintained at 85° C) where the thiophene was resolved from the mixture of C_4-hydrocarbons. The output of column 'A' was then passed through one cell of the detector (thermal conductivity) while the other cell acted as a reference. By operating a three-way valve the mixture of C_4-hydrocarbons, already separated from thiophene in column 'A' and leaving the first cell of the detector, was injected into column 'B'. As soon as the peak characteristic of thiophene started to appear on the chart recorder (by operating the same three-way valve) the thiophene (issuing from column 'A' and through the detector) was collected in a liquid nitrogen trap. The three-way valve was then returned again to its initial position and the polarity of the detector changed before each component of the C_4 mixture reached the second cell of the detector. This time the first cell of the detector was used as a reference cell.

A typical chromatogram is shown in Figure 2.4 and the gas chromatographic conditions used to record it are given below.

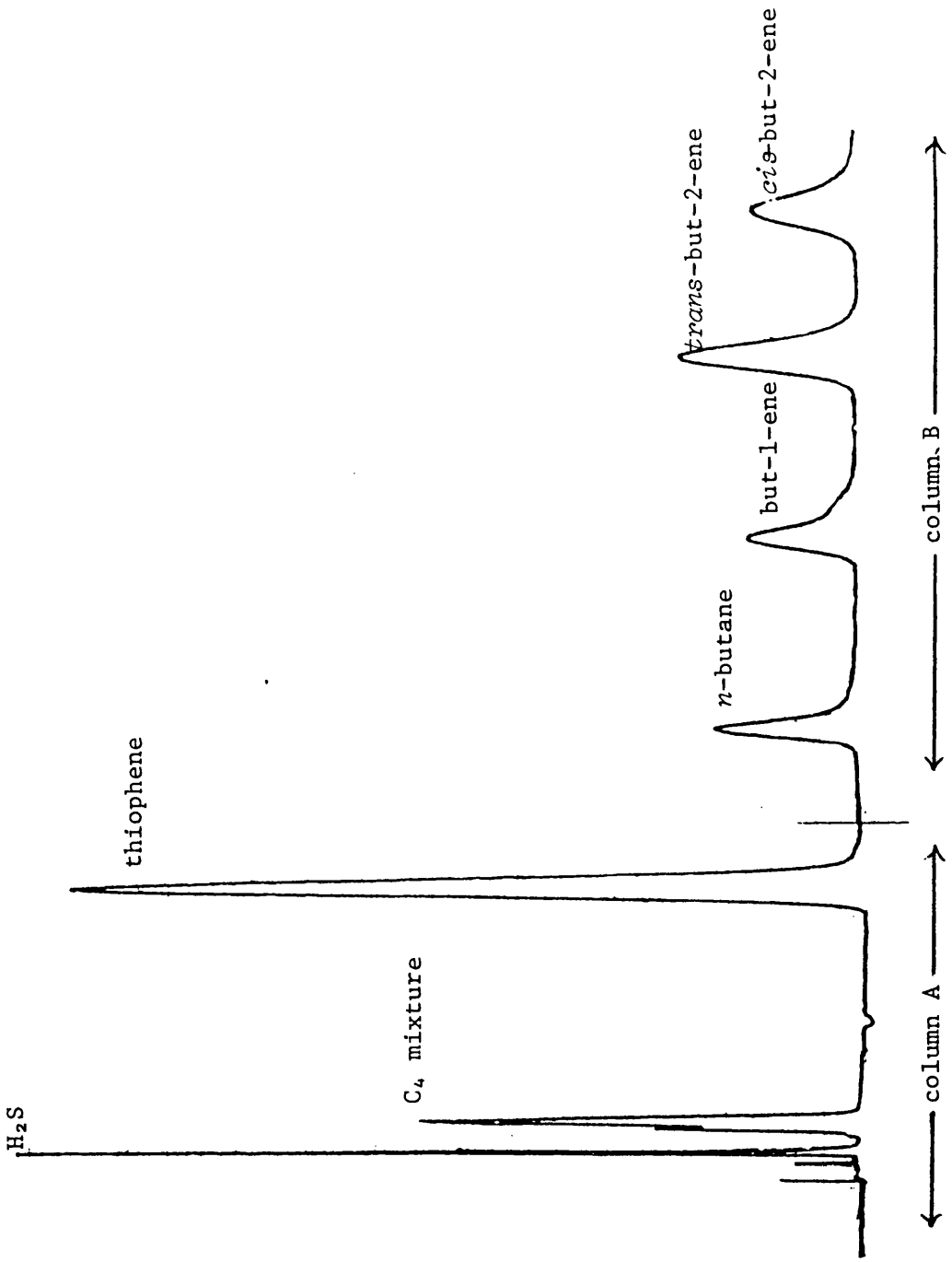

Figure 2.4 Typical chromatogram showing the separation of the different products

Volume of sample	10 ml
Temperature of detector	175° C
Temperature of injector	100° C
Oven temperature for column 'A'	85° C
Bath temperature for column 'B'	0° C
Current intensity setting	No.2
Attenuation	16, range 1, for thiophene 4, range 1, for C_4 mixture
Chart speed	1 cm/min
Carrier hydrogen flow rate	60 ml/min

b) Calibration of the gas chromatograph - According to Kaiser[65] the following conditions are required for the quantitative evaluation of gas chromatographic results:

(i) The detector must have a linear response.

(ii) The operating conditions of the gas chromatograph during calibration and analysis must be kept completely constant. The ratio of area to number of moles should be equal to a constant. The calibration graphs for the chromatograph used in the present investigation, shown in Figure 2.5, indicates a linear response of the detector for thiophene and hydrogen sulphide.

As the straight lines in Figure 2.5 do not overlap, it suggests that an equal concentration of different substances in the carrier gas does not generate an equal response of the detector. As a result of this, it appears that a parameter called the response factor, f, (constant for a particular compound) is needed for quantitative estimation for

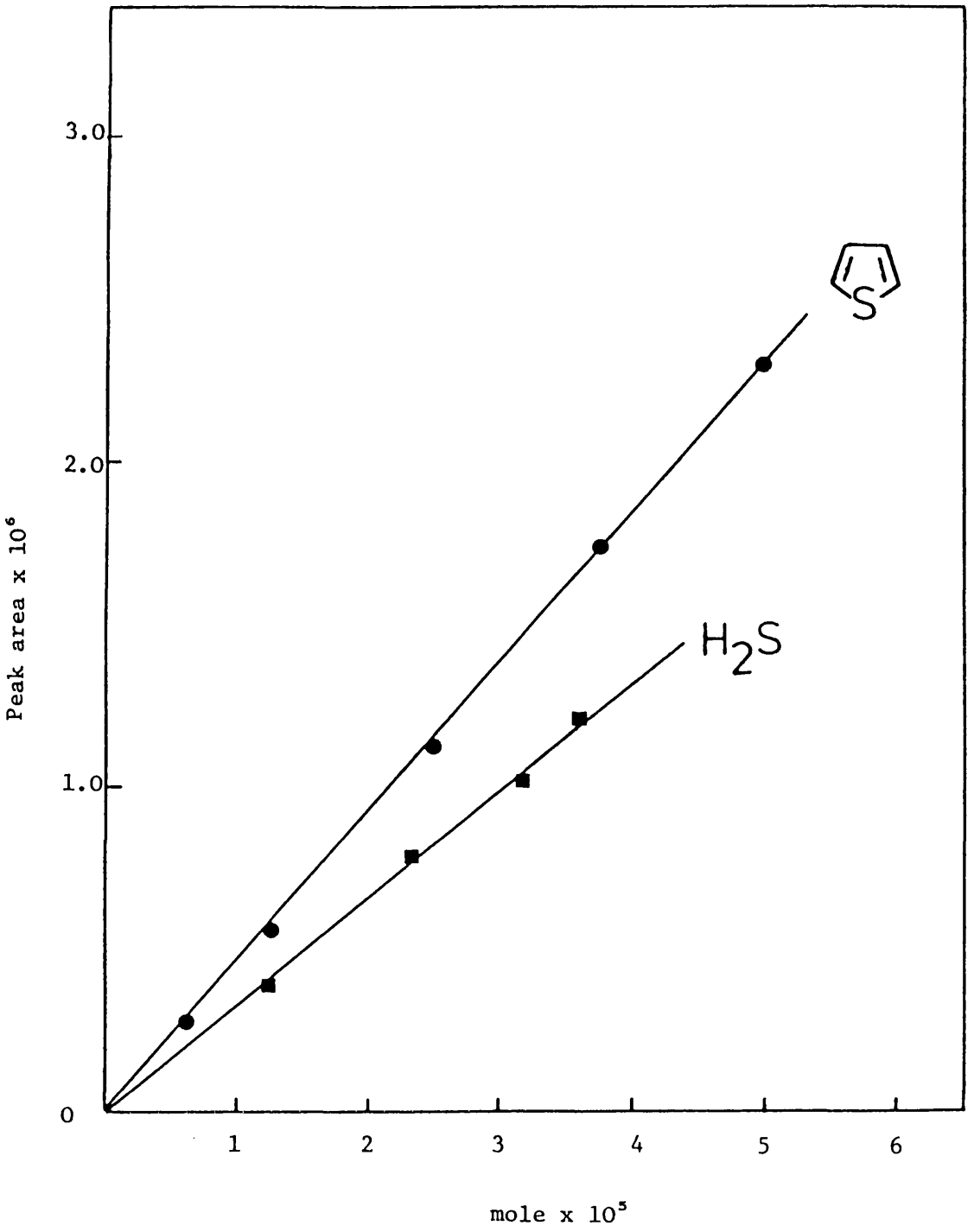

Figure 2.5 Calibration curves for thiophene and hydrogen sulphide

the concentration of components in a mixture.

The response factor is determined from the inverse of the slope of the plot of peak area against number of moles (see Figure 2.5). By using the response factor and the peak areas of the various components in a mixture, quantitative estimations of any component can be found from the following relation:

$$\% \text{ Subs}_i = \frac{f_i A_i \times 100}{f_1 A_1 + f_2 A_2 + \ldots + f_n A_n} \qquad (2.3)$$

where i = 1, 2, 3 .... n and f_i is the response factor of component i.

For the analysis, the relative response factor was used for all the components by taking the thiophene response factor as reference. The relative response factors of the compounds of interest are given below:

Substance	Relative response factors (F)
Thiophene	1.00
Hydrogen sulphide	1.33
Mixture of C_4 hydrocarbons	1.19

The relative response factor for a mixture of C_4 hydrocarbons was obtained indirectly from the ratio of areas of hydrocarbon sulphide to the areas of total C_4 hydrocarbons produced during the hds reaction.

(4) Operational procedure

(i) Start-up

A precise amount of catalyst was weighed in a high precision analytical balance and placed into the reactor. The next step was to leak-test the system. These tests were carried out in the catalytic system, and in the helium and hydrogen lines by bringing the circuit

up to 15 psi above atmospheric pressure using helium. Then all valves were closed at the line exit. If within 1 h no decrease in pressure was observed, it was assumed that there were no appreciable leaks.

For the measurement of hds activity of the catalyst, the saturator was charged with 300 ml of thiophene and left in the water bath at T = 300 K for about 12 h before the experiment was commenced.

(ii) Pretreatment of catalyst

Once the reactor has been loaded with catalyst and the system leak-tested, helium was allowed to flow through the reactor at the rate of 100ml/min and the temperature raised to 150° C. After 90 min the reactor temperature was increased gradually to 400° C. The helium flow was cut off and a mixture of 10% hydrogen sulphide in hydrogen (100ml/min) was allowed to flow through the reactor for 14 h. This pretreatment procedure was the same for catalytic measurement and for reaction kinetic experiments.

(iii) Steady state

After pretreatment of the hydrogen sulphide catalyst, the gas flow was stopped, allowing only hydrogen to pass through the reactor for 1 h. The reactor was set to the desired reaction temperature (400° C for activity tests and 260-320° C for reaction kinetic studies). Once the reaction temperature was attained, hydrogen was adjusted to the desired flow rate and thiophene was allowed to flow through the system. Sampling for the gas chromatographic analysis was then commenced and continued periodically until no change was evident in the variation of each chromatographic peak, *i.e.*, steady state was reached. Two or three more samples were taken as representative of the steady state and used for calculation of the data presented in the thesis.

2.2 Physical Characterisation

(1) Introduction

A great deal of interest has been shown by many different research groups in the characterisation of hydrodesulphurisation catalysts. Massoth[41] has recently reviewed some of the techniques applied to molybdena catalysts.

Standard characterisation techniques have been well developed for metallic catalysts and acidic-type catalysts. Such standard techniques have, however, not yet been well developed for characterising supported oxide or sulphide catalysts. Hence, sufficient information is lacking on how these characterisation studies may be related to the catalyst activity.

The characterisation technqiues generally applied to the hds catalysts can be divided into two broad categories:

(i) Non spectroscopic methods:

a) *X*-ray diffraction
b) Electron microscopy
c) Adsorption measurements
d) Magnetic measurements

(ii) Spectroscopic methods:

a) Diffuse reflectance
b) Electron spin resonance
c) Photoelectron (ESCA)

In this chapter the underlying principles of some of the characterisation techniques are presented, which have been applied to the series of hds catalysts prepared for the present investigation.

(2) Diffuse reflectance spectroscopy

(i) Principle

Several workers[19,46,66-68] have successfully used diffuse reflectance spectroscopy for the qualitative determination of cobalt and molybdenum on $CoO-MoO_3/\gamma-Al_2O_3$ hydrodesulphurisation catalysts in both oxide and sulphide forms

This technique involves measurement of the amount of radiant energy reflected from the surface of a sample. Data are generally reported as % reflectance:

$$R\% = \frac{I}{I_o} \times 100 \qquad (2.4)$$

where I = intensity of radiant energy reflected from the sample and I_o = intensity of radiant energy reflected from a standard reflecting surface.

Specular reflectance is simply a mirror - like reflection from a polished surface. Diffuse reflectance refers to a reflected radiant energy which has been partially absorbed and partially scattered by a surface having a poorly defined angle of reflection. The reflected light from such a surface depends on the particular nature of the medium under consideration. This is the main distinction from specular reflectance.

In diffuse reflectance techniques, the intensities of absorption at various wavelength in a reflectance spectrum is expressed as the Kubelka-Munk function, $f(R_\infty)$, calculated from the % reflectance at the respective wavelength.

$$f(R_\infty) = \frac{(1 - R_\infty)^2}{2R_\infty} \qquad (2.5)$$

where R_∞ is the reflectance at the wavelength of absorption. The theory related to the development of this equation is given in detail elsewhere.[69]

The relation between $f(R_\infty)$ and the concentration, c, of the absorbing species is given by

$$\log f(R_\infty) = \log c + \log \varepsilon/s \qquad (2.6)$$

where ε is the extinction coefficient and s is the scattering coefficient.

(ii) Experimental

U.v.-visible diffuse reflectance spectra of the series of lithium-containin- catalysts were recorded by using magnesium oxide as a reference (100% reflectance).

The spectrometer used was a Pye Unicam SP 700C fitted with the standard commercial Pye Unicam reflectance attachment. The spectrometer was capable of scanning from 180 nm to 2500 nm using a deuterium lamp below 333 nm and a tungsten lamp between 333-2500 nm. A photomultiplier tube was used to detect the reflected radiation below 666 nm and a lead sulphide detector above 666 nm. The spectrometer scan was linear with respect to energy and time. All the samples were ground into a very fine powder. The sample holder was a circular stainless steel disc (diameter 37 mm, depth 5 mm) fitted with glass windows. It had two compartments: one was used to contain the sample of catalyst while the other was used to contain the reference. The spectra were recorded by scanning the energy range from 250-1100 nm.

(3) *X*-ray diffraction

(i) Principle

A beam of *X*-rays striking a crystal becomes diffracted by the planes of the crystal in the same way as a grating diffracts ordinary light.

The relationship between the wavelength λ, the angle of diffraction θ, and the distance between the planes in the crystal d, is given by the Bragg equation:

$$n\lambda = 2\,d\sin\theta \qquad (2.7)$$

where n is the order of diffraction. If the *X*-ray beam is monochromatic,

there will be only a limited number of angles, θ, of diffraction depending upon the wavelength of the *X*-ray and the interplanar spacing. If, instead of a single crystal, a polycrystalline powder sample (in which the particles are randomly oriented, but some are so placed as to satisfy Bragg's law) is placed in the *X*-ray beam, a continuous cone of diffracted rays will be produced. The diffracted *X*-ray patterns can be recorded in several ways as follows:

a) Using simple powder cameras
b) Using focusing cameras
c) Using powder diffractometers

In order to record the diffracted *X*-ray pattern of the samples the third method was used. Figure 2.6 shows the basic arrangement for a powder diffractometer. The sample holder plate rotates about an axis at O, and the counter travels on a circle centred at O; the two motions are coupled so that the incoming beam and the radiation to the receiving slit are both inclined to the specimen at the same angle.

Since the incident beam is divergent and each diffracted *X*-ray makes an angle of 2θ with the appropriate ray of the incident beam, the diffracted beam is convergent. The arrangement in Figure 2.6, in which the source slit, receiving slit and sample holder all lie in a circle to which the specimen is tangential, has a semi-focusing effect. However, the specimen is so small compared with the distance between the source (or receiving) slit and the sample that the arrangement described provides a good approximation to true focusing.

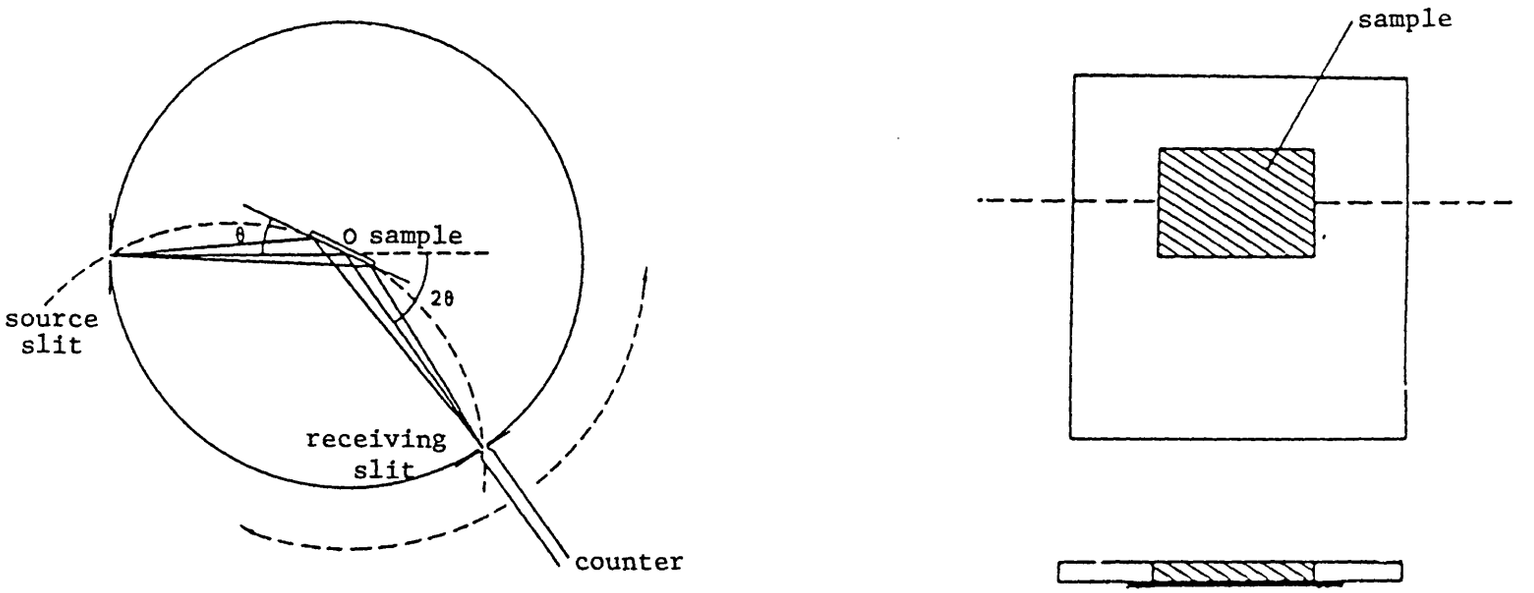

Figure 2.6 (a) general arrangement of powder diffractometer; (b) sample holder

(ii) Experimental

X-ray diffractograms of all the lithium-containing catalysts were recorded using a Phillips *X*-ray generator (PW 1730/10) equipped with nickel filter, copper Kα radiation, a diffractometer (Phillips, model 1050/25), a Xenon proportional counter (PW 1965) and a chart recorder. For sample preparation, each catalyst was ground to a very fine powder ($\gtrsim$ 300 mesh) and by using the back loading method[70] the sample was put into a sample holder of the following dimensions: 2 cm long, 1 cm wide and 1 mm depth. The sample was placed in the path of the *X*-ray. The scanning of the diffracted beam covered the range $10^\circ \lesssim 2\theta \lesssim 100^\circ$.

(4) B.E.T. surface area and pore volume distribution

(i) Principles

The molecules in the surface layer of a solid are bound on one side to inner molecules and there is an imbalance of atomic and molecular forces on the other side. The surface molecules attract gas or liquid molecules in order to satisfy these latter forces. The attraction may be either physical or chemical, depending on the system involved and the temperature employed. The nature of the forces acting in physical adsorption are of the same kind as van der Waals forces, chemical adsorption being more energetic than physisorption. As B.E.T. surface area measurement involves physisorption, but not chemisorption, the following paragraph will be devoted to the discussion of the salient features of the former only. The theories related to the measurement of either B,E.T. surface area or pore size distribution have been given in detail by many workers.[71-73]

a) B.E.T. surface area - Physical adsorption (physisorption) is frequently used to measure the total surface area of a porous solid. Several equations to describe physical adsorption have been derived by Langmuir, but the equation ascribed to Brunauer, Emmett and Teller is the one most widely used. The langmuir isotherm is derived by assuming a dynamic equilibrium between adsorbed molecules and molecules in the gas phase, assuming an energetically uniform surface and that each site only accommodates one molecule up to the extent of one monolayer.

With these assumptions the equation may be written as:

$$\frac{V}{V_m} = \frac{b_p}{1 + b_p} \text{ or } \frac{p}{V} = \frac{1}{bV_m} + \frac{p}{V_m} \qquad (2.8)$$

where V = volume adsorbed at the pressure p, V_m = volume of the monolayer and b = constant related to the heat of adsorption.

Often it has been found that very few systems obey the Langmuir equation. The deviation of the experimental results from this equation has been attributed to a non-uniformity of the surface, both physical and energetic.

The Brunauer, Emmett and Teller (B.E.T.) method extends the postulates of the Lantmuir isotherm to apply to multilayer adsorption and assumes that the heat of adsorption beyond the first layer is equal to the heat condensation.

Now equation (2.8) (the B.E.T. equation) can be adapted for multi-layer adsorption by rearranging it to:

$$\frac{p}{V(p_s-p)} = \frac{1}{V_m c} + \frac{(c-1)}{V_m c}\frac{p}{p_s} \qquad (2.9)$$

where V = volume adsorbed at pressure p, V_m = monolayer volume, p_s = saturation pressure and c = constant for a particular temperature, related to the heat of adsorption.

Equation (2.9) is a linear function of p/p_s. In practice, the range of linearity of relative pressure (p/p_s) is from 0.05-0.3 and this equation can be applied to the determination of surface area by plotting

$$\frac{p}{V(p_s-p)} \textit{ versus } \frac{p}{p_s}$$

Calculation of the slope (m) and the intercept (i) allows the determination of V_m according to the following equation:

$$V_m = \frac{1}{m+i} \qquad (2.10)$$

Converting V_m to the number of molecules adsorbed and from the known area covered by a single adsorbed molecule (in this case N_2), the total area per unit mass s, can be evaluated by:

$$s = \frac{V_m \times N_o}{22400}\,\alpha \qquad (2.11)$$

where N_o is Avogadro's number (6.623×10^{23}), α = area covered by a single adsorbed molecule (for N_2 adsorption, $\alpha = 16.2$ Å^2, see reference 74).

b) Pore size distribution - There are two established methods for measuring the distribution of the pore volume: 1) mercury penetration; this method depends on the fact that mercury has a significant surface tension and does not wet most catalytic surfaces. Mercury can therefore be forced into pores of narrow diameter and the relationship between applied pressure and the pore radii in the system enables the size distribution to be computed and 2) nitrogen adsorption-desorption; in this method adsorption of N_2 is continued until the nitrogen pressure approaches the saturation value ($p/p_s = 1$). At this stage all the void volume is filled with adsorbed and condensed nitrogen. Then a desorption isotherm is traced by lowering the pressure step-wise and measuring the amount of N_2 desorbed.

In this research project, nitrogen adsorption-desorption was employed to investigate pore size distribution of the catalysts. The basic principles of the method are given below.

If a cylindrical pore in a solid of a radius r_c is not filled with condensate, but has its wall blanketed with a condensed layer of thickness t, the radius of the free space r is $(r_c - t)$. The opening radius is related to the relative pressure of the condensed liquid forming its boundary by the well-known Kelvin equation:

$$r = r_c - t = - \frac{2\sigma \ V \cos\theta}{RT \ \ln \ (p/p_s)} \qquad (2.12)$$

where σ = surface tension (8.85×10^{-3} N m^{-1} for N_2), V = molar volume of the condensed liquid (34.6×10^{-6} m^3/mole for N_2), and θ = contact angle between surface and condensate (assumed to be 0).

The thickness t depends on the nitrogen relative pressure. The exact relation has been the subject of considerable study, but the relation proposed by Halsey (given below) is generally used.

$$t = A(\ln \frac{P_s}{P})^{-1/3} \qquad (2.13)$$

where A is related to the average thickness of a single layer of adsorbed molecules.

Using the value of A = 6.05, as suggested by earlier workers,[74,75] the equation (2.13) can be written as:

$$t = 6.05\ (\ln \frac{P_s}{P})^{-1/3} \qquad (2.14)$$

where t is expressed in Å.

The method used in these calculations of pore size distribution is a modification of Pierce's method[76] by Orr and Dellavalle.[72] A brief description of the steps involved is given below. The data required are obtained from the experimental desorption isotherm. During desorption each amount of gas desorbed (ΔV) is composed of the gas evaporated from the inner capillaries ΔV_r and the gas evaporated from the film on the walls of the unfilled pores (ΔV_f). So,

$$\Delta V_r = \Delta V - \Delta V_f \qquad (2.15)$$

ΔV is determined directly from the isotherm while ΔV_f can be evaluated by taking into account the areas of the wall covered by film ($\Sigma \Delta s_p$) and the diminution in the thickness of the film (Δt).

$$\Delta V_f = \Delta t \, \Sigma \Delta s_p \tag{2.16}$$

where $\Sigma \Delta s_p$ represents all the pore surface area except that of filled pores. At each desorption increment the volume of the pores is calculated by:

$$\Delta V_p = \Delta V_r \left(\frac{\bar{r}_c}{\bar{r}_c - t} \right)^2 \tag{2.17}$$

while the surface area attributable to any group of pores Δs_p is, by geometrical considerations, twice the pore volume of that group ΔV_p divided by the average pore radius of the group $\bar{r}_c$.

$$\Delta s_p = 2 \frac{\Delta V_p}{\bar{r}_c} \tag{2.18}$$

When the above steps are followed through the whole desorption branch, one can plot a cumulative pore volume distribution curve as shown in Figure 3.15 given in Chapter 3.

c) Adsorption-desorption isotherms characterisation - Most physisorption isotherms may be placed in one of the five types, frequently referred to as the Brunauer, Deming, Deming and Teller (B.D.D.T.) classification. Physisorption isotherms often exhibit hysteresis cycles (adsorption and desorption follow different paths). Various types of isotherms and hysteresis loops are shown in Figures 2.7 and 2.8 respectively. This classification will be used to characterise the isotherm used in the present study.

(ii) Experimental procedure for the measurement of surface area and pore size distribution

Determination of the B.E.T. surface area and pore size distribution of all the catalysts were carried out by physical adsorption of nitrogen

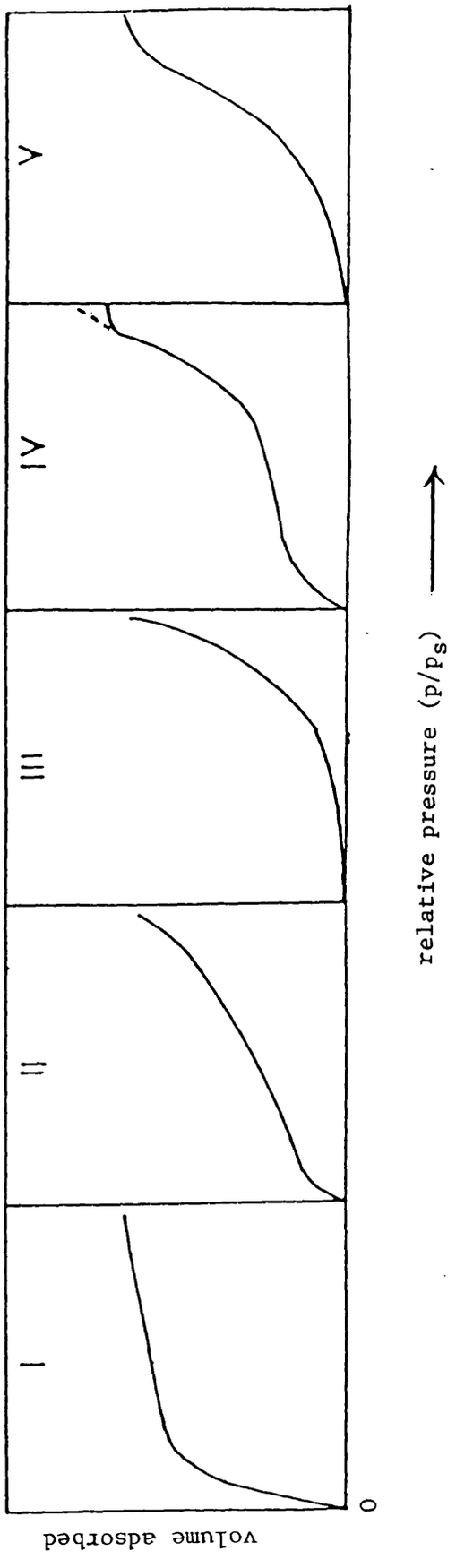

Figure 2.7 B.D.D.T. classification of adsorption isotherms

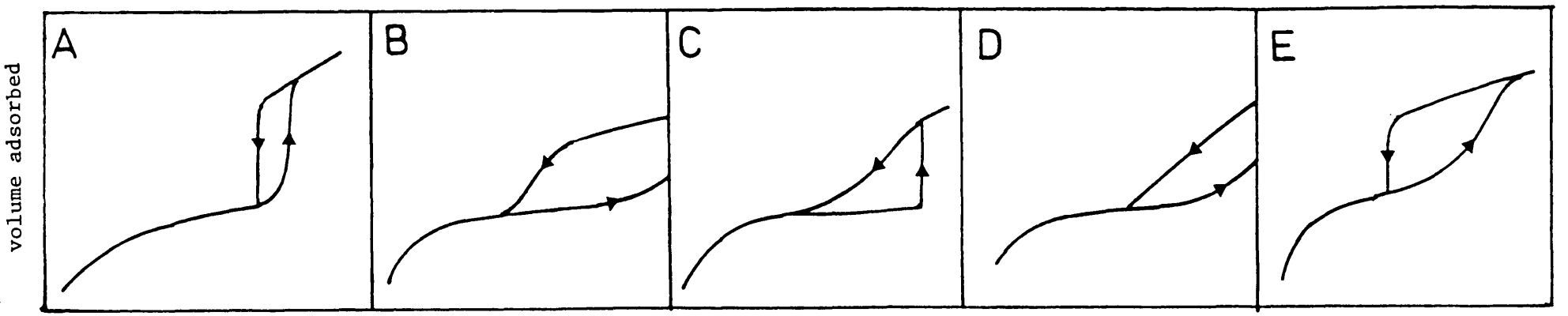

Figure 2.8 Classification of hysteresis loops of isotherms[73]

Type A: tubular-shaped capillaries, ink bottle-shaped capillaries (open and closed)

Type B: open slit-shaped capillaries with parallel walls, ink bottle pores (very wide body)

Type C: spheroidal pores, open and closed ink bottle pores (different sizes)

Type D: capillaries with large body radii and different sizes of short, narrow necks

Type E: spheroidal cavities with same entrance diameters

at liquid nitrogen temperature (77 K). An apparatus capable of recording surface area - pore volume data (micromeritic, model 2100 D, U.S.A.) was employed and basically consists of the following sections:

1) gas handling system (helium, nitrogen);
2) vacuum system (rotary pump backed by an oil diffusion pump);
3) pressure recording system (pressure transducer coupled with a digital pressure indicator);
4) sample handling system (sample container, heating mantles, and liquid nitrogen bath).

Analytical determinations were conducted by the following procedure. A known amount of sample (about 0.5 g) was introduced into a glass sample bottle which, in turn, was attached to one of the ports of the instrument. The sample bottles were evacuated ($< 10^{-3}$ mmHg) and heating mantles were placed around each of them. The samples were then degassed at 200° C for about 16 h, under high vacuum ($< 10^{-5}$ mmHg). Once the samples were completely degassed, the heating mantles were removed and the sample bottles were placed in liquid nitrogen baths. The dead space measurement was carried out using helium. For surface area measurement nitrogen gas was introduced into the manifold of known volume (27.71 ml) to attain a pressure of about 250 mmHg. The exact pressure was recorded as p_1. Then the valve connecting the manifold with the sample bottle was opened. Sufficient time was given to achieve equilibrium pressure which was noted at p_2. The sample bottle was then isolated by closing the valve.

The above procedure was repeated by gradually increasing the initial pressure p_1. Each time the equilibrium pressure p_2 was noted. This was continued until p_2 reached saturation pressure and thus a full adsorption isotherm was obtained. To obtain the desorption isotherm, the desorption of nitrogen was followed by gradually decreasing the initial pressure p_1 and recording the equilibrium pressure p_2. The desorption isotherm recorded in this way was used to determine the pore size distribution.

(5) Electron spin resonance (e.s.r.) or electron paramagnetic resonance (e.p.r.)

(i) Principle

Electron resonance is a branch of absorption spectroscopy in which a radiation of microwave frequency is absorbed by molecules possessing unpaired electrons. The phenomenon has been designated by the names e.p.r. or e.s.r.

The theory of e.s.r. spectroscopy is given in some detail in reference 77. However, the basic principles can be summarised as follows. For an electron of spin $s = \frac{1}{2}$, the spin angular momentum quantum number can have values of $m_s = \pm \frac{1}{2}$, which, in the absence of a magnetic field leads to a doubly degenerate spin energy state. When a magnetic field is applied this degeneracy is resolved. The lower energy state has the spin magnetic moment aligned with the field corresponding to a quantum number $m_s = -\frac{1}{2}$, while the high energy state $m_s = +\frac{1}{2}$ has its moment opposed to the field. A transition between the two different electron spin energy states occurs upon absorption of a quantum of radiation (in the radio frequency or microwave region). The

energy (E) of the transition is

$$E = h\nu = g\beta Ho \qquad (2.19)$$

where h = Planck's constant, ν = frequency of radiation, β = Bohr magneton, Ho = the field strenth, and g = the spectroscopic splitting factor.

The quantity g is a tensor quantity. The actual value of g for a free electron is 2.0023. In general, the magnitude of g depends upon the orientation of the molecules containing the unpaired electron with respect to the magnetic field.

E.s.r. spectra can be obtained by varying either the frequency or the field strength. In practice it is simpler to vary the latter. The spectrum is presented by plotting the intensity of adsorption against the strength of the field. However, e.s.r. spectra are usually presented as first derivative curves. A typical spectrum is shown in Figure 3.16. There are a number of factors other than those which are ascribed to instrument design which affect line width. Broadening of the line width due to spin-lattice relaxation results from the interaction of paramagnetic ions with thermal vibration of the lattice. For some compounds the spin-lattice relaxation time is sufficiently long to allow the observation of the spectra at room temperature, while for others the spin-lattice relaxation time is so short that no spectra at room temperature is observed. Since relaxation time increases as temperature decreases, many transition metals need to be cooled to liquid N_2, H_2 or He temperatures before good spectra are observed.

(ii) Experimental

The e.s.r. spectra of a series of lithium-containing catalysts were recorded. Prior to recording of the spectra, the samples were treated in two different ways:

a) reduction in a hydrogen stream at 400° C, and
b) reduction and sulphidation with a mixture of hydrogen sulphide (10% volume) in hydrogen at 400° C.

The experimental procedure used for pretreatment of the catalyst was substantially similar for both the reduction and the reduction plus sulphidation pretreatment.

The reactor was loaded with a known amount of catalyst [0.5000 g for sample with 0.0% lithium and the weight of the lithium-containing samples was determined following the relation given by equation (2.1)]. The reaction temperature was raised to 150° C while 100 ml/min of helium was flowing through the reactor. After 90 min the temperature was gradually raised to 400° C and then the helium supply was stopped and a flow of 100 ml/min of either pure hydrogen or a mixture of 10% volume of hydrogen sulphide in hydrogen was allowed through the reactor for 14 h. The hydrogen or the sulphiding mixture of $H_2S + H_2$ was stopped and the catalyst kept in a stream of helium until the reactor cooled down to room temperature. The helium flow was then stopped and the inlet and outlet of the reactor were closed in order to prevent air contacting the catalyst, which would affect the state of paramagnetic species. The reactor was dismounted and the sample transferred to the appendix attached to the reactor (see Figure 2.2). The appendix containing the sample was placed in the resonance cavity of an e.s.r.

spectrometer (Varian, model E3) for recording the spectra at 20° C. The *X*-band e.s.r. spectra of the samples was recorded at 9.5 GHz. The magnetic field was modulated by 100 kHz and the first derivative of the spectrum was recorded. α,α-diphenyl β-picrylhydrazyl (DPPH) was used for calibration of the magnetic field.

CHAPTER 3

RESULTS AND DISCUSSION OF CATALYTIC MEASUREMENT AND CHARACTERISATION STUDIES

3.1 Introduction

In the field of hds catalysis there is growing interest in attempts to understand the chemistry of the cobalt molybdate system. The literature survey (Chapter 1) suggests that the structure of the cobalt molybdate system has not yet been clearly understood. Without this information, preparation of catalysts with improved activity is limited. Knowledge about changes in structure and catalytic activity caused by modifying the catalyst might be helpful and provide a better understanding of the role of the catalyst in the hds reaction. A series of lithium containing cobalt molybdate catalysts was therefore prepared in order to investigate the effect of lithium as a second promoter and also to obtain some information about the relationship between structure and selectivity as well as activity.

In this chapter the results of catalytic activity measurements obtained by using a fixed bed flow microreactor, together with results obtained by using various physical characterisation techniques will be described. A general discussion based on these results will be presented at the end of this chapter.

3.2 Activity Measurement

(1) Identification of reaction products, measurement of conversion and product distribution at stead state of hds reaction

Reaction products were identified chromatographically by using various standard calibration bottles containing pure compounds. Thus it was established that hydrogen sulphide, *n*-butene (NB), but-1-ene (1B), *cis*-but-2-ene (CB) and *trans*-but-2-ene (TB) were the primary reaction

products. In addition, small amounts of lighter hydrocarbons (cracked products) were also formed. These latter products were neglected during the analysis of the results. Neither butadiene nor tetrahydrothiophene were found in the reaction products.

The lithium catalysts were reduced and sulphided prior to the measurement of the steady state catalytic activity (thiophene conversion into C_4 hydrocarbons) under the conditions described earlier in Chapter 2. The conversion of thiophene was followed as a function of time on stream for all the catalysts studied. In all cases a steady state of conversion was reached after about two hours of contact of thiophene feed with the catalyst. The steady state conversion and product distribution data are given in Appendix B-1. The activity of the lithium series of catalysts can be plotted either as a function of Li/Co, or Li/Mo atomic ratio, or simply as Li wt %. The results of the present investigation are expressed in terms of Li/Co atomic ratio. This arises from a comparison between the results of this present study and those of Kelly and Ternan,[61] both of which were presented as a function of several parameters, *e.g.*, Li/Co, Li/Mo, Li/(Co + Mo) atomic ratios (see Figure 3.1). It can be seen from the figure that when the catalytic activity is plotted only as a function of the Li/Co ratio, both sets of results produce a similar pattern.

Figures 3.2 - 3.5 show the plots of thiophene conversion and product distribution against the lithium to cobalt atomic ratio. It can be seen from Figure 3.2 that the catalytic activity for thiophene conversion passes through a maximum at about Li/Co = 2 and then the activity decreases with increase in Li/Co. The activity of the catalysts, with Li/Co > 5, drops below that of the catalyst not containing any lithium.

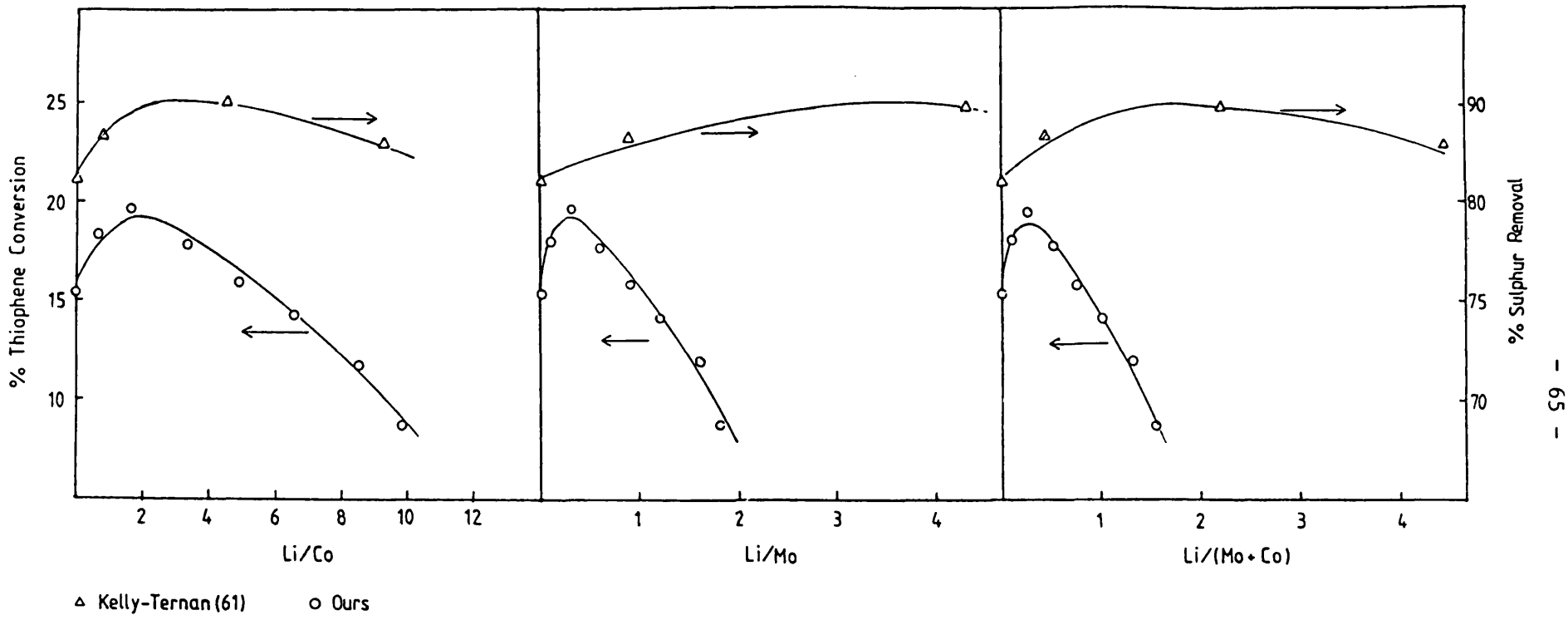

Figure 3.1 Comparison of the catalytic activity of hds of thiophene in the present investigation with the results of catalytic sulphur removal studies reported by Kelly and Ternan[61] as a function of Li/Co, Li/Mo and Li/(Co + Mo) atomic ratio.

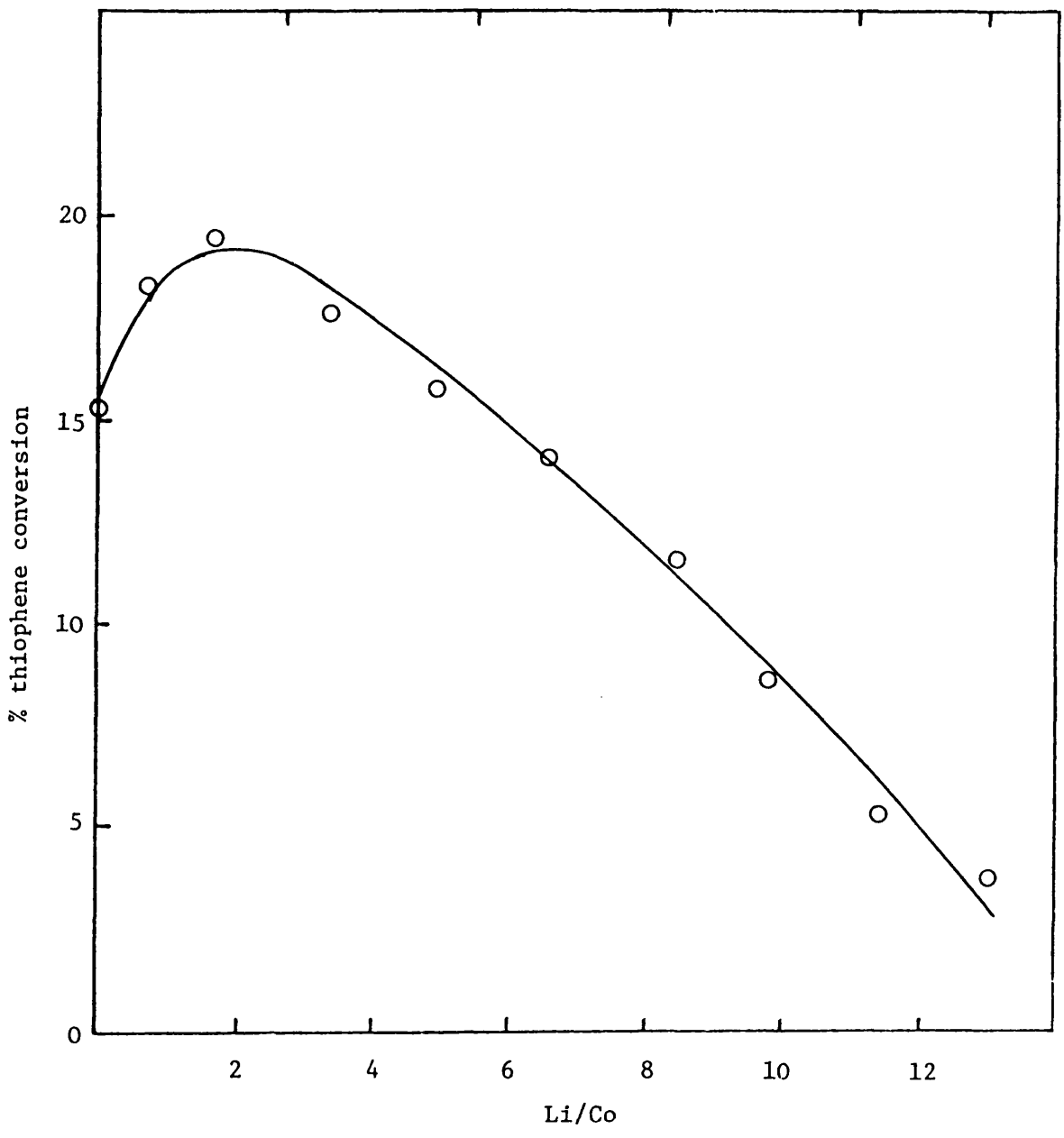

Figure 3.2 Variation of the thiophene conversion with Li/Co atomic ratio (t = 400° C and p = 1 atm).

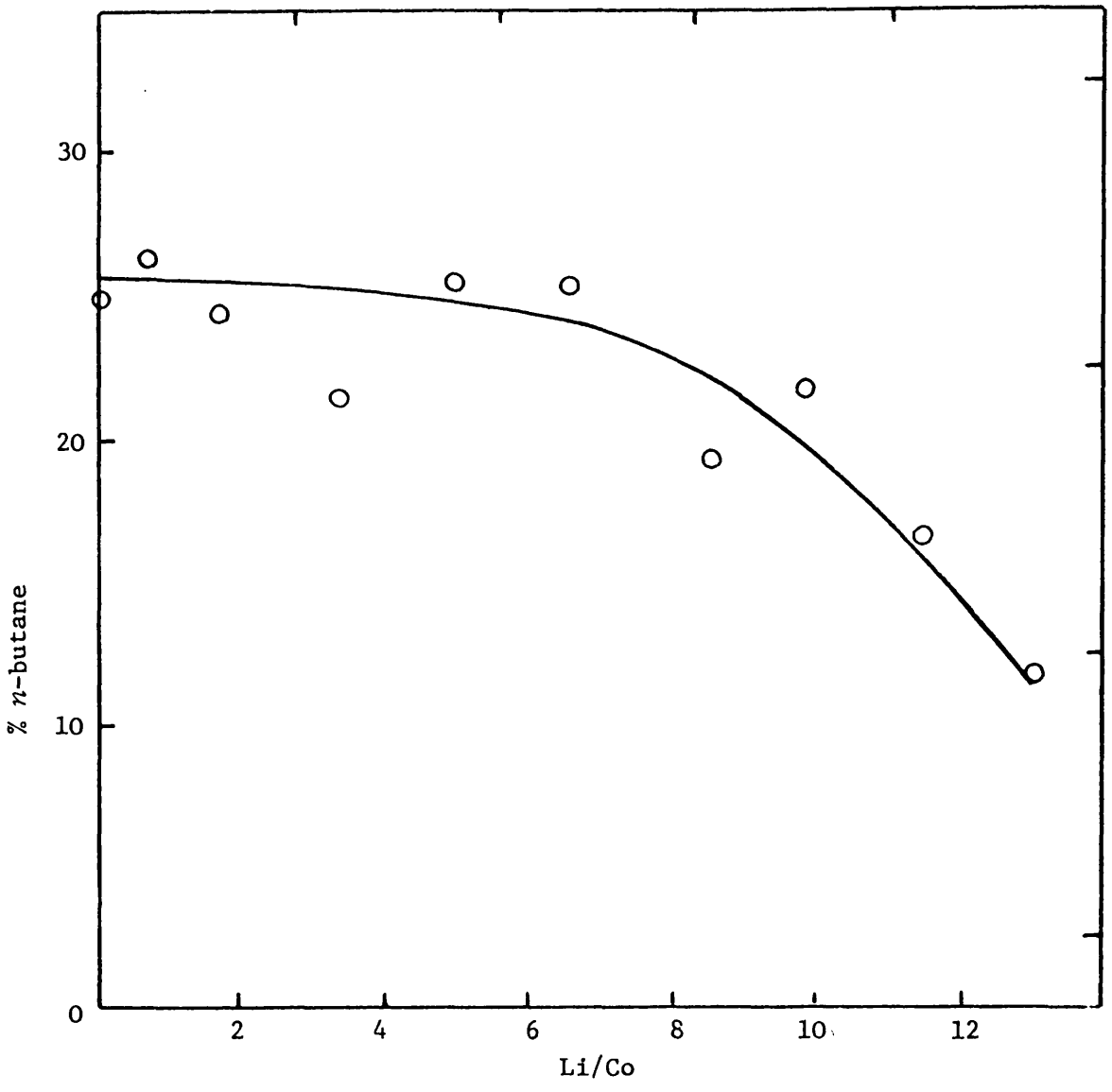

Figure 3.3 Plot of the percentage of *n*-butane in the C_4 products against Li/Co atomic ratio.

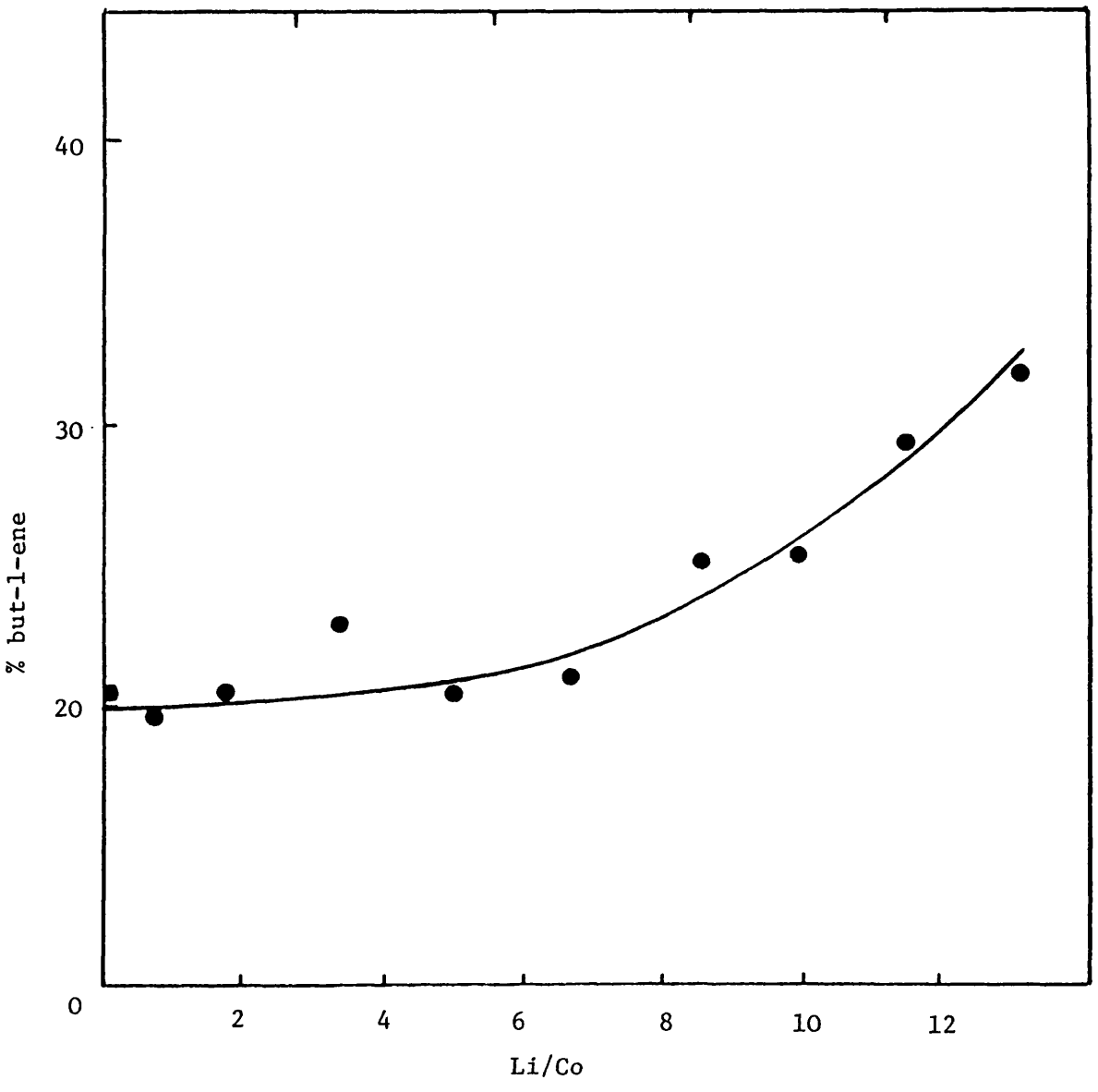

Figure 3.4 Plot of the percentage of but-1-ene in the C_4 products against Li/Co atomic ratio.

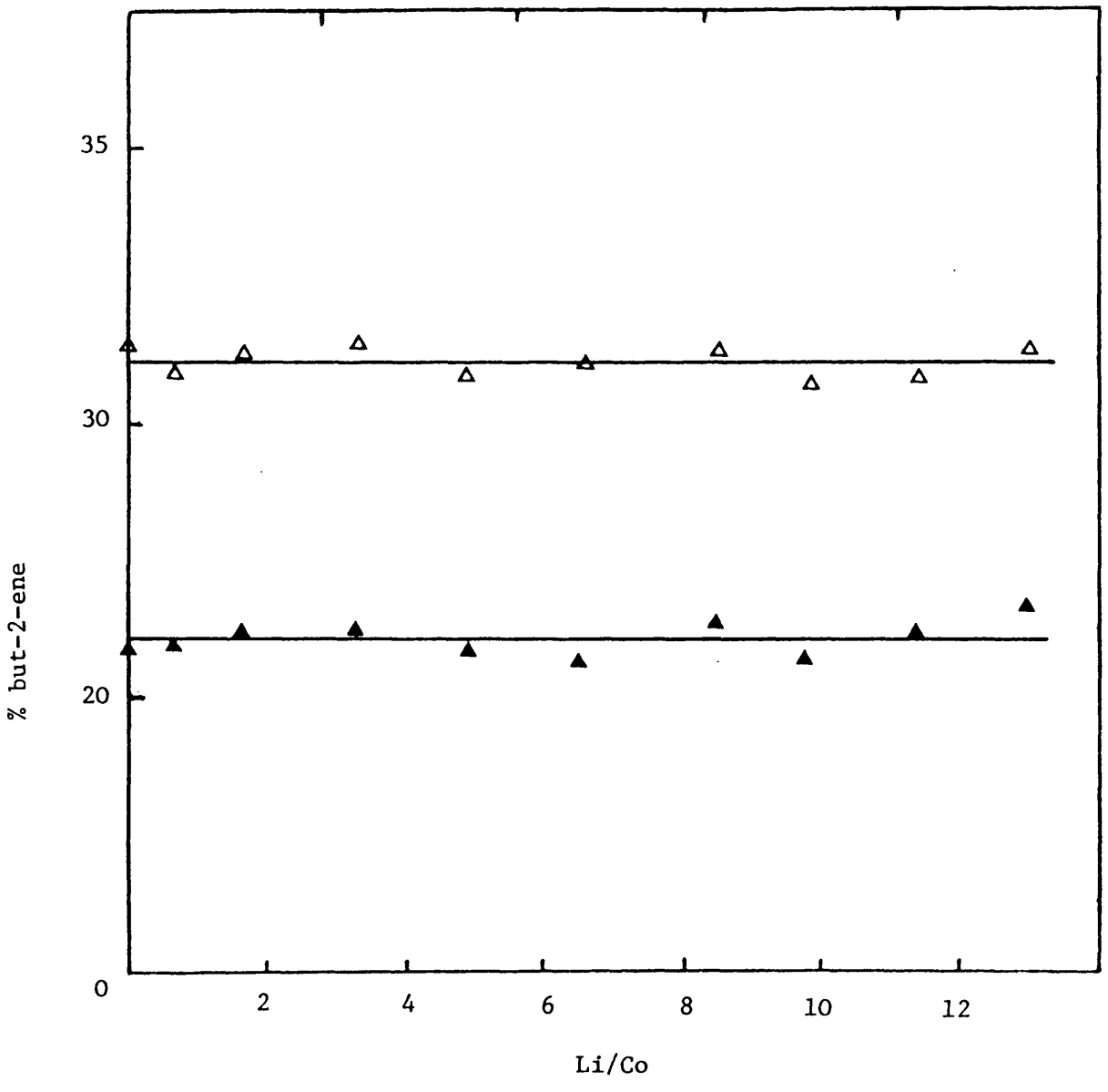

Figure 3.5 Plots of the percentage of *trans*-but-2-ene (△) and *cis*-but-2-ene (▲) in the C_4 products against Li/Co atomic ratio.

The *n*-butane distribution remains almost constant in the range $0 \lesssim$ Li/Co $\lesssim 6.5$, as shown in Figure 3.3. However, for higher values of the Li/Co ratio it decreases. But-1-ene distribution also appears to be constant in the range $0 \lesssim$ Li/Co $\lesssim 6.5$, as shown in Figure 3.4, but increases for higher values of Li/Co ratios. Finally, Figure 3.5 shows that the distribution of *cis*-but-2-ene and *trans*-but-2-ene over the whole range of Li/Co ratios remains unchanged.

The ratio of butane/total C_4 or butane/total butanes is normally considered to be a measurement of hydrogenation activity.[79] As in the present case, both *cis*- and *trans*-but-2-ene remains constant for all the catalyst samples, so the ratio butane/but-1-ene can be taken as a measure of the extent of hydrogenation. From the plot of butane/but-1-ene against Li/Co ratio (Figure 3.6), it can be seen that the selectivity for hydrogenation remains constant up to Li/Co $\simeq$ 5, beyond which it decreases quite sharply. As the distribution of *cis*- and *trans*-but-2-ene remains unaltered over the whole range of Li/Co ratio, this result also suggests that the increase in but-1-ene (see Figure 3.4) beyond Li/Co ~ 6 takes place at the expense of normal butane formation.

Another important reaction occurring during the hds of thiophene is the isomerisation of double bonds associated with the carbon chain, such as (i) but-1-ene $\rightleftharpoons$ *cis*- or *trans*-but-2-ene and (ii) *cis*-but-2-ene $\rightleftharpoons$ *trans*-but-2-ene. Let us now consider the effect which the addition of lithium to a Co-Mo catalyst has on its isomerisation properties. Figure 3.7 shows the variation of but-1-ene/total but-2-ene and *cis*-but-2-ene/*trans*-but-2-ene for various Li/Co ratios. The plots indicate

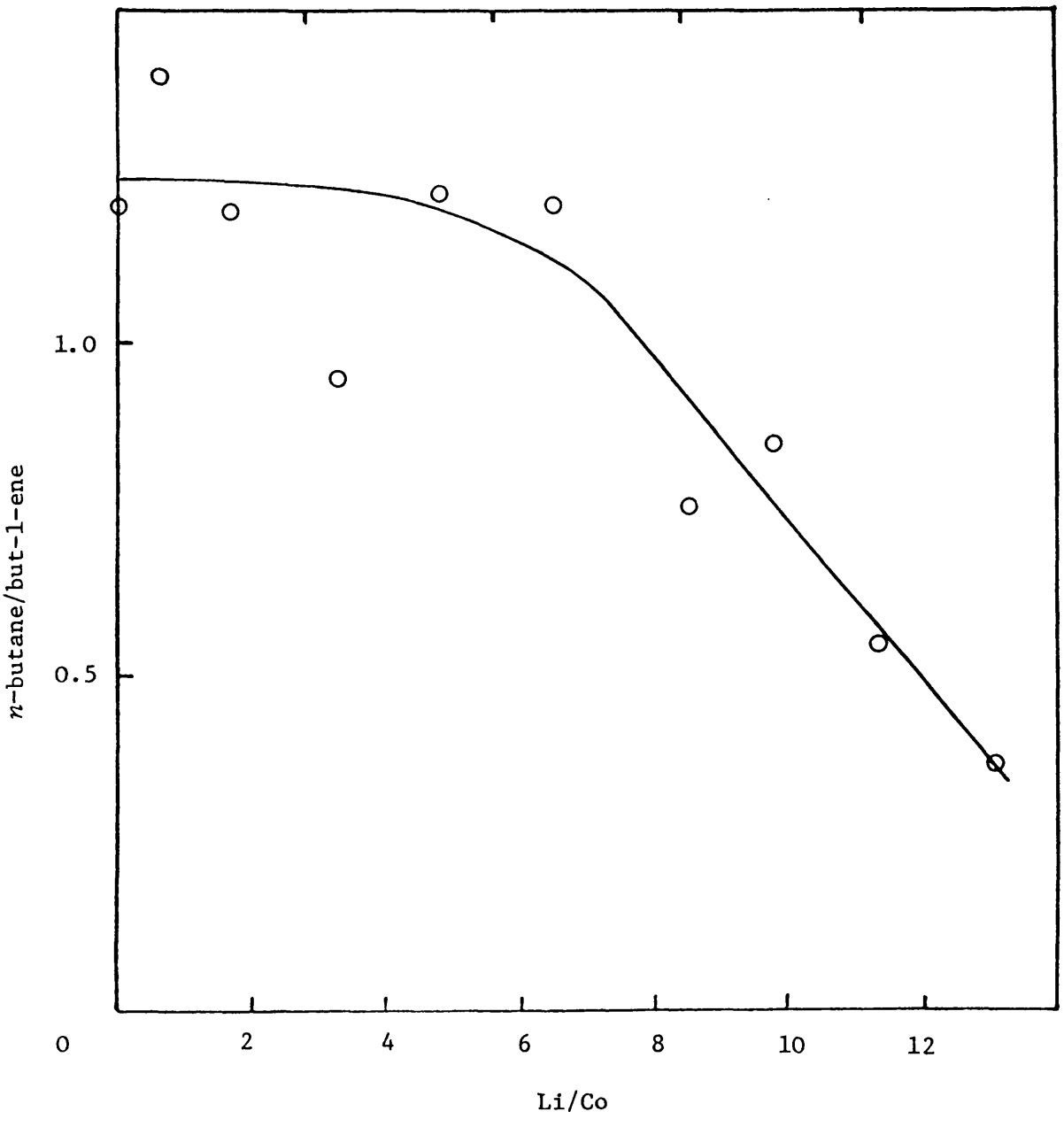

Figure 3.6 Variation of hydrogenation (*n*-butane/but-1-ene) activity of the catalysts with Li/Co atomic ratio.

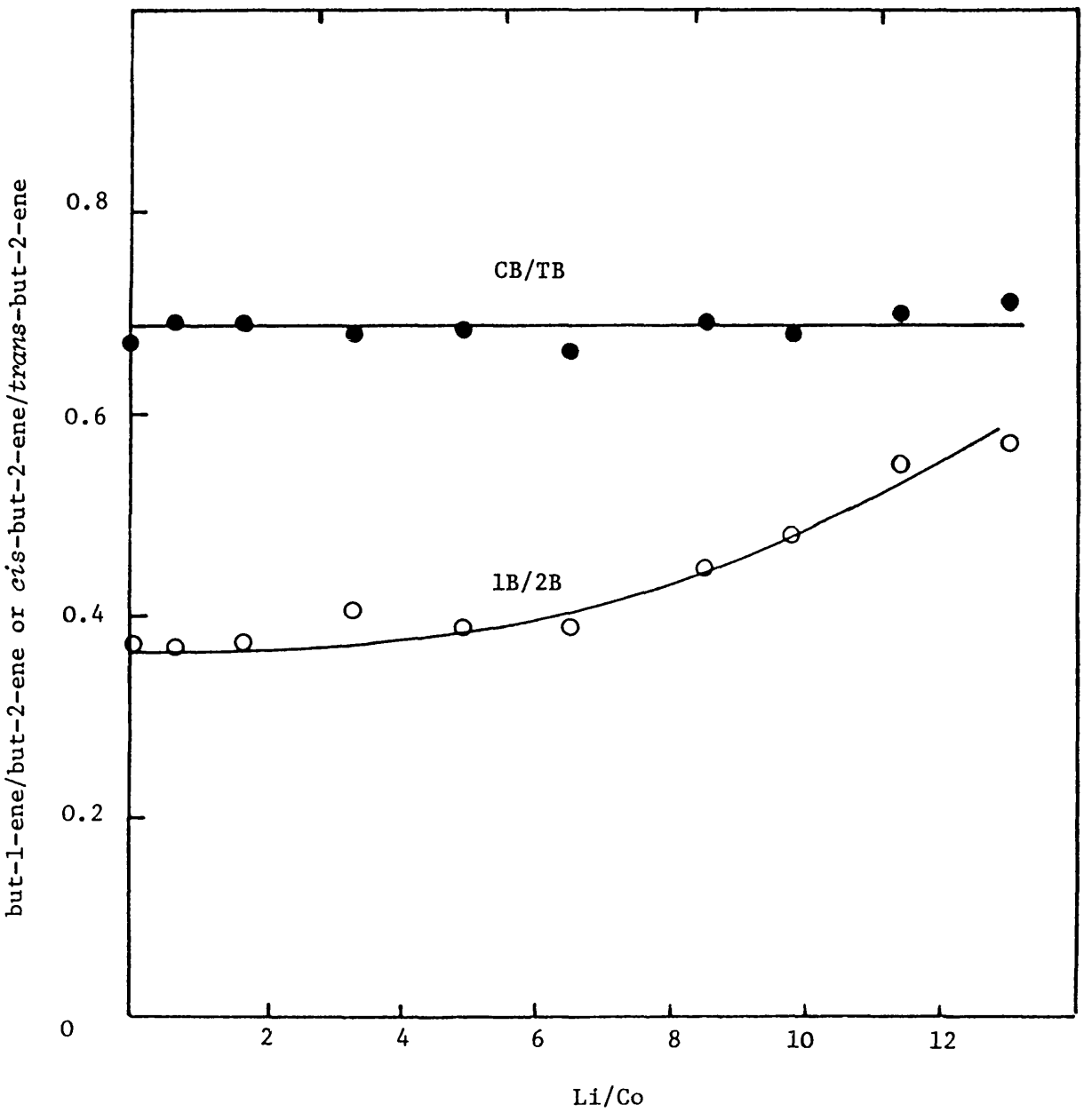

Figure 3.7 Variation of isomerisation activity (but-1-ene/but-2-ene and *cis*-but-2-ene/*trans*-but-2-ene) of the catalysts with Li/Co atomic ratio.

that the selectivity for isomerisation towards either *cis*- or *trans*-but-2-ene does not change with increase in lithium content of the catalyst, as might be expected from the product distribution (see Figure 3.5). However, the selectivity for isomerisation from but-2-ene to but-1-ene remains unchanged only up to Li/Co ~ 6, beyond which it increases.

From the results of this investigation it is clear that both the hydrogenation and hydrogenolysis activity of the hds catalyst are affected by the addition of lithium to Co-Mo/γ-Al_2O_3. In order to obtain information about the influence of lithium addition on the structure of the cobalt molybdate system, characterisation of the samples was undertaken by using a number of physical techniques.

3.3 Physical Characterisation

(1) U.v.-visible reflectance spectra

Transition metal ions supported on an inert matrix exhibit absorption bands due to electronic transitions in the u.v.-visible and near infra-red region of the spectrum. These absorption frequencies are characteristic of certain arrangements of molecules within their environment. A series of reflectance spectra were recorded for several lithium containing catalysts, as well as for a catalyst without lithium.

Figure 3.8 shows the spectrum of CoO-MoO_3/γ-Al_2O_3 (Li/Co = 0) which was typical of the spectra of all the lithium containing samples shown in Appendix A-1. Each spectrum consists of two groups of bands. One broad band is in the range 32000-40000 cm^{-1}, and it attributed to molydenum in both co-ordination states (tetrahedral and octahedral).[41] The second group of absorption bands is in the range 17000-18000 cm^{-1} and is due to

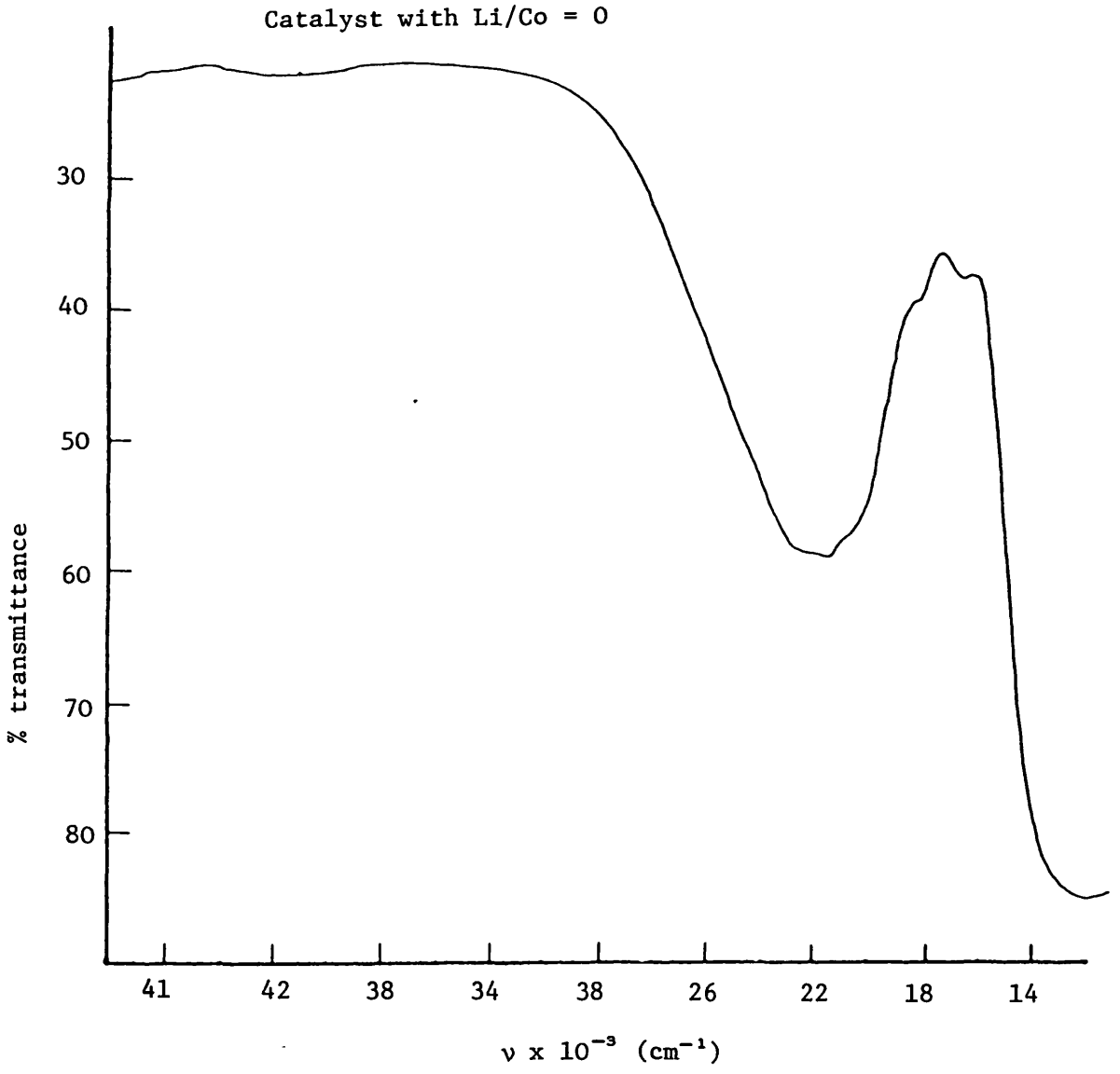

Figure 3.8 A typical reflectance spectrum of the lithium containing catalyst series (corresponding to the catalyst with no lithium).

Co^{2+} (tetrahedral).[66] A small amount of cobalt may be present in octahedral co-ordination as Co_3O_4, which was reported by Martinez *et al.*[78] as a result of magnetic susceptibility measurements. However, the octahedral fraction of Co^{2+} ion is difficult to detect[78] in the presence of tetrahedral Co^{2+} because the absorption band due to the octahedral Co^{2+} ion is very small (~ 50 times) compared to the band given by the same amount of the tetrahedral Co^{2+} ion.

No appreciable difference was observed in intensity of absorption bands for cobalt as the lithium content in the catalyst series was varied. This is shown in Figure 3.9, where the transmittance due to cobalt is plotted against the Li/Co ratio. No broadening of the molybdenum band was observed with increasing amounts of added lithium, unlike that reported by Martinez *et al.*[78] who worked on a series of catalysts with different cobalt content. They found a broadening of the molybdenum band and suggested that this broadening was due to Co enhancing the dispersion of molydenum over the γ-Al_2O_3 surface.

(2) X-ray studies

X-ray diffraction patterns recorded for the lithium series of catalysts are shown in Figure 3.10. The patterns of all the lithium containing catalysts and that of the Co-Mo/γ-Al_2O_3 catalyst are identical (see Figure 3.10). A comparison of *X*-ray diffraction patterns of an hds catalyst (Co-Mo/γ-Al_2O_3) and several other oxides, *i.e.*, Al_2O_3, MoO_3, CoO, Li_2O, and $CoAl_2O_4$ are shown in Figure 3.11. All the patterns in Figure 3.10 are again similar to the diffraction pattern of γ-Al_2O_3 given in Figure 3.11. The *X*-ray diffraction patterns due to any

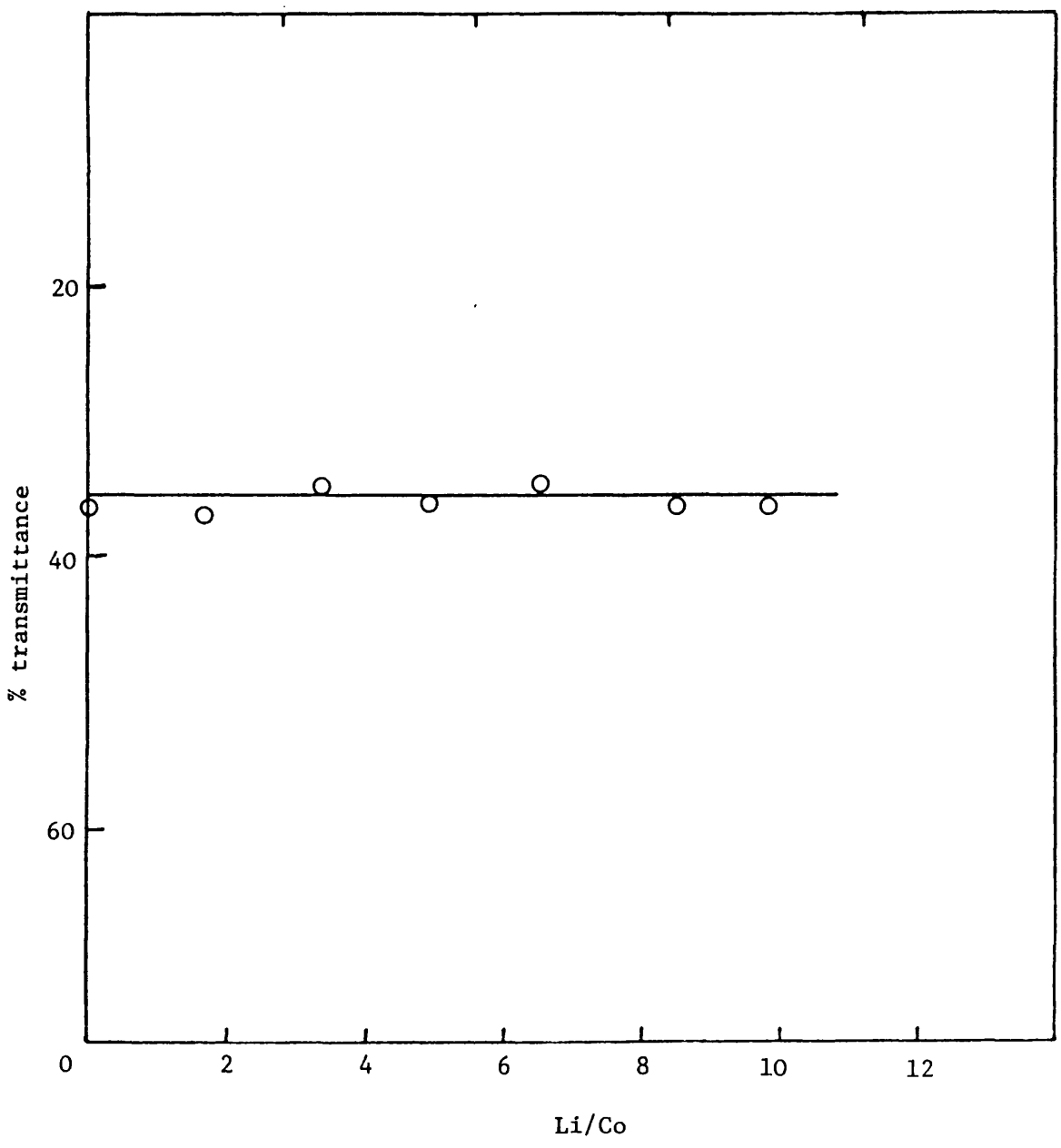

Figure 3.9 Variation of the tetrahedral cobalt signal intensity (% transmittance) with the Li/Co atomic ratio.

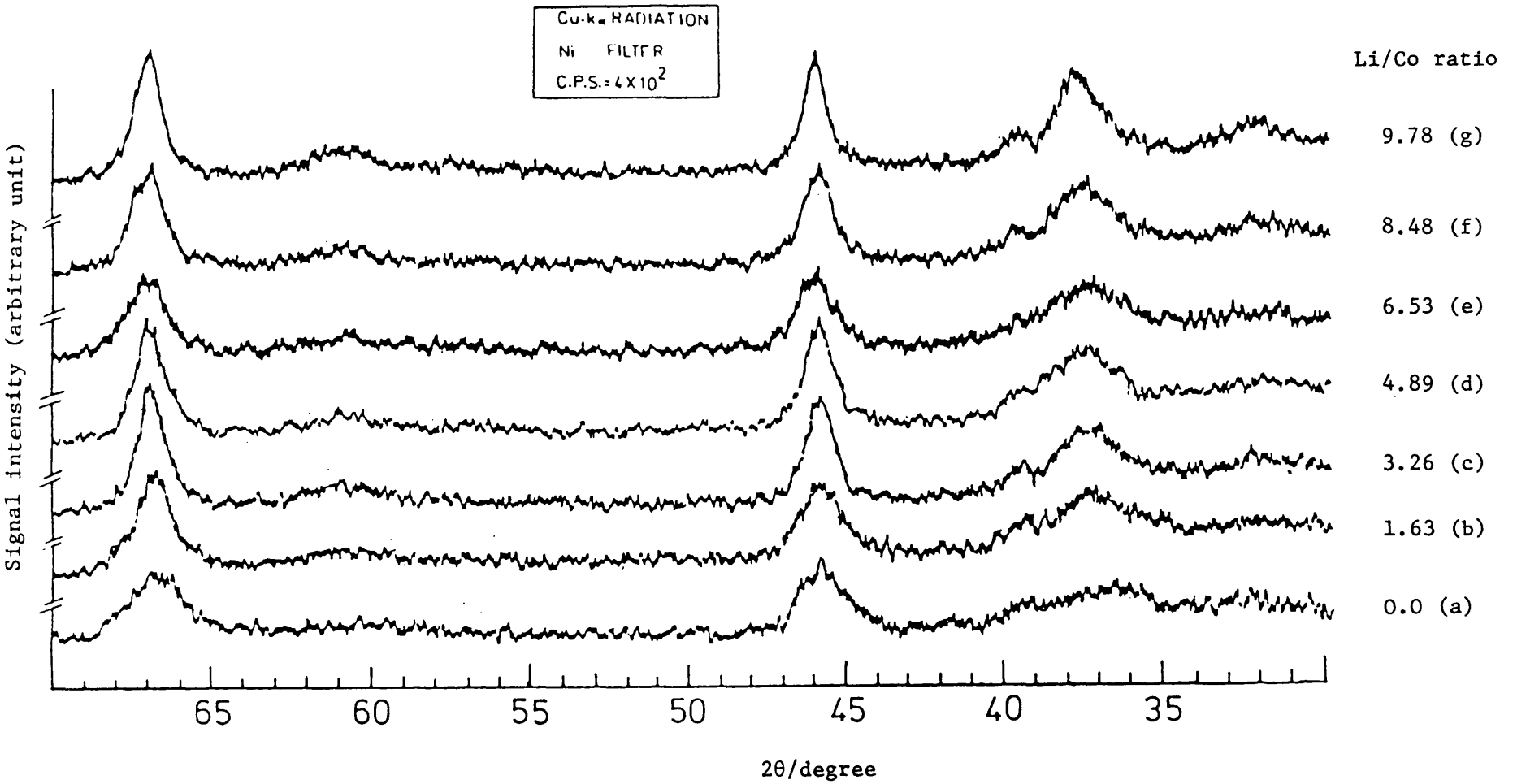

Figure 3.10 *X*-ray diffraction patterns of some hds catalysts: (a) $CoO-MoO_3/\gamma-Al_2O_3$ (Co = 1.3 wt %, Mo = 11.65 wt %) and (b)-(g) $Li_2O-CoO-MoO_3/\gamma-Al_2O_3$.

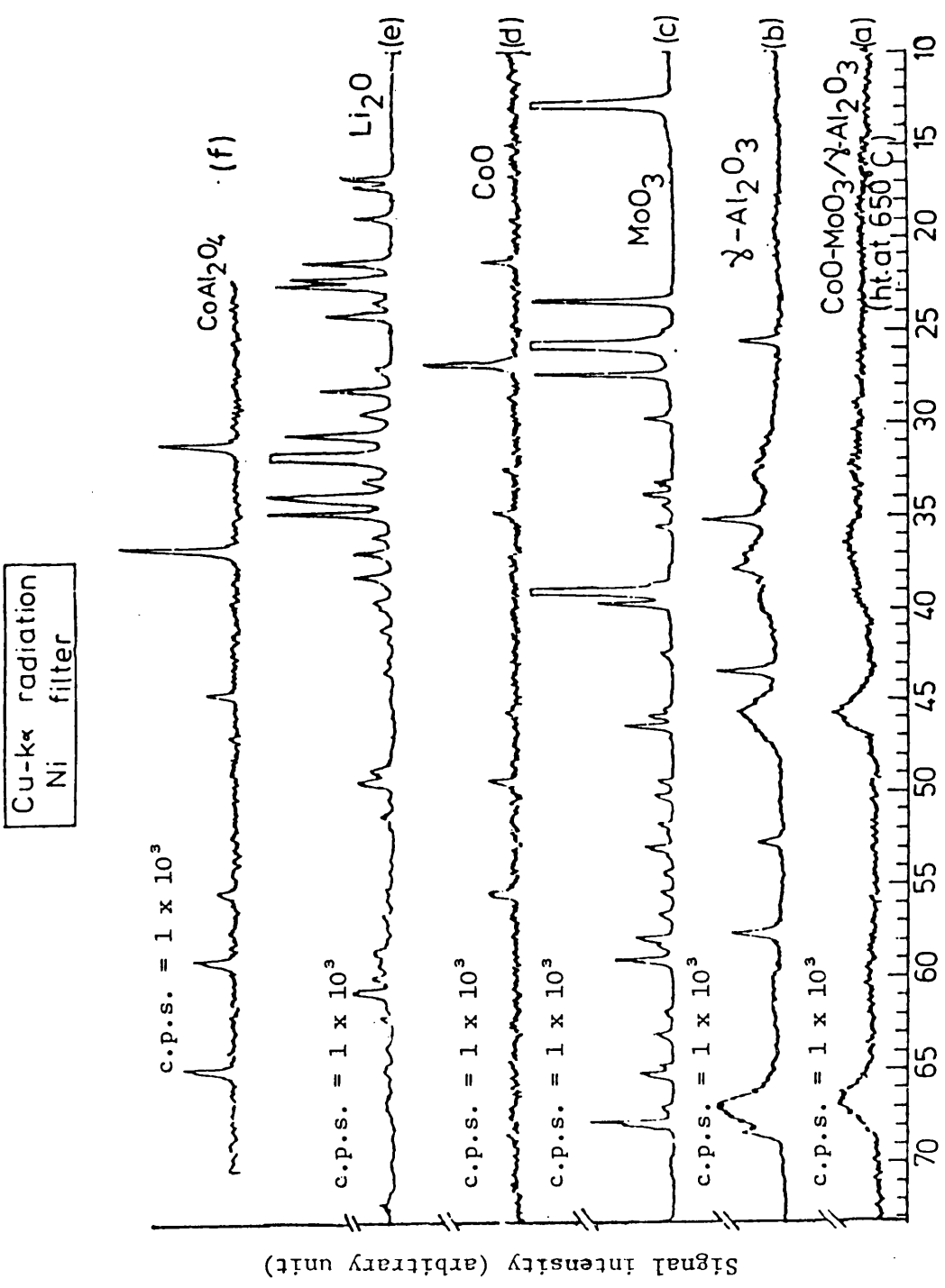

Figute 3.11 X-ray diffraction patterns of an hds catalyst (a), γ-Al_2O_3 (b), MoO_3 (c), CoO (d), Li_2O (e) and $CoAl_2O_4$ (f).

constituent oxide (see Figure 3.11) is obviously not visible at all in the patterns of the series of catalysts investigated (see Figure 3.10). This is perhaps due to the fact that their amounts are relatively small compared with that of γ-Al_2O_3. The main characteristic of the patterns given in Figure 3.10 is that the peak height increases (width decreases and hence intensity remains constant) with increasing lithium content. The sharpening of the peak in the *X*-ray diffraction patterns suggest that the addition of lithium increases the crystallinity of the support (γ-Al_2O_3). As γ-Al_2O_3 possesses a pseudo-spinel structure and forms a major part of the catalyst under investigation, it was not possible to obtain from *X*-ray studies information about the presence of other compounds such as cobalt molybdate ($CoMO_4$), cobalt aluminate ($CoAl_2O_4$), cobalt oxide (Co_3O_4) *etc.*, which also possess spinel structure and which may be present in CoO-MoO_3/γ-Al_2O_3 and lithium doped CoO-MoO_3/γ-Al_2O_3.

(3) Physisorption methods

(a) BET surface area and isotherm analysis

The full isotherms (adsorption and desorption branch at liquid nitrogen temperature) were recorded for all the catalysts of the series. The results are presented in Appendix A-3. To compute the surface areas of the catalysts, the initial part of the adsorption branch of the isotherms was used. Figure 3.12(a) and (b) show the BET plots. The calculated BET surface area for the catalyst series, together with the values of the monolayer capacity, Vm, and the constant C in the BET equation, are recorded in Appendix A-4. Figure 3.13 shows the plot of the BET surface area against the Li/Co ratio for all the catalysts studied. It can be seen from the plot that in the composition

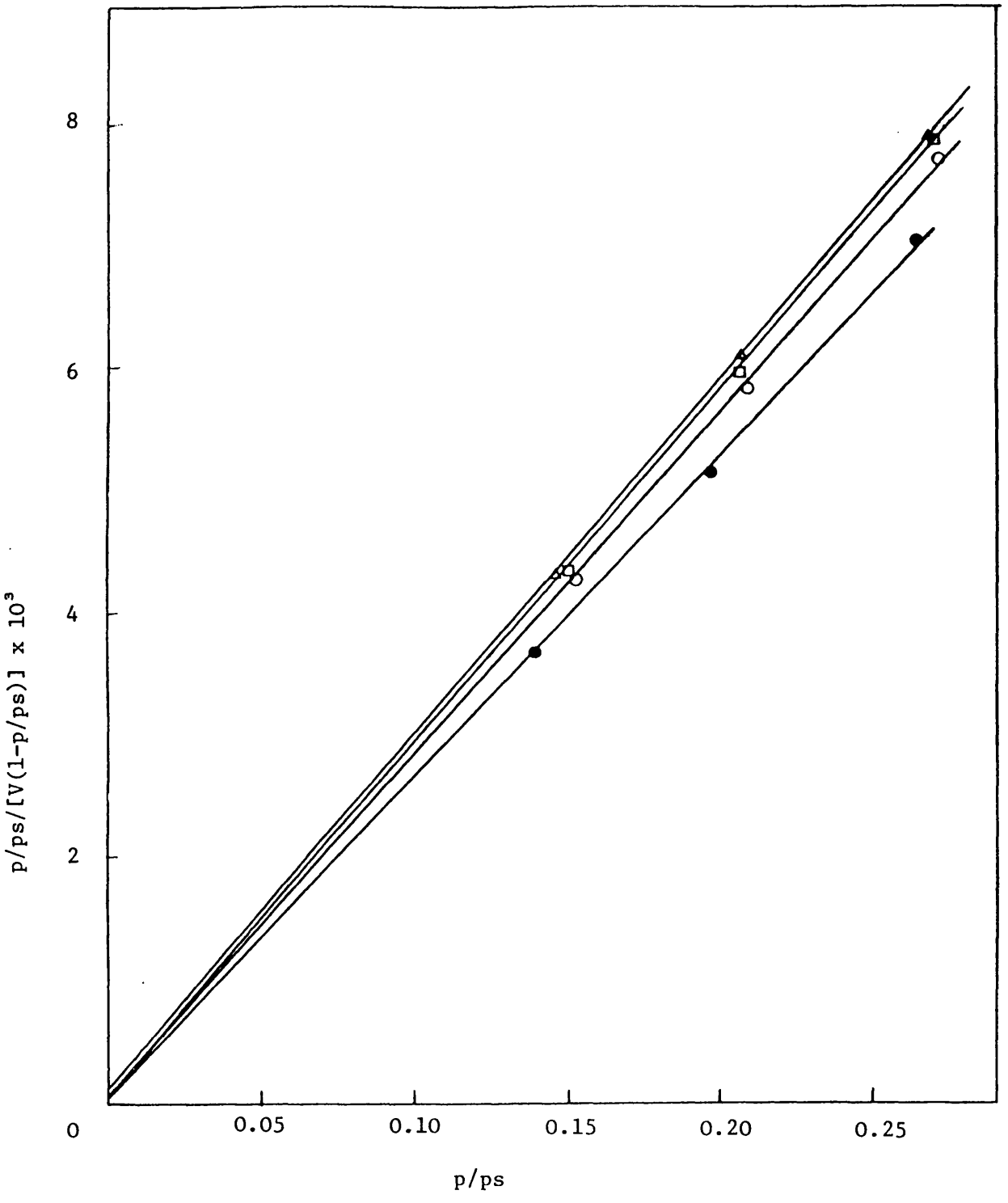

Figure 3.12(a) BET plot for the lithium containing catalyst series for catalyst with Li/Co atomic ratio of 0.0 (●), 1.63 (○), 3.26 (□) and 4.89 (△).

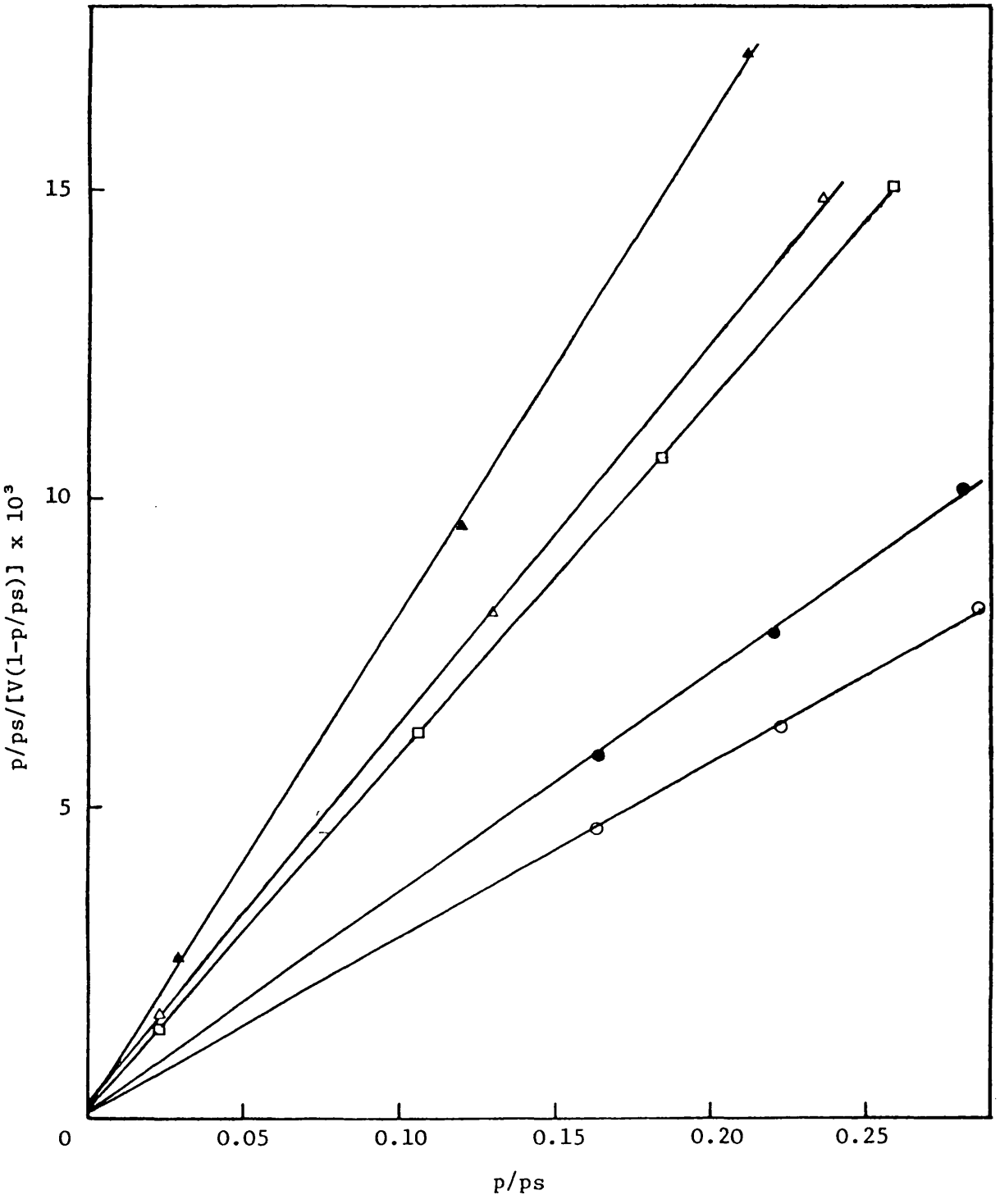

Figure 3.12(b) BET plot for the lithium containing catalyst series for catalyst with Li/Co atomic ratio of 6.53 (○), 8.48 (●), 9.78 (□), 11.43 (▲) and 13.06 (△).

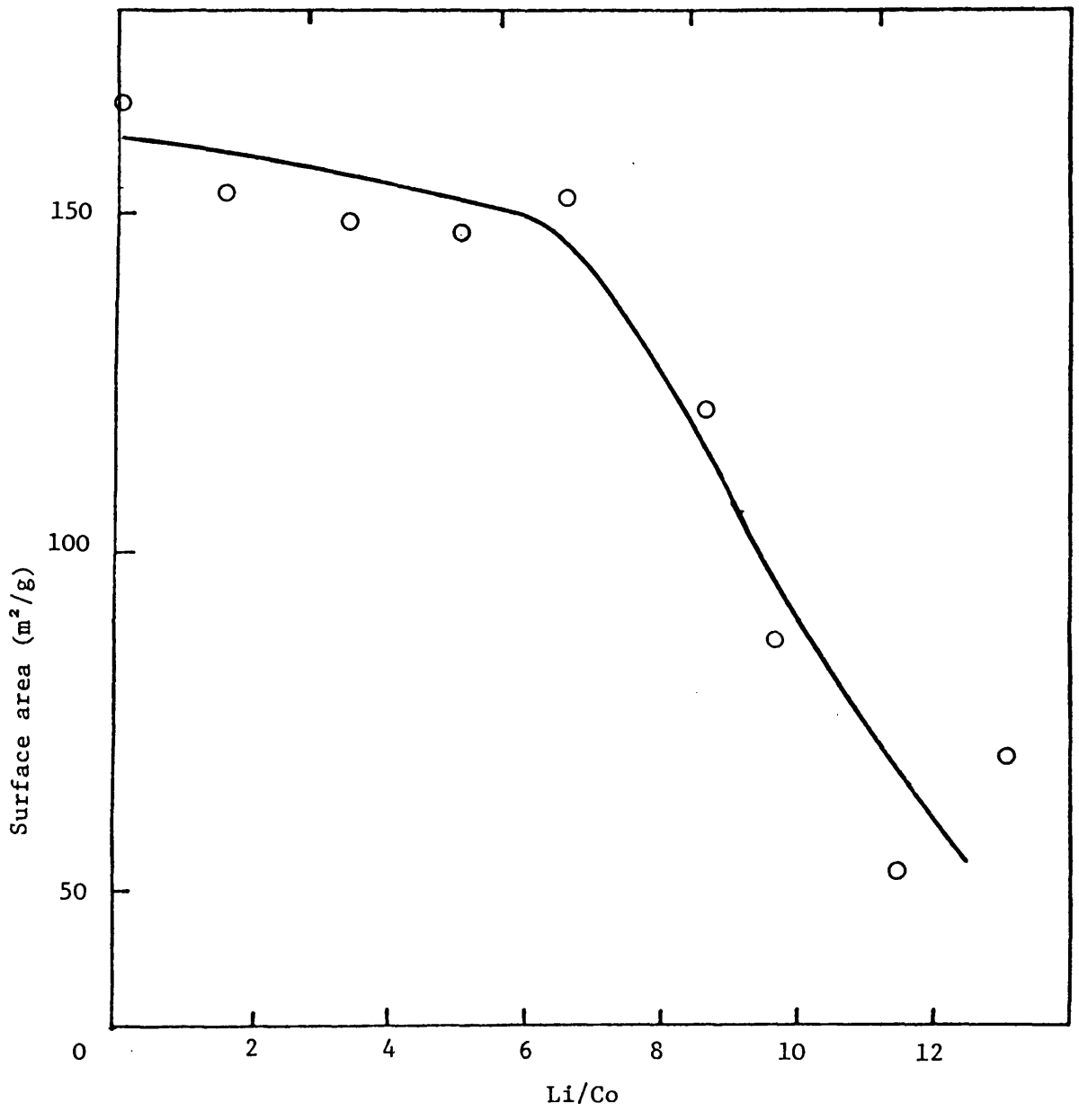

Figure 3.13 Variation of the surface area for the lithium containing catalyst series with Li/Co atomic ratio.

range $0 \lesssim Li/Co \lesssim 6.5$, the lithium addition to the catalyst does not have any influence on the surface area. However, for $Li/Co > 6.5$ the lithium causes a sharp decrease in the surface area of the catalysts.

It is known that the shape of the isotherm is highly dependent on the nature of the adsorbent surface.[71] For solids containing mesopores (20-500 Å), capillary condensation takes place in the middle or upper part of the isotherm, whereas for solids with micropores, pore filling occurs at a low relative pressure (p/p_s). An indication of the nature of the adsorption process may be obtained by inspection of the isotherm shape. Figures 2.7 and 2.8 [Section 2.2(4)] show the classification of the adsorption isotherms and the classification of characteristic hysteresis loops which are most frequently encountered.

To investigate the effect of lithium addition on the nature of the adsorbent surface (γ-Al_2O_3 support), full isotherms at liquid nitrogen temperature for the catalyst series are plotted in figures 3.14(a)-(i) by using the data recorded in Appendix A-3. The isotherms in these figures do not seem to correspond completely to any individual isotherm pattern in the BDDT classification. They appear, however, to be a combination of type II and type IV isotherms (see figure 2.7). Their hysteresis loops correspond mainly to type A in de Boer's classification (see Figure 2.8) and it is associated with capilliary condensation in mesopores.

It can also be observed from these figures that catalysts with low lithium content present a quite large hysteresis loop, indicating a wide distribution of mesopores. However, as the lithium content increases, the size of the hysteresis loop decreases, which suggests that a fraction of the mesopores disappears.

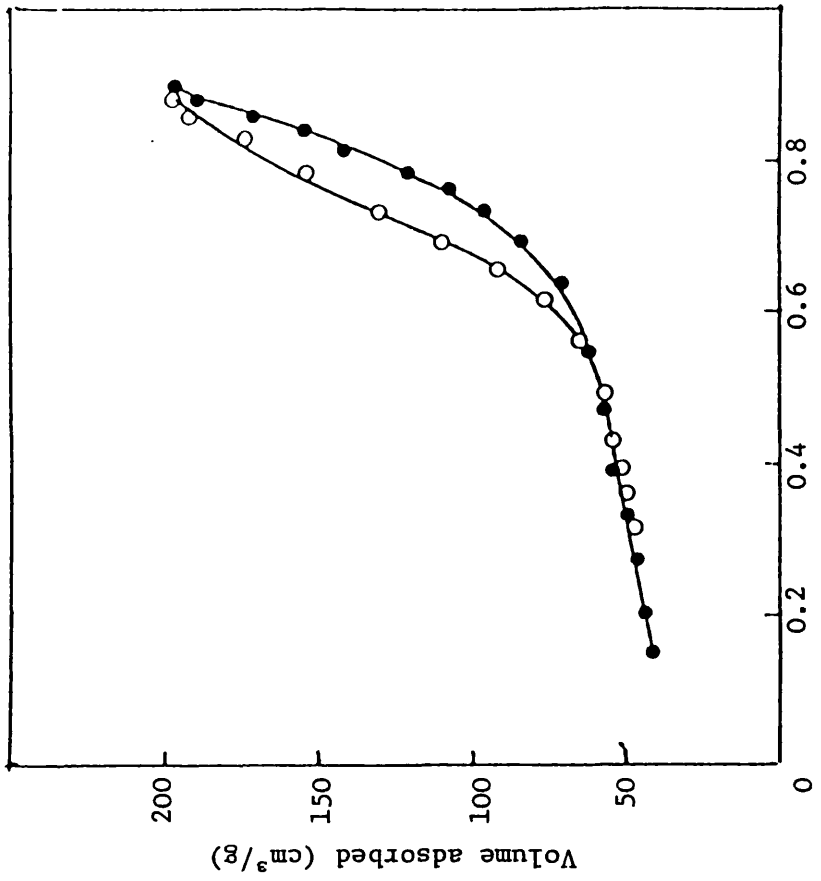

(a) catalyst with Li/Co = 0

(b) catalyst with Li/Co = 1.63

● adsorption
○ desorption

Figure 3.14 Adsorption-desorption isotherms for the lithium containing catalyst series.

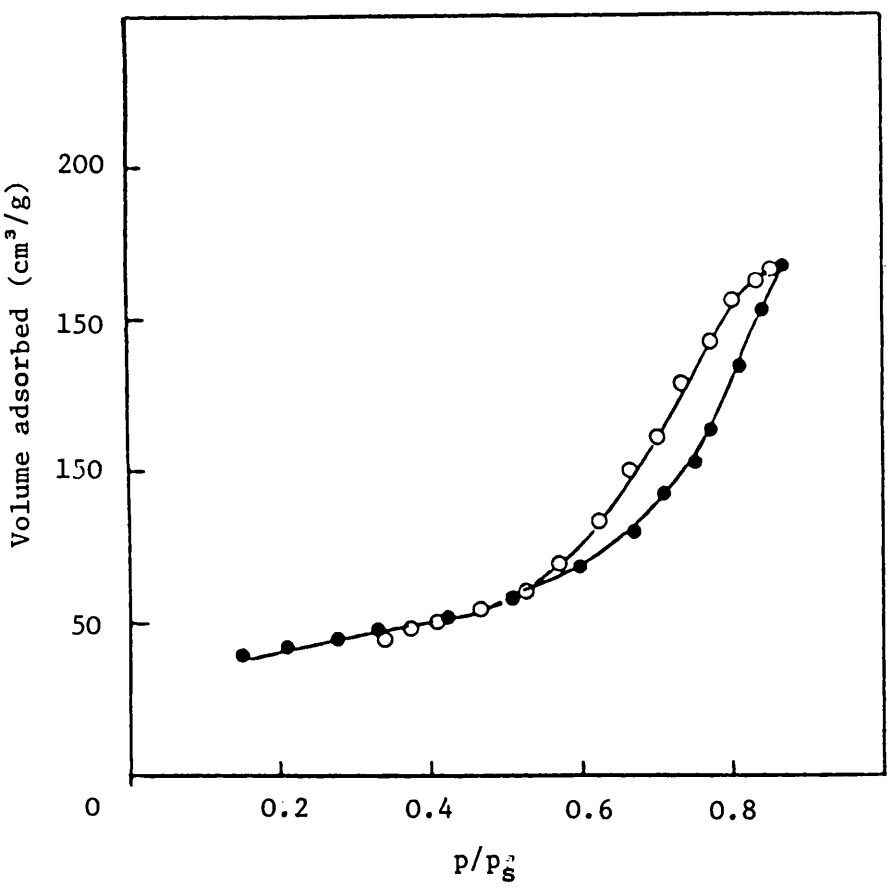

(c) catalyst with Li/Co = 3.26

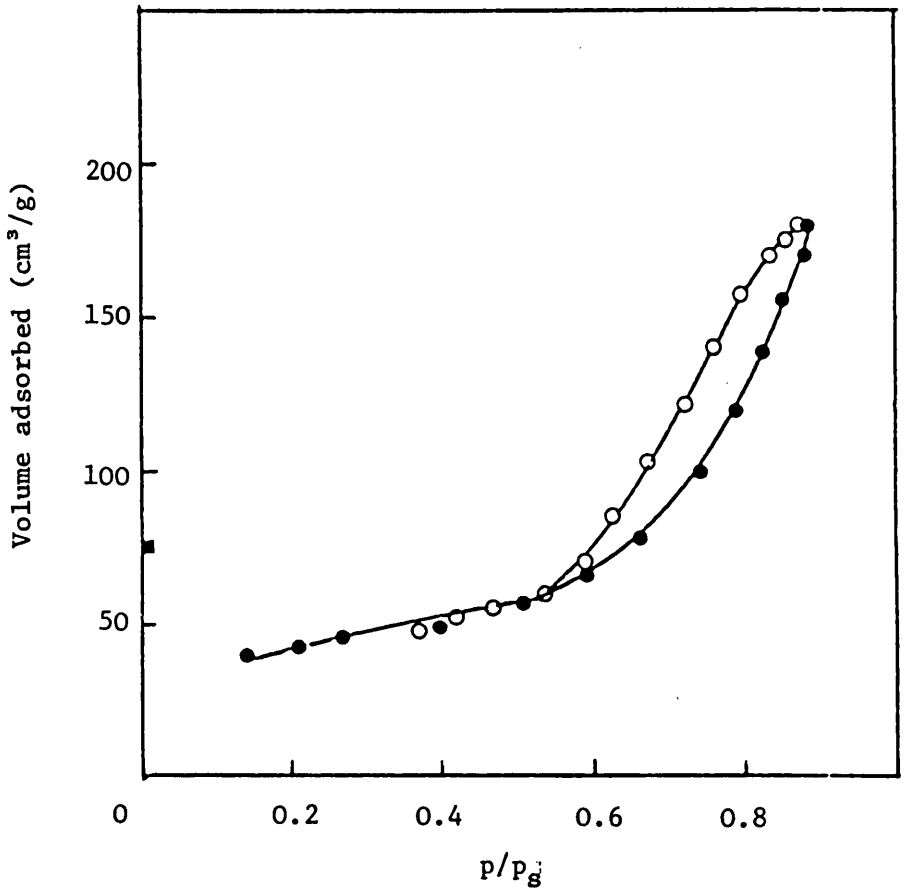

●adsorption

○desorption

(d) catalyst with Li/Co = 4.89

Figure 3.14 Adsorption-desorption isotherms for the lithium containing catalyst series.

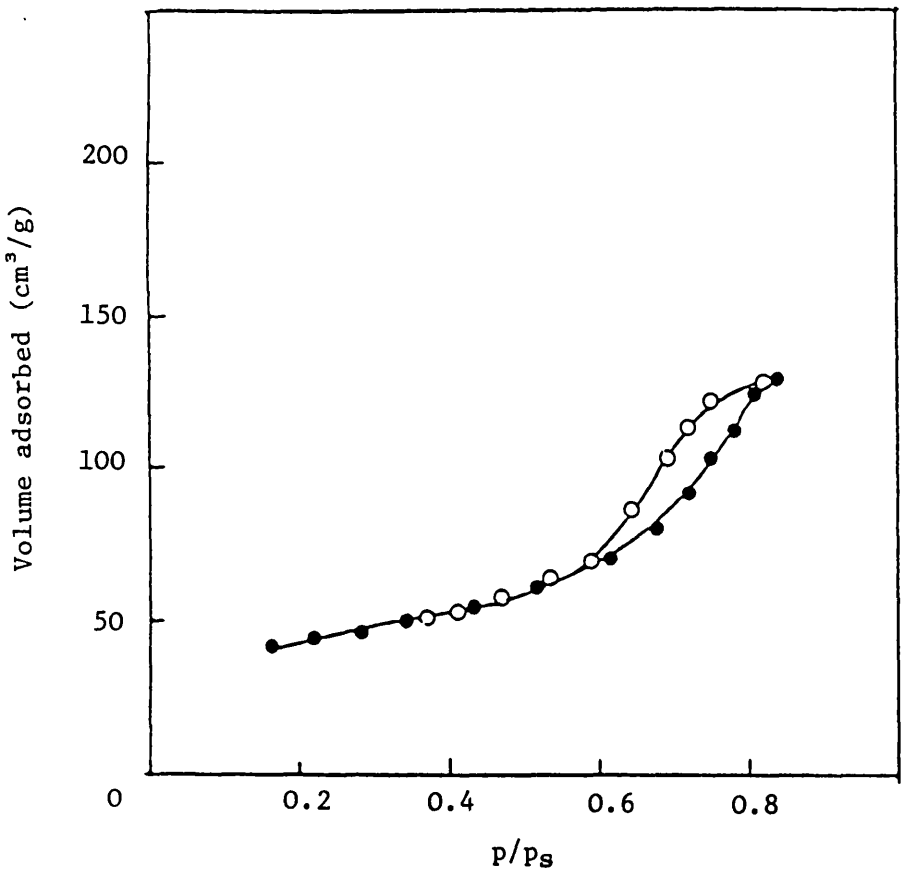

(e) catalyst with Li/Co = 6.53

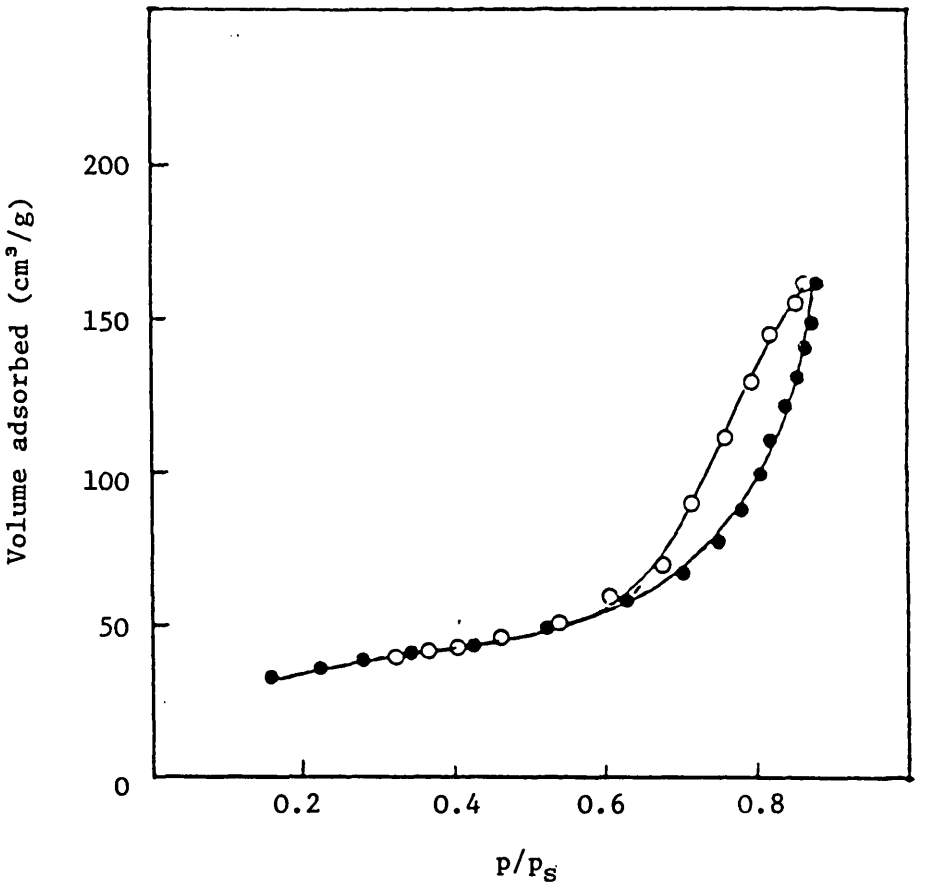

●adsorption

○desorption

(f) catalyst with Li/Co = 8.48

Figure 3.14 Adsorption-desorption isotherms for the lithium containing catalyst series.

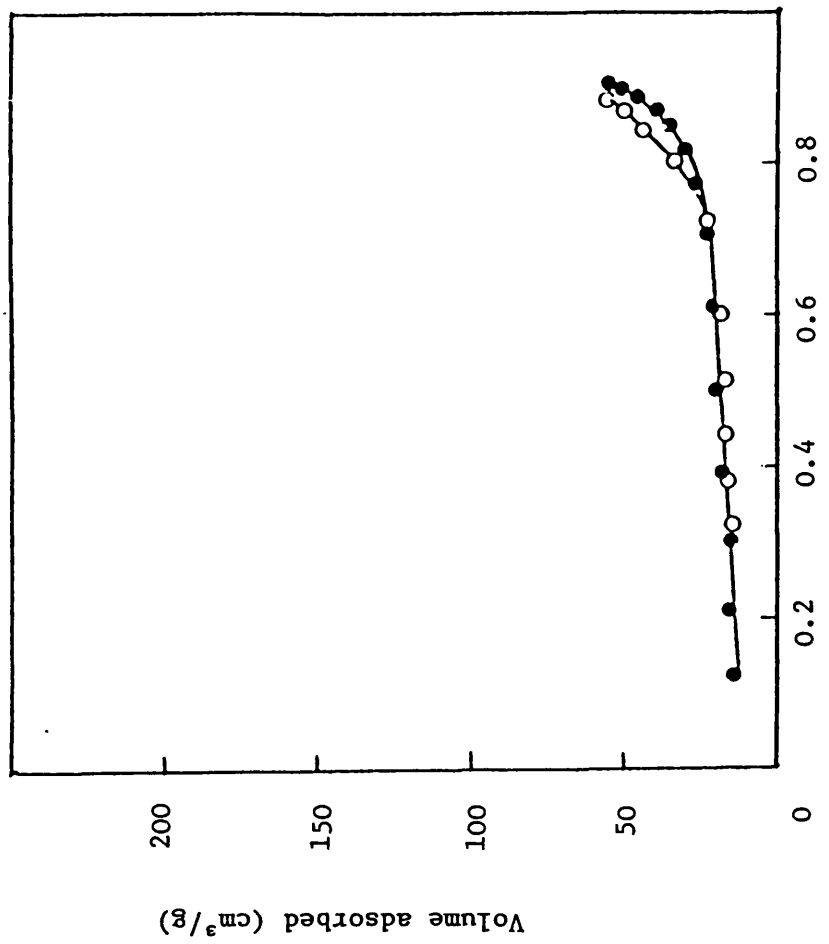

(g) catalyst with Li/Co = 9.78

(h) catalyst with Li/Co = 11.43

Figure 3.14 Adsorption-desorption isotherms for the lithium containing catalyst series.

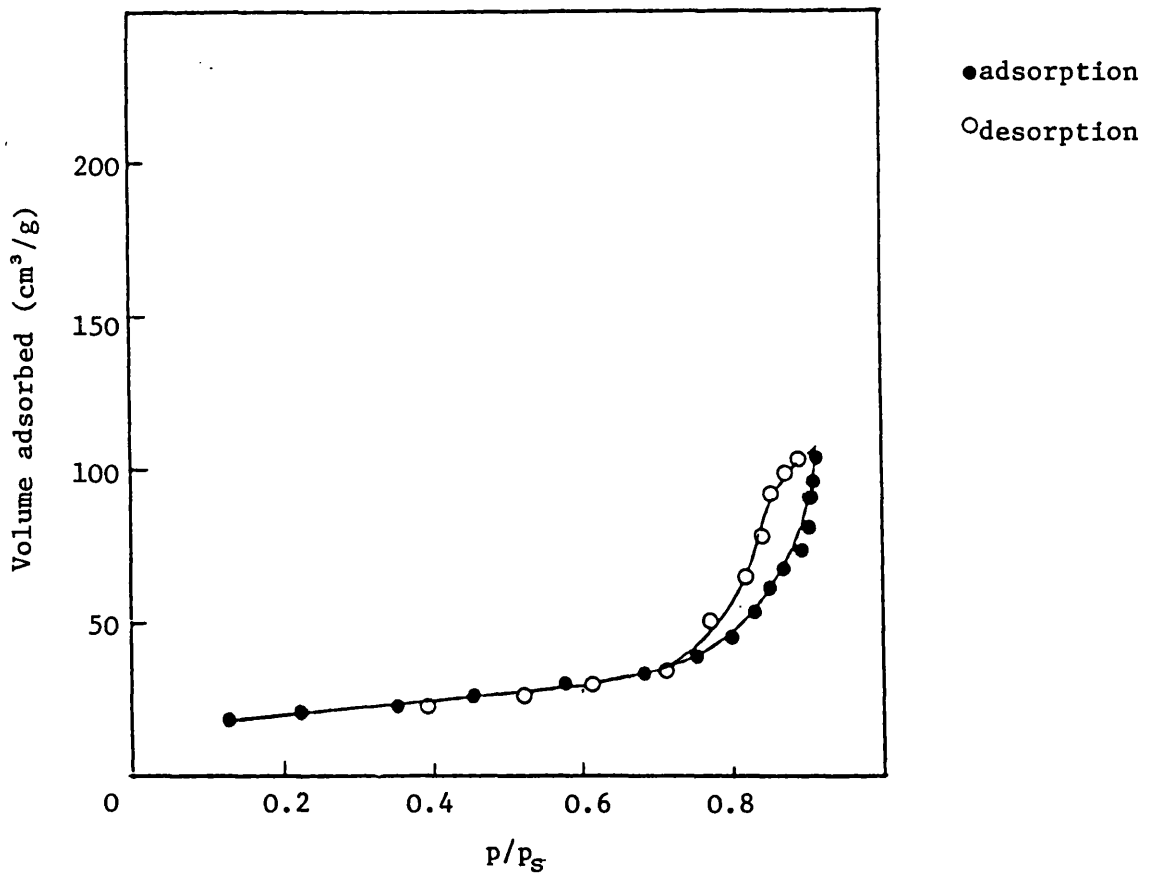

(i) catalyst with Li/Co = 13.06

Figure 3.14 Adsorption-desorption isotherms for the lithium containing catalyst series.

(b) Pore size distribution

The pore size distribution of the series of catalysts were determined by the method of Orr and Dellavalle[72] using desorption data extracted from the isotherms shown in Figure 3.14 (a)-(i). The results of the pore size distribution analysis are recorded in Appendix A-5 and plotted in Figure 3.15. From this latter figure it can be seen that for catalysts in the composition range $0 \leqslant Li/Co \lesssim 6.5$, pore size distributions do not differ significantly. For the remaining catalysts (*i.e.*, with Li/Co > 6.5) the pore size distributions do alter. For samples with high Li content (Li/Co > 6.5), pores with relatively small radii (20 Å) disappear first and, with further increase in the lithium content, larger pores progressively disappear.

For all the catalysts of the series, almost 100% of the volume is occupied by pores with radii less than 95 Å. It has been found that, for some catalysts, the accumulative surface area (determined by pore size distribution) $\Sigma\Delta s_p$ is much higher than the BET surface area. This points to severe irreversibility in the process responsible for the desorption branch, and thus to a bottle-neck effect.[79]

(4) Electron spin resonance spectra

An e.s.r. signal is observed when unpaired electrons are present in the sample. Thus the e.s.r. technique can provide information about the oxidation state of the metal present in the catalyst. The signal is very sensitive to small concentrations of any paramagnetic species.

It was discovered earlier[41] that reduced MoO_3/Al_2O_3 produced a rather large e.s.r. signal which was attributed to the Mo^V species. The

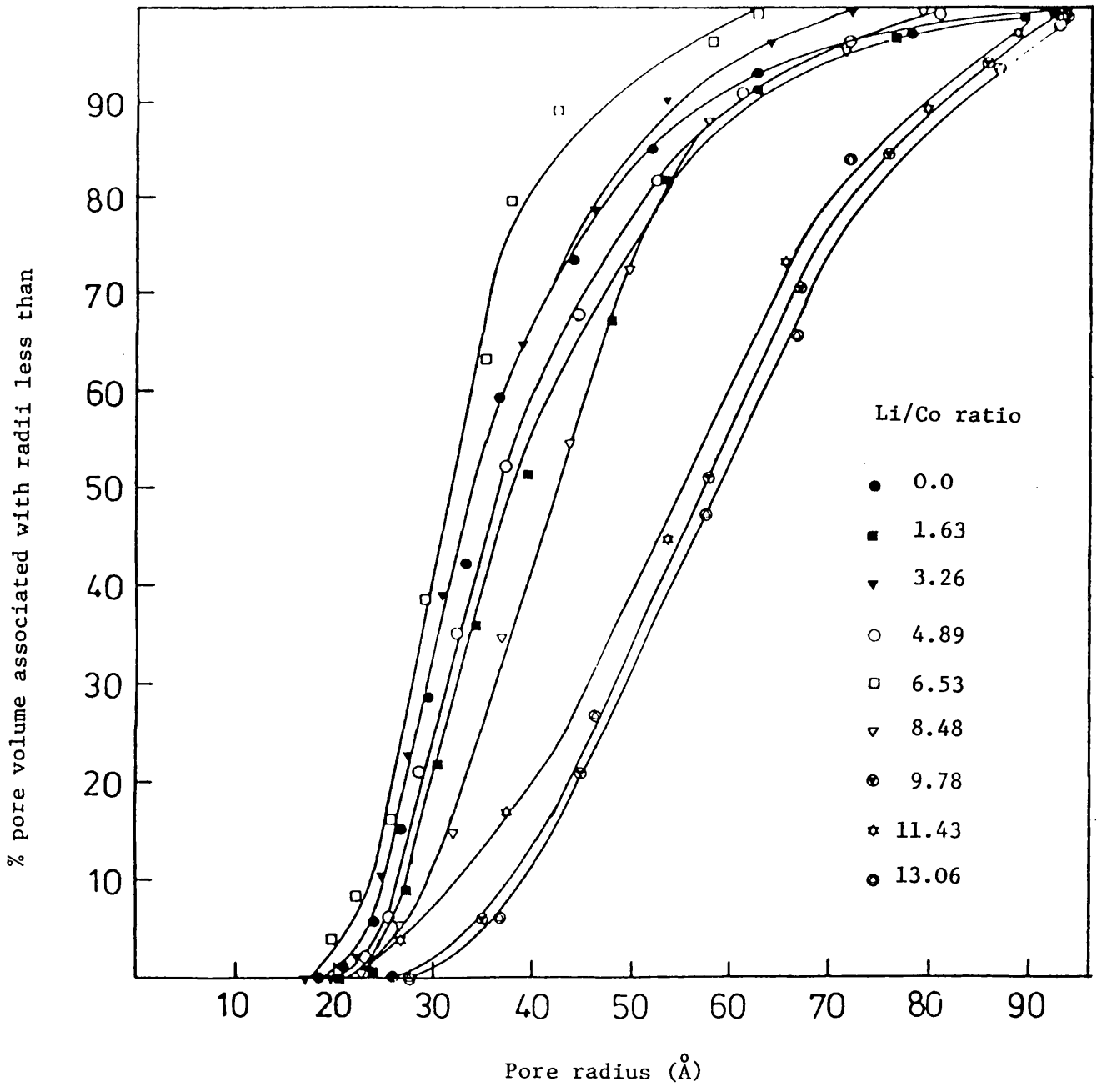

Figure 3.15 Pore volume distribution for the lithium containing catalyst series.

e.s.r. signal is characterised by its g value (spectroscopic splitting factor) which was found to be 1.930 for Mo^{V}.[82] In general, the Mo^{V} species is believed to be an intermediate in the reduction of Mo^{VI} to lower valencies. In the present study the effect of the addition of lithium on the reducibility of cobalt molybdate was investigated and for this purpose, studies have been made in two ways:

(a) reduction of the catalysts in an atmosphere of hydrogen;

(b) reduction plus sulphidation of the catalyst in a mixture of hydrogen sulphide in hydrogen (10 v % H_2S in H_2).

(a) Reduction of the series of catalysts in hydrogen

A typical e.s.r. spectrum for the series of catalysts is shown in Figure 3.16. The spectra for the remaining samples are given in Appendix A-2(i). The signal intensity was very strong and is attributed to Mo^{V} on the basis of its calculated g value of 1.927 and which corresponds well with the value reported in the literature.[80]

As the peak-width remains constant in each case, the peak height in each e.s.r. spectrum has been taken as a measure of the intensity of the Mo^{V} (see Figure 3.17). The peak intensities are plotted against the Li/Co atomic ratio as shown in Figure 3.17. It can be seen from Figure 3.17 that there is a decrease in the e.s.r. signal intensity of Mo^{V} species as the Li/Co atomic ratio increases from 0 to 5. However, this is followed by a sharp increase in the intensity of the e.s.r. signal as the Li/Co ratio increases to 6.5, beyond which the signal intensity decreases.

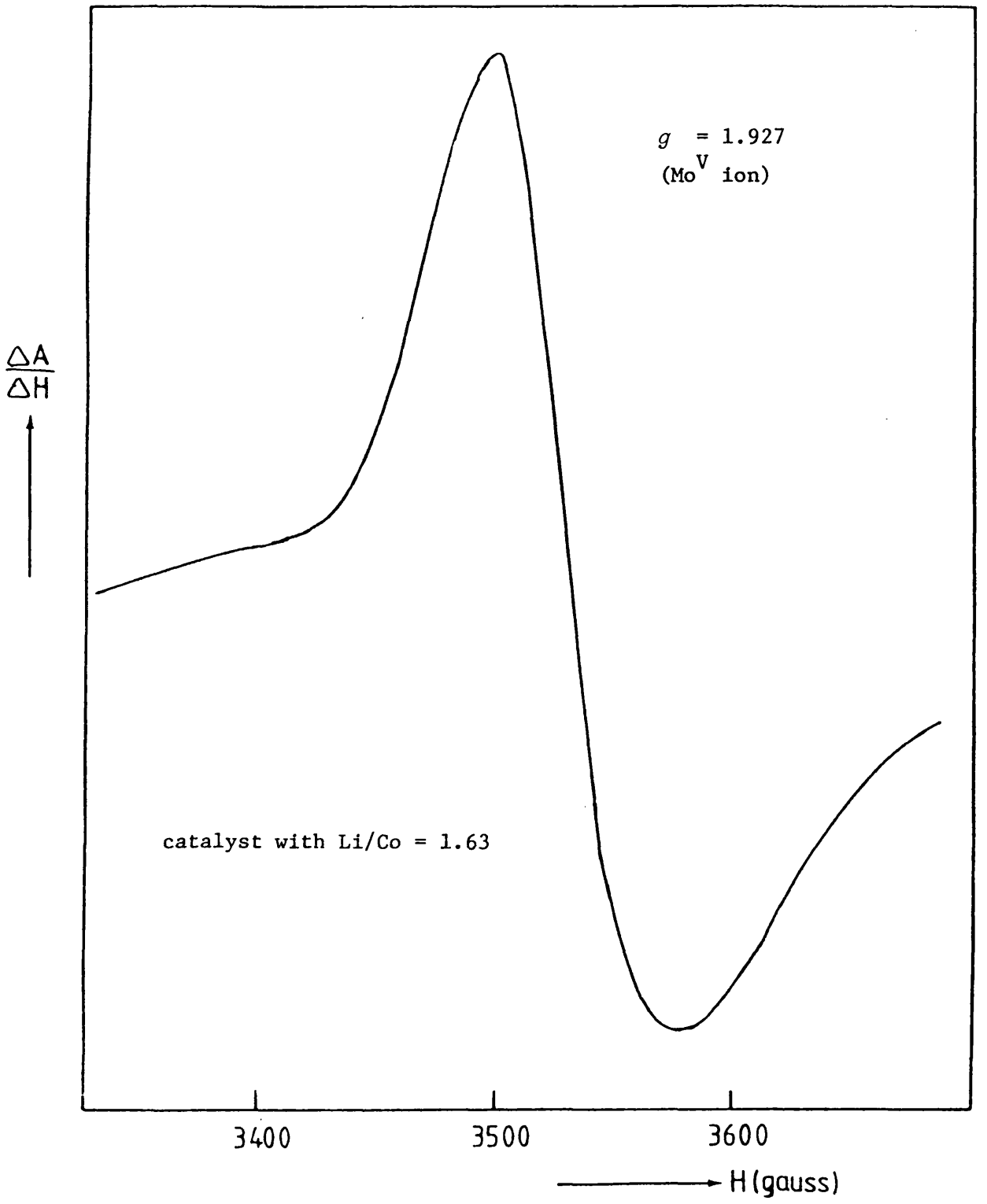

Figure 3.16 A typical e.s.r. spectrum for the lithium containing catalyst series pretreated with hydrogen.

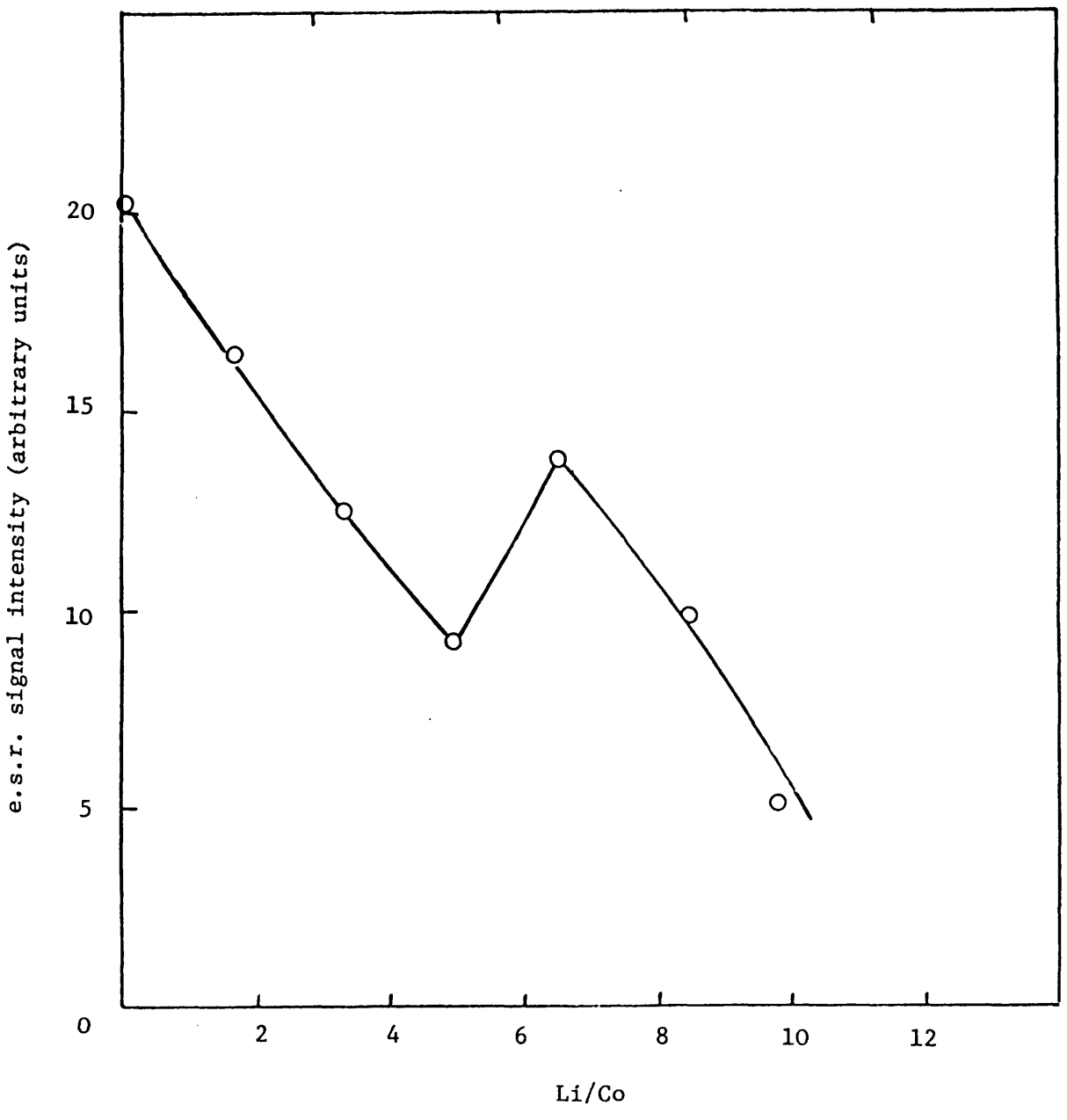

Figure 3.17 Variation of the e.s.r. signal intensity due to the Mo^{V} ion with Li/Co atomic ratio for the lithium containing catalysts series pretreated with hydrogen.

The results will be discussed and interpreted in the following section, together with the results of e.s.r. studies of the catalysts after treatment with hydrogen sulphide and hydrogen. However, at this stage it is worth noting that lithium addition does, in fact, affect the reducibility of molybdenum in the catalysts.

(b) Reduction and sulphidation of the series of catalysts

Figure 3.18 shows an e.s.r. spectrum of a lithium containing catalyst (Li/Co = 1.63). It is typical of the spectra of samples in the series which are presented in Appendix A-2(i). The results show that, apart from the signal corresponding to the Mo^{V} species, there are two new signals whose g values are 1.976 and 1.991 respectively. The e.s.r. signal intensity of all the catalysts are plotted against their Li/Co atomic ratio in Figure 3.19. For convenience, and as a means of direct comparison, the data plotted in Figure 3.17 (reduction plus sulphidation) have been combined and plotted in Figure 3.20. All the signal intensities have been normalised for the same receiver gain. It can be observed from Figure 3.20 that the Mo^{V} signals obtained from $H_2S + H_2$ treatment are much smaller than those obtained from H_2 treatment over the whole composition range ($0 \lesssim$ Li/Co $\lesssim 10$). The results suggest that the reduction of Mo^{VI} to Mo^{V}, or to lower valence states, is enhanced in the case of sulphide species. This is supported by the appearance of two new extra signals in the case of sulphided samples: the peak with g = 1.991 is attributed to Mo^{III} species,[81,82] while the other, with a g value of 1.976, remains unidentified.

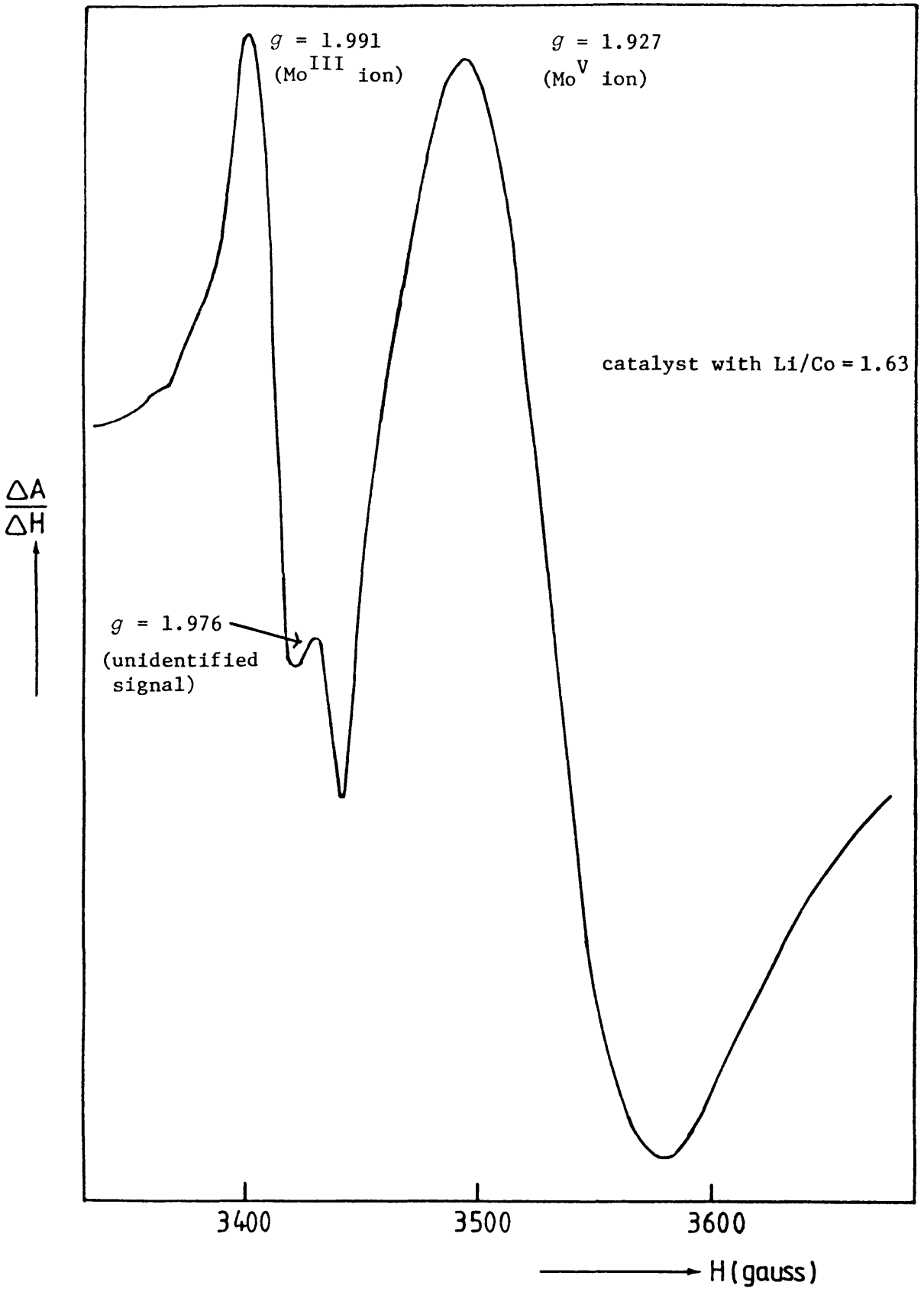

Figure 3.18 A typical e.s.r. spectrum for the lithium-containing series pretreated with a mixture of 10 v % hydrogen sulphide in hydrogen.

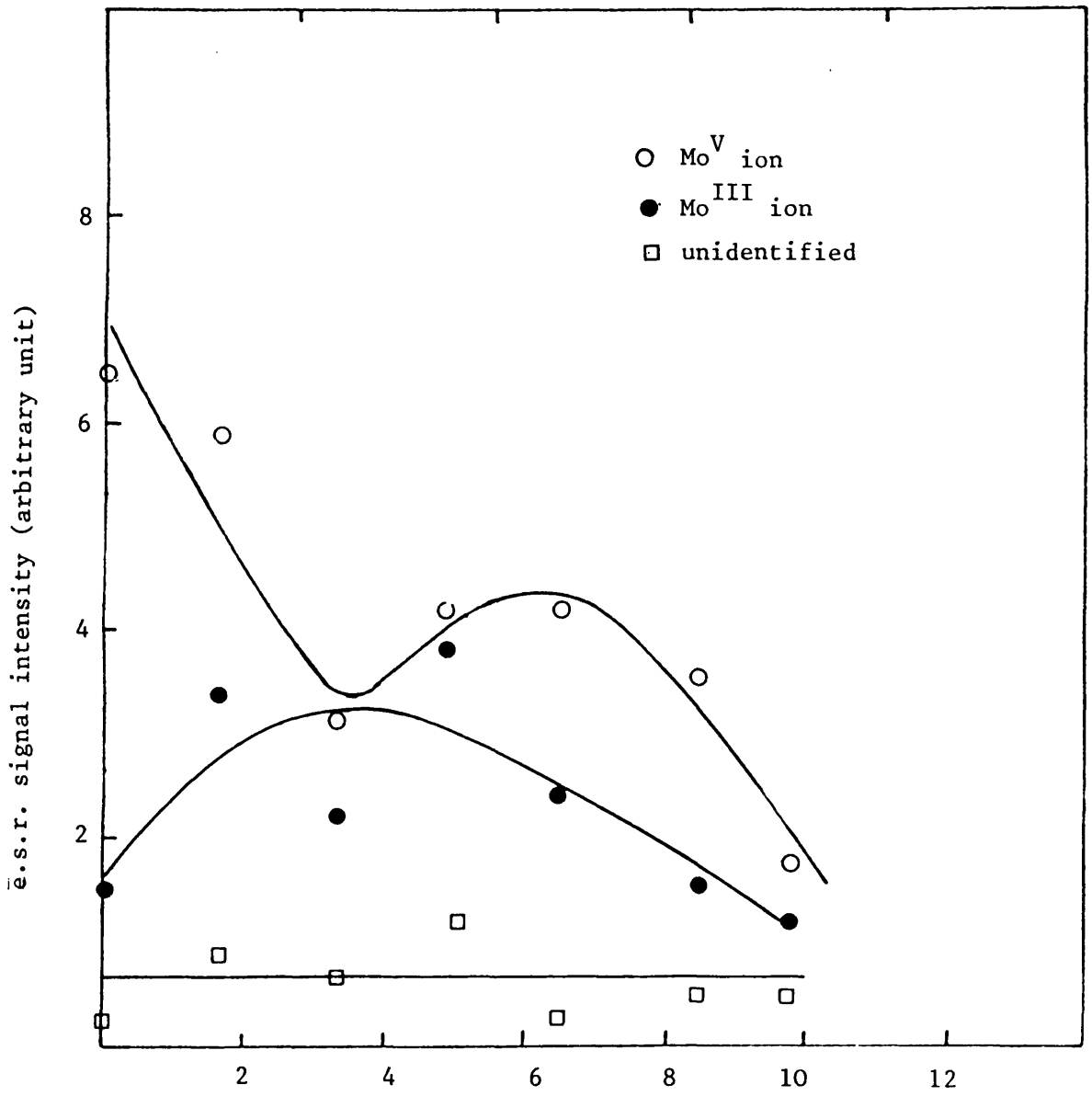

Figure 3.19 Variation of the e.s.r. signal intensity with Li/Co ratio for the lithium containing catalyst series pretreated with a mixture of 10 vol % of hydrogen sulphide in hydrogen

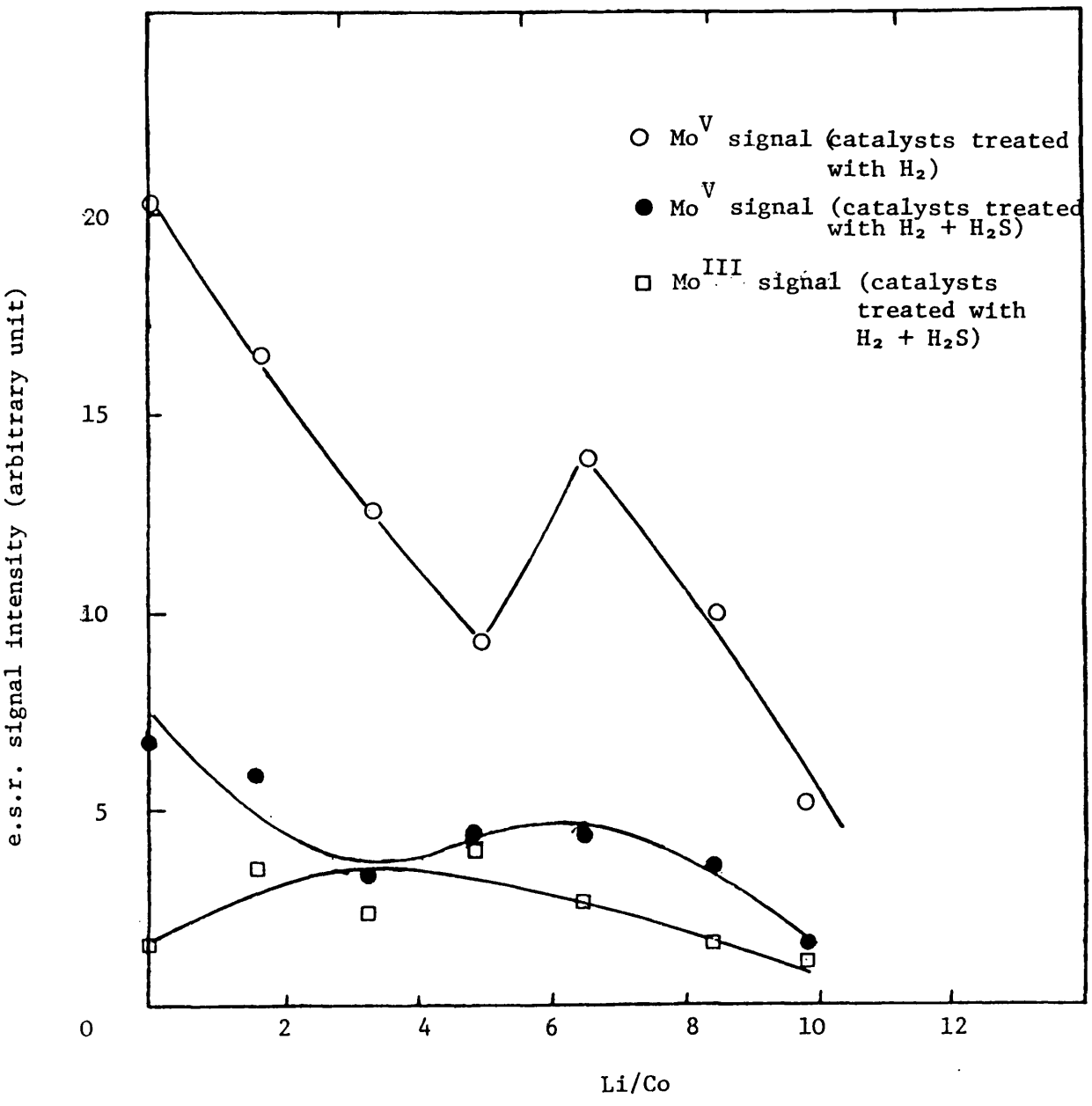

Figure 3.20 Comparison of the e.s.r. signal intensity of reduced catalysts and reduced plus sulphided catalysts against Li/Co atomic ratio.

From a close examination of the experimental results on the reduction and sulphidation experiments (given in Figure 3.19), it can be seen that the Mo^{III} signal intensity attains a maximum value as the Li/Co ratio increases from 0 to 4. This suggests that the reduction of the Mo^{V} species is enhanced as the Li/Co ratio increases to 4. For higher values of the Li/Co ratio (> 4) the Mo^{III} e.s.r. signal intensity begins to decrease while the Mo^{V} signal intensity increases until the Li/Co ratio is about 6.5. This suggests that for values of Li/Co > 4, the reducibility of molybdenum is suppressed by lithium addition. As the Li/Co ratio increases beyond 6.5, the intensity of the Mo^{V} signal begins to diminish again while the Mo^{III} signal continues decreasing. A possible explanation of this phenomenon may be found by superimposing the plots of surface area (see Figure 3.13) and the Mo^{V} and Mo^{III} signal intensities against the Li/Co atomic ratio as shown in Figure 3.21. It has been demonstrated by pore size distribution measurements (see Figure 3.15) that the presence of large amounts of lithium causes the gradual disappearance of a fraction of the pores of the catalysts with a concomitant sharp decrease in surface area. This could be the reason for noting the decrease in the formation of Mo^{V} and Mo^{III} species explained by the decrease in the availability of molybdenum species for reduction. Figure 3.21 shows that both the Mo^{V} signal intensity and the surface area begin to decrease at about the same Li/Co atomic ratio ($\sim$ 7).

In order to elucidate the effect of lithium on the reducibility of molybdenum for catalysts with Li/Co > 7, the signal intensity of Mo^{V} and Mo^{III} per unit surface area were plotted (Figure 3.22).

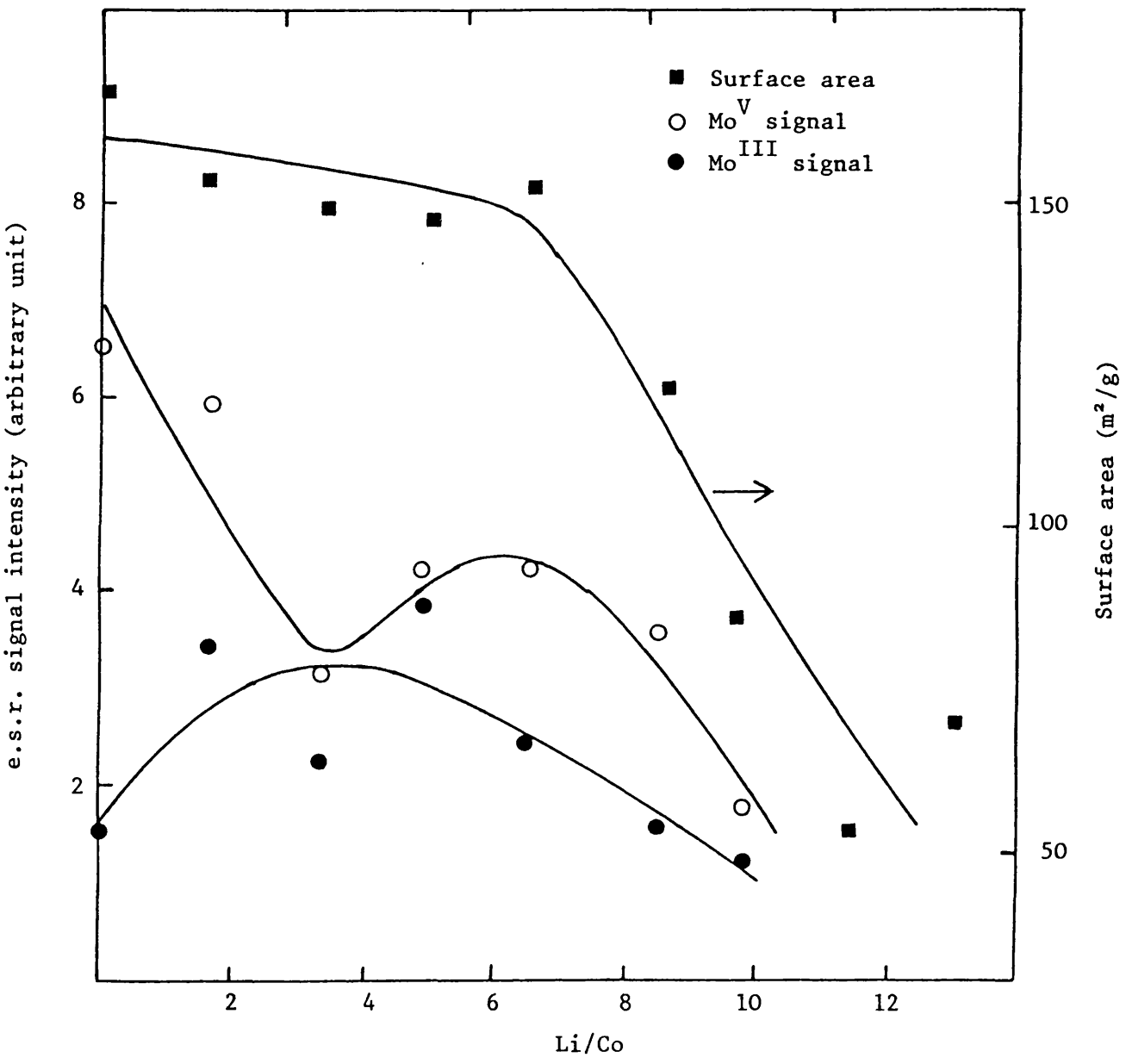

Figure 3.21 Plot of Mo^{V} and Mo^{III} e.s.r. signal intensities and surface area against the Li/Co atomic ratio

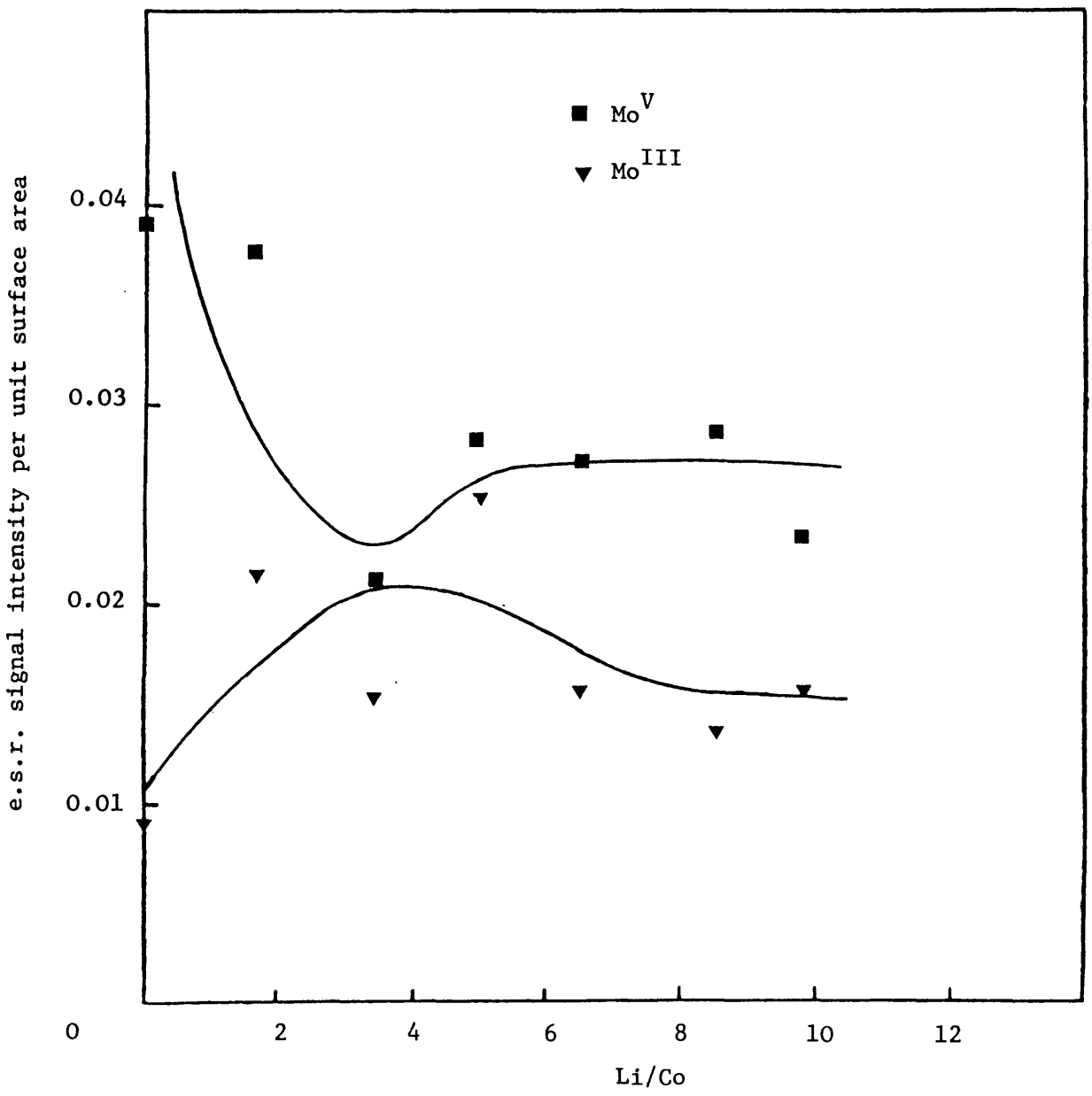

Figure 3.22 Plot of e.s.r. signal intensities per unit surface area against Li/Co atomic ratio.

The intensity of Mo^{V} and Mo^{III} signal per unit surface area in the range of composition Li/Co > 7 remains almost constant, which suggests that the addition of lithium above Li/Co = 7 does not affect the reducibility of molybdenum. For the range of composition $0 \lesssim Li/C \lesssim 7$, where the surface area of the catalysts remains almost constant, the reducibility of molybdenum is clearly affected.

In the case of the catalysts treated with hydrogen, a similar explanation to that given above regarding the effect of lithium on the reducibility of molybdenum can be exploited to interpret the observed variation in the Mo^{V} signal intensity with Li/Co ratio (see Figure 3.17). This explanation may, however, be somewhat speculative because no signal due to the Mo^{III} species was detected in the case of samples treated with hydrogen. The reason for not observing any Mo^{III} signal in the case of samples treated with hydrogen (unlike those treated with hydrogen plus hydrogen sulphide) is that the extent of reduction over the whole range of composition ($0 \lesssim Li/Co \lesssim 10$) is much less in the former case than in the latter, as was pointed out earlier in this section (see Figure 3.20).

3.4 Interpretation of the Catalytic Activity in Terms of Physico-chemical Properties

The lithium series of catalysts used in the present investigation were subjected to physico-chemical characterisation tests, both for the oxide and sulphide forms. *X*-ray diffraction, u.v.-visible reflectance spectroscopy, measurement of the BET surface area and pore size distribution analysis were used to study the catalysts in their oxide form, while e.s.r. spectroscopy was used for the catalysts treated with either H_2 or $H_2S + H_2$ mixtures.

The X-ray studies did not provide any information regarding the structural change of the catalysts due to Li^+ addition (see Figure 3.17), but reflectance studies did show that the addition of lithium does not affect the structural (tetrahedral and octahedral) environment of Co^{2+} or Mo^{6+} ions [see Section 3.3 (1)]. However, the information obtained from physisorption and e.s.r. studies might be used to explain the hds activity of lithium doped Co-Mo/Al_2O_3 catalysts. This is offered as an interpretation in the following section.

(1) Hds reaction

The results of the catalytic activity and surface area measurement for the lithium series of catalysts are given in Figure 3.23. On the basis of these results, the catalyst series can be divided into three ranges:

(a) range $0 \lesssim Li/Co \lesssim 3$ where the activity increases but the surface area remains constant;

(b) range $3 \lesssim Li/Co \lesssim 6.5$ where the catalytic activity decreases without any change in surface area;

(c) range $Li/Co > 6.5$ where both the activity and surface area decrease.

Although the surface area remains constant over the range $0 \lesssim Li/Co \lesssim 6.5$, it decreases sharply for high values of Li/Co atomic ratios (> 6.5). Therefore, in order to understand the effect of lithium addition (independent of surface area) on the catalytic activity, the activity was normalised on the basis of unit surface area and plotted against Li/Co ratios as shown in Figure 3.24. The scattering of the data in this plot is due mainly to the fact that the ratios of activity to surface area were calculated by using the respective experimental values and not by taking data from the graph representing

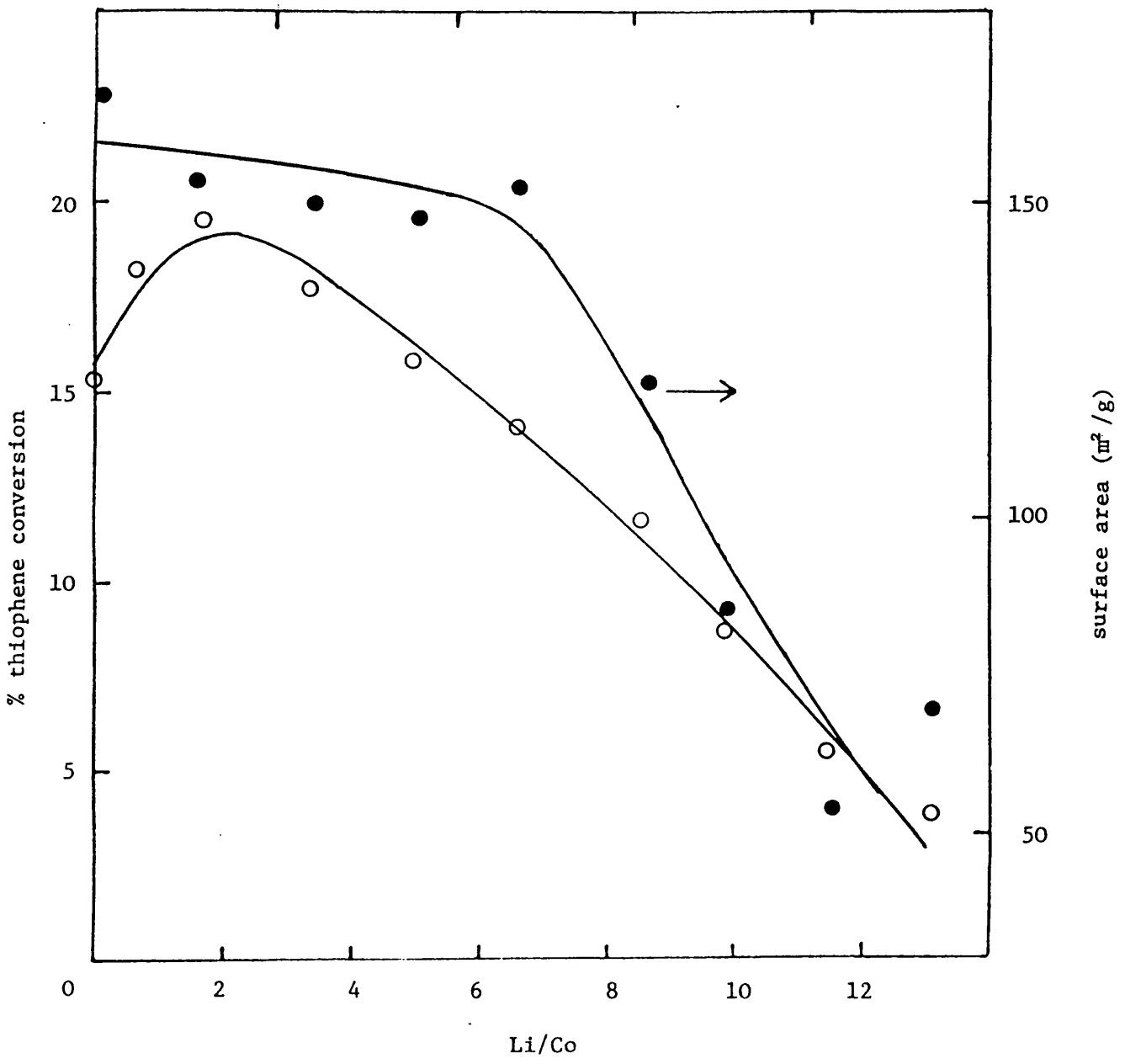

Figure 3.23 Plot of thiophene conversion and surface area *versus* Li/Co atomic ratio.

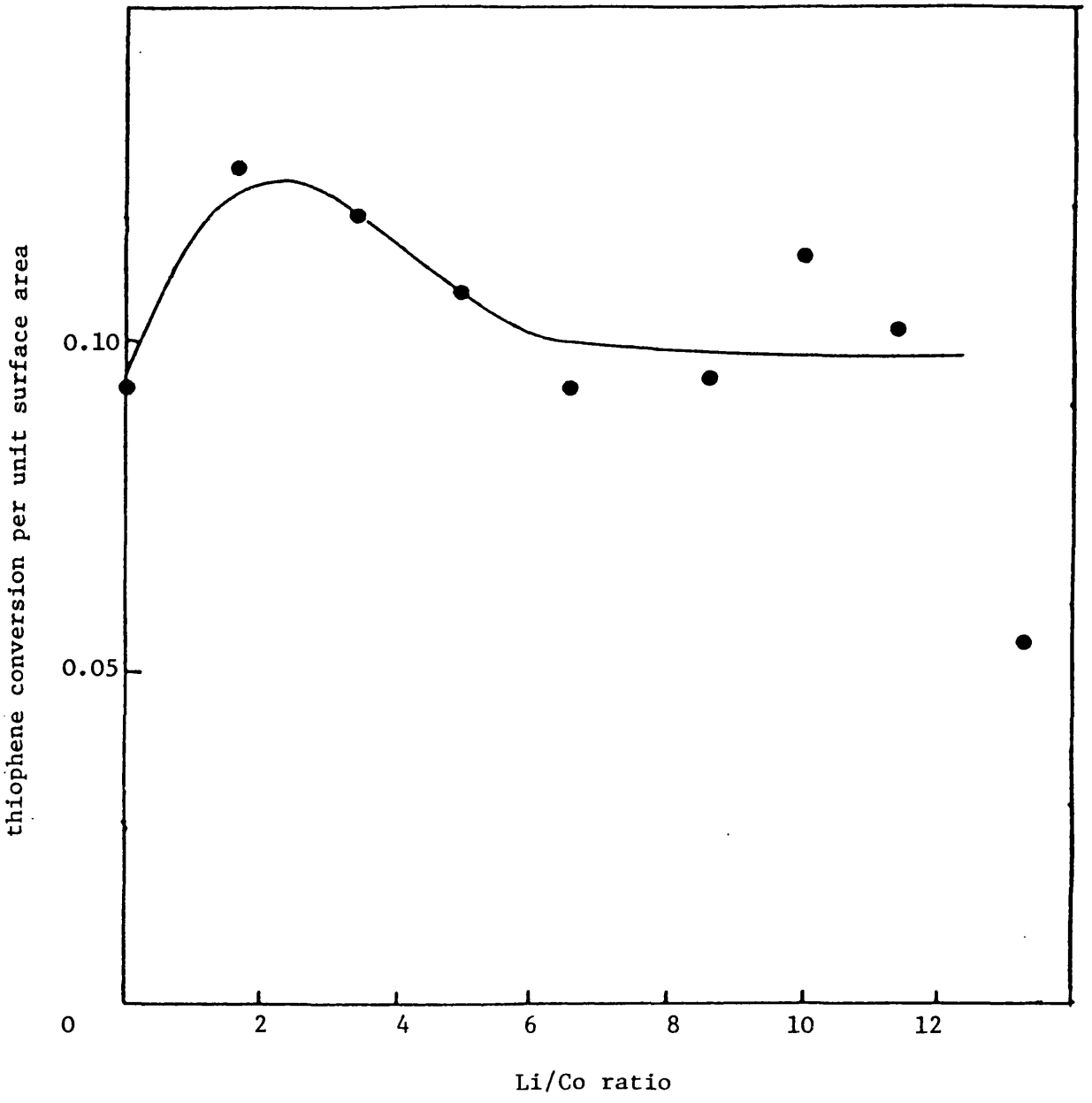

Figure 3.24 Plot of hds activity per unit surface area of the catalyst against Li/Co atomic ratio.

the average trend.

From Figure 3.24 it is clear that the addition of lithium over the first two ranges ($0 \lesssim Li/Co \lesssim 3$) and ($3 \lesssim Li/Co \lesssim 6.5$) affects the hds activity of the catalysts, whereas further addition of lithium (third range, $Li/Co > 6.5$) has no effect on the activity at all.

These results of catalytic studies could be interpreted in terms of the reducibility of molybdenum as affected by the lithium addition which has been revealed by the e.s.r. studies [see Section 3.3 (4)]. The main deductions arising from the e.s.r. studies are given below.

From the pattern of the variation of Mo^{V} and Mo^{III} signal intensities with Li/Co atomic ratio (see Figures 3.19 and 3.22), it appears that the reducibility of molybdenum as influenced by lithium addition can also be divided roughly into three similar composition ranges:

(a) range ($0 \lesssim Li/Co \lesssim 4$) where addition of lithium increases the reducibility of molybdenum;
(b) range ($4 \lesssim Li/Co \lesssim 7$) where addition of lithium hinders the reduction of molybdenum;
(c) range ($Li/Co > 7$) where the addition of lithium has no effect on the reducibility of molybdenum.

In the first range of composition ($0 \lesssim Li/Co \lesssim 4$) the activity increases with the simultaneous increases in the reducibility of molybdenum. The catalytic activity, in the second range of composition ($4 \lesssim Li/Co \lesssim 7$), begins to decrease, together with a decrease in the reducibility of molybdenum. For the catalysts in the composition range $Li/Co > 7$, both the cataltyic activity and the reducibility of molybdenum are not significantly affected by increasing the lithium content. From the above discussion, a direct correlation between the reducibility of molybdenum

and hds activity of the catalysts over the whole range of composition ($0 \leqslant Li/Co \leqslant 13$) is therefore apparent.

It was suggested by Desikan and Amberg[14] that hydrodesulphurisation reactions are associated with molybdenum. This means that any alteration caused in any way to the molybdenum species is likely to affect the desulphurisation reaction. The result of the present investigation does, indeed, support this view. Further support for the correlation between activity and reducibility of hds catalysts has been provided by the work of Ratnasamy *et al.*,[58] in addition to work of Thomas *et al.*[83]

In a recent report, Kelly and Ternan[61] claim that addition of small amounts of lithium to the Co-Mo catalyst enhances its sulphur removal capacity, as observed in the present studies. These authors explained their results in terms of changes in catalyst electronic properties caused by the addition of the metal. The same authors did not perform any experiment to characterise the catalysts either physically or chemically. It is thus probable that their explanation is purely speculative. However, the results of the present catalytic studies are supported by the results of characterisation studies.

It is known[82] that Mo^{IV} species (promoted by the Co^{II} ion) are active sites for hds reaction in Co-Mo/Al_2O_3 catalysts. The present study revealed that the variation of both the catalytic activity and the concentration of Mo^{III} species with respect to the Li/Co ratio, follows the same pattern (see Figures 3.2 and 3.19). Therefore, it would not be unreasonable to suppose that, in addition to Mo^{IV}, Mo^{III} may play an important role as an active species in hds reactions. The role of Mo^{III}

as an active species in hds catalysts has been suggested by earlier workers.[40,84]

(2) Isomerisation and hydrogenation reaction

Studies of isomerisation and hydrogenation reactions occurring simultaneously with the desulphurisation of thiophene have been reported by Amberg and co-workers.[11,15] They associated the desulphurisation and hydrogenation reactions with the strength of acidic sites (Lewis type) of the catalyst.[15] It is well known[85] that the alumina used as support could also catalyse the isomerisation reactions for olefin compounds. However, results of other investigations suggest that, apart from alumina, there are other major components in the sulphide catalyst which might have isomerisation properties. Among these components are:

(a) MoS_2 (studied by Kieran and Kemball[21]);

(b) Co_9S_8 (investigated by Lewis[86]);

(c) a cobalt-sulphur catalyst (patented by Germana and Pollitzer[87]) for selective isomerisation of olefin.

As a standard hds catalyst (sulphided CoO_3-MoO_3/Al_2O_3) may contain a mixture of all these species responsible for isomerisation reactions, the understanding of the problem of olefin isomerisation during thiophene hydrodesulphurisation is far from clear.

Two types of isomerisation reaction occur simultaneously during the hydrodesulphurisation of thiophene: (a) Isomerisation between *cis*- and *trans*-but-2-ene, and (b) isomerisation of but-1-enes and but-2-ene (*cis* and *trans*). The general scheme of these reactions is given below:

but-1-ene

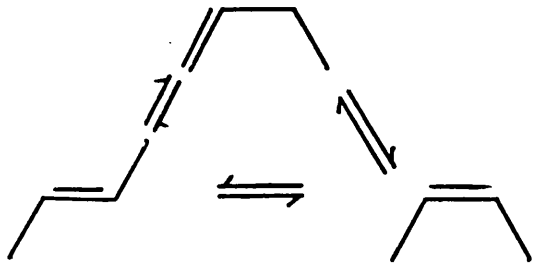

trans-but-2-ene *cis*-but-2-ene

The results of the present investigation concerning the isomerisation reaction occurring during the hds of thiophene are given in Figure 3.7. These results, together with the results for the hydrogenation reaction (given in Figure 3.6) can be explained on the basis of the deductions of Desikan and Amberg.[15] They studied the thiophene desulphurisation simultaneously with the hydrogenation reaction. It was concluded that two kinds of acidic site (Lewis type), one strongly acidic and the other having a low affinity for electrons, were present in the sulphide cobalt-molybdate catalyst. The strong acidic sites are sufficiently electrophilic to interact with the olefin and to hydrogenate them, while the weak sites are considered to be associated with the bulk of the desulphurisation in the hydrogenolysis of thiophene. However, the authors did not attribute these sites to any particular chemical species present in the catalyst, nor did they specify any particular site as being responsible for isomerisation. Nevertheless, they clearly mentioned that there is an interaction between the acidic sites and the olfeins. Apart from this, no clear information is available regarding the sites responsible for isomerisation on a $CoO-MoO_3/\gamma-Al_2O_3$ catalyst. However, a possible explanation of the results observed for the isomerisation and hydrogenation reactions (see Figures 3.6 and 3.7) are postulated. The

strong acidic sites may be considered to be responsible for hydrogenation reactions, as proposed by Desikan and Amberg.[15] These sites could also be associated with the isomerisation reaction between but-1-ene and but-2-ene. Figures 3.6 and 3.7 show that both the hydrogenation and isomerisation (but-1-ene to but-2-ene) reactions are affected when the amount of lithium present in the catalyst increases beyond Li/Co = 6.5. This is perhaps due to the fact that the strong acidic sites, which are likely to be responsible for isomerisation, are affected by the addition of large amounts of alkali metal (Li), although such effect is not significantly noticeable at low concentrations. From Figure 3.7 it can be seen that the ratio of *cis*- to *trans*-but-2-ene remains unchanged over the whole range of Li/Co ratios.

The weak acidic sites may be responsible for the isomerisation between *cis*- and *trans*-but-2-ene. These weak electrophilic sites are, perhaps, not affected at all by the amount of lithium added to the present series of catalysts. The large difference in electron affinity between the strong acid sites and weak sites, which are both present in the catalyst, causes the addition of lithium to affect the former sites more than the latter.

CHAPTER 4

STUDIES ON THE KINETICS OF THE HDS REACTION AND MODELLING OF THE KINETIC DATA

4.1 Introduction

Knowledge of the kinetics of a reaction is essential for the successful design of catalytic reactors. Therefore, in order to predict accurately the conversion, yield and product selectivity, reliable kinetic models are required which can provide a good description of the kinetics of the hds reaction. Mathematical techniques of kinetic modelling have been extensively discussed in the literature, such as chemical engineering texts and reviews.[88-93]

Generally, the mathematical modelling of the kinetics of catalytic reactions is carried out by using either a simple power function law (P.L.) or the Langmuir, Hinshelwood, Hougen and Watson (LH-HW) approach. Before giving more detailed information regarding these two approaches, it is important to mention how the kinetic data are obtained experimentally.

(1) Intrinsic kinetic region

The process of gaseous reaction over a particular catalyst is very complex. It involves the transport of reactants and products to and from the bulk of the gaseous phase and the catalyst surface, adsorption and desorption of reactants and products and also the chemical transformation occurring on the active sites of the catalyst. Two types of transport processes can be identified, namely external and internal transport. The chemical transformation involves three steps: chemisorption of at least one of the reactants, chemical reaction and desorption of the products. Any of the steps involved in either the transport processes or chemical transformation may be rate limiting and therefore the controlling factor in determining the reaction rate.

In order to obtain intrinsic kinetic data, experiments must be carried out under conditions where the transport effects, either mass or heat transfer, are negligible or at least minimised. In the present work various experimental tests were carried out to determine the intrinsic kinetic region where transport effects were negligible. Under such conditions, models of the rate of reaction were based only on the steps involved in the chemical transformation. The choice of kinetic models as well as their discrimination is based mainly on the mechanistic information of the reaction presented in Chapter 1.

4.2 Power Law Rate Model

Let us consider a general reaction of the form:

$$A + B \longrightarrow C + D \qquad (4.1)$$

The rate of reaction may be written:

$$r(P_i, T) = k(T) f(P_i, T) \qquad (4.2)$$

The constant k is the reaction rate constant which depends only on the temperature T. This constant k is often represented according to the law proposed by Arrhenius

$$k = A.e^{-E/RT} \qquad (4.3)$$

where A = pre-exponential factor approximately independent of temperature;

E = apparent activation energy; and

R = gas constant.

The function f(Pi,T) depends mainly on the partial pressure of the reactants, products and inhibitors. This function may also depend on the temperature. Very often f(Pi,T) is temperature independent and to a high degree of approximation can be written as:

$$f(Pi,T) = \prod_i Pi^{n_i} \tag{4.4}$$

where n_i is the order of reaction with respect to each of the 'i' species. Then the rate of reaction is represented as:

$$r = (Ae^{-E/RT}) P_A^{n_A} P_B^{n_B} P_C^{n_C} P_D^{n_D} \tag{4.5}$$

In cases where the experimental data have been forced to fit this type of rate expression it may be found that the orders of reaction vary with temperature. In such cases the observed correlation should be applied only in a restricted and specified temperature interval.

4.3 LH-HW Kinetic Models

The LH-HW approach was developed by Hougen and Watson[88] as an extension of the Langmuir-Hinshelwood kinetic theory of catalyst surfaces.[89] The LH-HW kinetic equations are the result of the application of Langmuir's adsorption theory to heterogeneous catalytic reactions. This theory provides a method for relating the equilibrium surface concentration of an adsorbed species to the partial pressure of that species. The Langmuir theory is based on the following assumptions:

(i) Adsorbed molecules are localised at definite sites on the surface.

(ii) The differential energy of adsorption is independent of the coverage.

(iii) The maximum possible adsorption corresponds to a monolayer.

(iv) The rate of adsorption is proportional to the product of the partial pressure and the number of unoccupied sites.

(v) The rate of desorption is proportional to the number of molecules adsorbed.

On the basis of these assumptions an expression for the fractional coverage of any species in terms of the partial pressure of all the species present may be derived considering that the adsorption and desorption steps are in equilibrium. This can be easily visualised from the following general irreversible reaction:

$$A + B \longrightarrow C + D \qquad (4.6)$$

The steps involved in the reaction on a surface site, S, could be written as:

(i)	$A + S \rightleftharpoons AS$	Adsorption of A	(4.7)
(ii)	$B + S \rightleftharpoons BS$	Adsorption of B	(4.8)
(iii)	$AS + BS \longrightarrow CS + DS$	Surface reaction of adsorbed A and B	(4.9)
(iv)	$CS \rightleftharpoons C + S$	Desorption of C	(4.10)
(v)	$DS \rightleftharpoons D + S$	Desorption of D	(4.11)

Suppose that A and B adsorb on a single site (as written above) and the surface reaction [equation (4.9)] is the rate limiting step. The other steps are assumed to be in equilibrium. Their adsorption equilibrium constant is given by:

$$K_i = \frac{\theta_i}{P_i \theta_s} \qquad (4.12)$$

$$(i = A, B, C, D)$$

where θ_i is the fractional coverage of the species 'i' and θ_s is the fraction of vacant sites. θ_i may be expressed as:

$$\theta_i = \frac{K_i P_i}{(1 + K_A P_A + K_B P_B + K_C P_C + K_D P_D)} \qquad (4.13)$$

$$(i = A, B, C, D)$$

If the species A requires n site for adsorption and species B m sites, the fractional coverage of A and B are then given by:

$$\theta_A = \frac{K_A P_A}{(1 + K_A P_A + K_B P_B + K_C P_C + K_D P_D)^n} \qquad (4.14)$$

$$\theta_B = \frac{K_B P_B}{(1 + K_A P_A + K_B P_B + K_C P_C + K_D P_D)^m} \qquad (4.15)$$

If the species A dissociates into two parts on adsorption, the fractional coverage of A becomes:

$$\theta_A = \frac{\sqrt{K_A P_A}}{(1 + \sqrt{K_A P_A} + K_B P_B + K_C P_C + K_D P_D)} \qquad (4.16)$$

Let us consider now that two different sites exist on the surface of the catalyst. Assuming that species A and C are associated with one kind of site, while species B and D are associated with another kind of site, the fractional coverage of A and B is given by:

$$\theta_A = \frac{K_A P_A}{(1 + K_A P_A + K_C P_C)^n} \tag{4.17}$$

$$\theta_B = \frac{K_B P_B}{(1 + K_B P_B + K_D P_D)^m} \tag{4.18}$$

The rate expression for the irreversible reaction may then be formulated as follows:

(a) According to the Langmuir-Hinshelwood mechanism (which assumes surface reaction between adsorbed molecules (A and B) as the rate limiting step:

$$r = k\theta_A\theta_B \tag{4.19}$$

(b) According to the Eley-Rideal mechanism (which assumes surface reaction between adsorbed species A and B in the gas phase as the rate limiting step):

$$r = k\theta_A P_B \tag{4.20}$$

(c) According to one of the Hougen-Watson mechanisms [which might, for example, assume that adsorption of A is the rate limit step ($\theta_A \simeq 0$)]:

$$r = kP_A\theta_S \tag{4.21}$$

The LH-HW rate model-building technique is based on Langmuir's theory of adsorption. The assumptions involved do not necessarily hold in practice. Boudart[94] and Weller[95] have critically discussed this technique, its applicability and its limitations. Furthermore, the LH-HW rate expressions are obtained by assuming that one step controls the overall rate of the reaction while the other steps are at equilibrium for all reaction temperatures. However, Thaller and Thodos[96] have shown that the rate limiting step could change depending on the operating condition. Apparently, it seems that the LH-HW model-building technique is of very limited application, but the fact remains that many catalytic reaction rates cannot be described adequately by using a simple model, especially when the reaction is inhibited by the reactants and/or by products.

(a) Discrimination between rival models

It may happen that more than one model describes mathematically the experimental rate data. This creates a need for selecting an appropriate model and discriminating between such a model and others on the basis of further information. Model discrimination between rival models may be achieved by both chemical and statiscally oriented approaches.

The chemical approach permits a choice of the rate expression based on knowledge obtained from physicochemical studies. The statistical approach allows a choice of model based on goodness of fit of the experimental data. Mezaki and Happel[97] have published a detailed review of the discrimination techniques for solid catalysed

gaseous reactions.

Another criterion which can be used to aid discrimination between LH rival models has been suggested by Boudart *et al.*[98]. they proposed a series of rules to examine the standard entropy (ΔS_a°) of adsorption (derived from the adsorption constant deduced from the models). These rules are:

Rule 1	$\Delta S_a^\circ < 0$	
Rule 2	$\lvert\Delta S_a^\circ\rvert < S_g^\circ$	S_g° standard entropy of the gas
Rule 3	$\lvert\Delta S_a^\circ\rvert < 10$ e.u.	1 e.u. = 1 cal/(mole K)
Rule 4	$-\Delta S_a^\circ < 12.2 - 0.0014\ \Delta H_a^\circ$	

The first two rules should be rigorously obeyed while the other are more or less empirical.

4.4 Results

(1) Intraparticle and interparticle mass transfer effects

In the present investigation various experimental tests were carried out to determine the intrinsic kinetic region where mass transport (external or internal) was not influencing the rate of reaction. Corrigan[99] described in detail how to conduct such tests. To check for external (interparticle) mass transfer, the reactor was loaded with different amounts of catalyst by keeping the ratio of mass of catalyst to total gas flow rate (W/F) constant. Conversion was then measured at various reaction temperatures. On the other hand, to check for internal (intraparticle) diffusion effects, the reactor was loaded each time with the same amount of catalyst using, in each case, different particle sizes.

Two catalysts were chosen for the hds kinetic studies (Li/Co = 0.0 and Li/Co = 1.63). However, the mass transfer limitation tests were carried out on the lithium free catalyst only since the physical characterisation studies (see Section 3. , Chapter 3) (BET surface, area and pore size distribution) indicated no significant difference between these two catalysts. The results of these tests are shown in Table 4.1. It can be seen from the table that (i) the conversion of thiophene remains unchanged when W/F is constant, (ii) change in particle size does not influence the rate of reaction. These results indicate that the effects of external and internal mass transfer are minimum in the range of temperature studied. Therefore the kinetic data collected over this range of conditions is believed to be close to true hds kinetics.

(2) Kinetics of the hds reaction over lithium free (Li/Co = 0.0) and 0.25 wt % Li cobalt molybdate catalysts (Li/Co = 1.63)

It is generally accepted[2,3] that the reaction of thiophene hydrodesulphurisation can be represented as a consecutive reaction (A → B → C) as shown below:

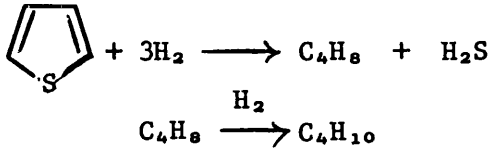

Kinetic data for the first reaction has been obtained over two cobalt molybdate catalysts (Li/Co = 0.0 and Li/Co = 1.63) by using a differential reactor working at atmospheric pressure. The kinetic

$W/F_{total} = 418 \frac{g}{mole\ s}$ $P_t = 20$ mmHg

mass of catalyst (mg)	80	50	44
% conversion at 260° C	0.62	0.59	0.60
% conversion at 320° C	2.1	1.9	2.2

(a) External mass transport test

	% Conversion at 260° C		% Conversion at 320° C	
P_t	Particle size		Particle size	
(mmHg)	150-180 μm	250-500 μm	150-180 μm	250-500 μm
11	0.83	0.76	2.4	2.5
20	0.53	0.59	1.9	1.9
31	0.44	0.43	1.6	1.5
57	0,35	0.36	1.5	1.3
101	0.20	0.21	0.91	1.0

(b) Internal mass transport test

Table 4.1 External and internal diffusion tests

data have been summarised in Appendix B-2 where the computations of the rate of disappearance of thiophene (r) is based on a material balance within an elementary volume of the tubular reactor. This equation is:

$$r = F_t \frac{dx}{dw} \qquad (4.22)$$

where F_t is the thiophene flowrate, W is the weight of catalyst and X is the conversion.

The experimental error ($\Delta r/r$) involved in the rate was found to be within 6%. It was calculated on the basis of the errors involved in F_t and X. The error in measuring the weight of the catalyst (W) was negligible compared to that involved in F_t and X.

The kinetic data obtained from the differential reactor employed, where the effect of reactants and products could be studied separately, are presented in the following way.

(i) Effect of thiophene concentration on the rate of reaction

Pure thiophene added to a stream of hydrogen enabled the effect of thiophene on the rate of the hds reaction to be investigated. The desired partial pressure of thiophene was set by adjusting the hydrogen flowrate and the delivery rate of thiophene. Figures 4.1 and 4.2 illustrate the effect of thiophene concentration on the rate of disappearance of thiophene over the two cobalt molybdate catalysts (Li/Co = 0.0, Li/Co = 1.63). Both the figures show clearly that the rate of the desulphurisation reaction is less than first order with respect to thiophene. The order of the reaction tends to zero, particularly at low temperatures and at relatively high partial pressure of thiophene.

The inhibition effect of thiophene on the rate of reaction has also been reported by earlier workers.[33-36] However, such claims that thiophene inhibits hds reaction are not entirely clear and this

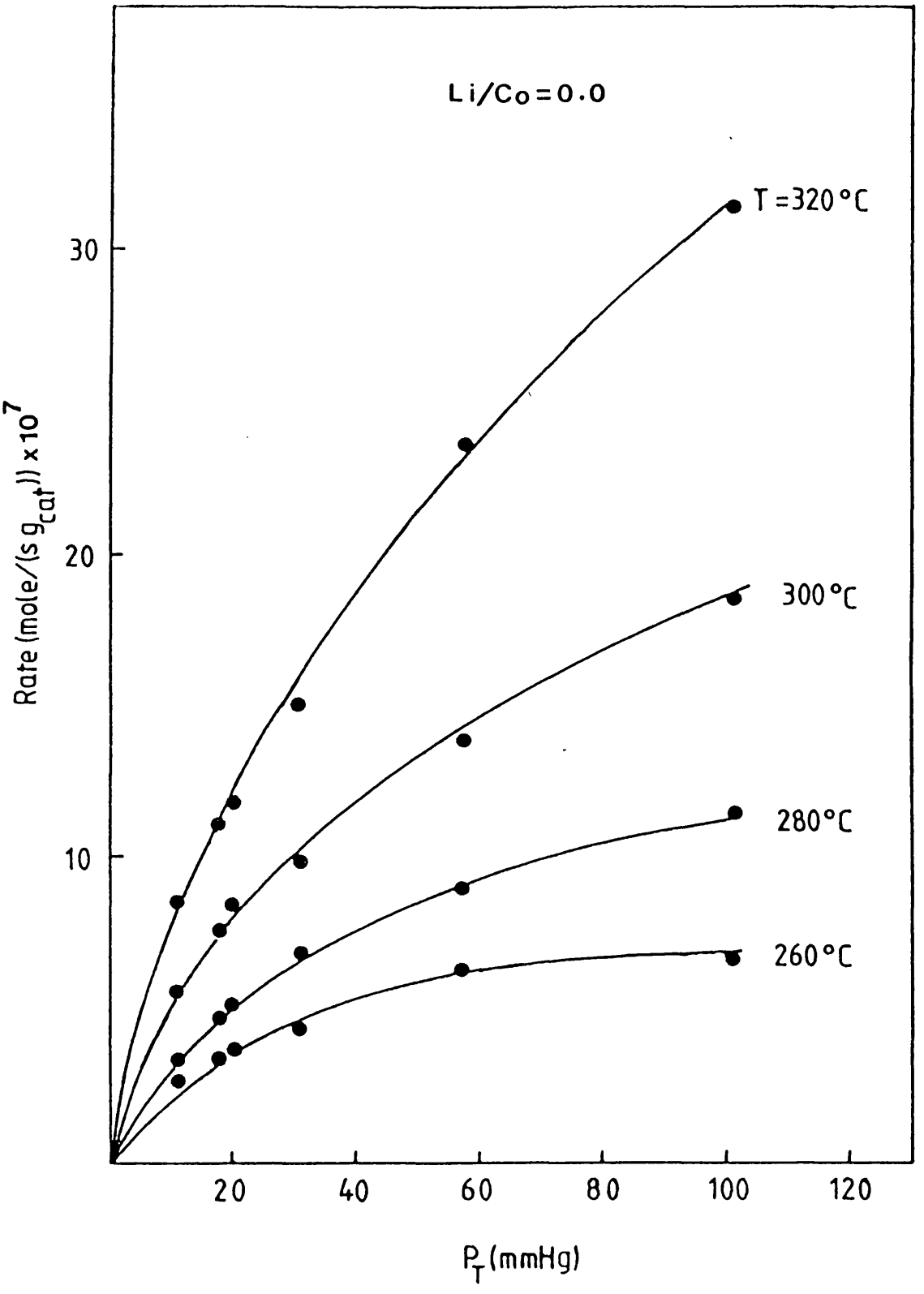

Figure 4.1 Variation of the rate of reaction with thiophene partial pressure at various temperatures for the lithium free cobalt molybdate catalyst (Li/Co = 0.0)

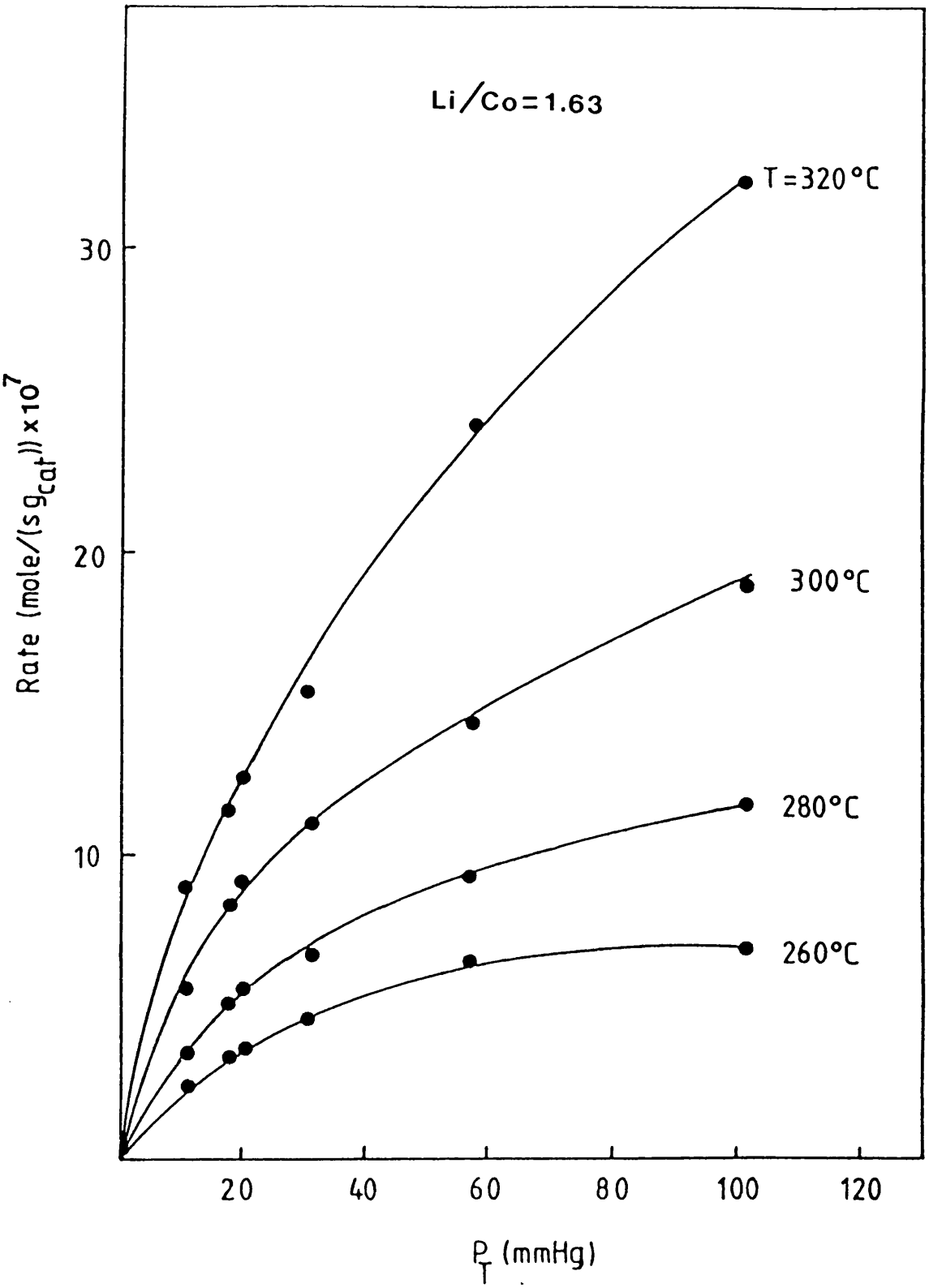

Figure 4.2 Variation of the rate of reaction with thiophene partial pressure at various temperatures for the cobalt molybdate catalyst with 0.25% lithium (Li/Co = 1.63)

will be discussed in detail in the subsequent section.

(ii) Effect of hydrogen sulphide concentration on the rate of reaction

The effect of hydrogen sulphide on the hds reaction rate was determined experimentally by using a mixed feed of hydrogen sulphide with thiophene and hydrogen. The partial pressure of thiophene was held constant for all the runs with mixed feed while the partial pressure of the hydrogen sulphide was adjusted by varying the hydrogen flow rate and thus keeping the total flow rate constant. The effect of the hydrogen sulphide on the rate of reaction is shown in Figures 4.3 and 4.4 for the two cobalt molybdate catalysts chosen for the kinetic studies. The inhibition effect of hydrogen sulphide was found to be very strong at low concentrations of H_2S. This suppression effect on the rate of reaction is more marked as the temperature of the reaction increases.

4.5 Discussion of the Kinetic Results

No significant difference between the rates of reaction has been found for either of the two cobalt molybdate catalysts (Li/Co = 0.0; Li/Co = 1.63) over the range of temperature studied. These results seem to conflict with the results of activity studies on these two catalysts reported in Chapter 3. However, the sample with Li/Co = 1.63 showed higher hds activity than that of the sample with Li/Co = 0.0 in spite of the fact that the reaction kinetics are identical on both the samples. A possible reason may be that the maximum temperature of the reaction for the kinetic test (320° C) was lower than that used for activity tests (400° C).

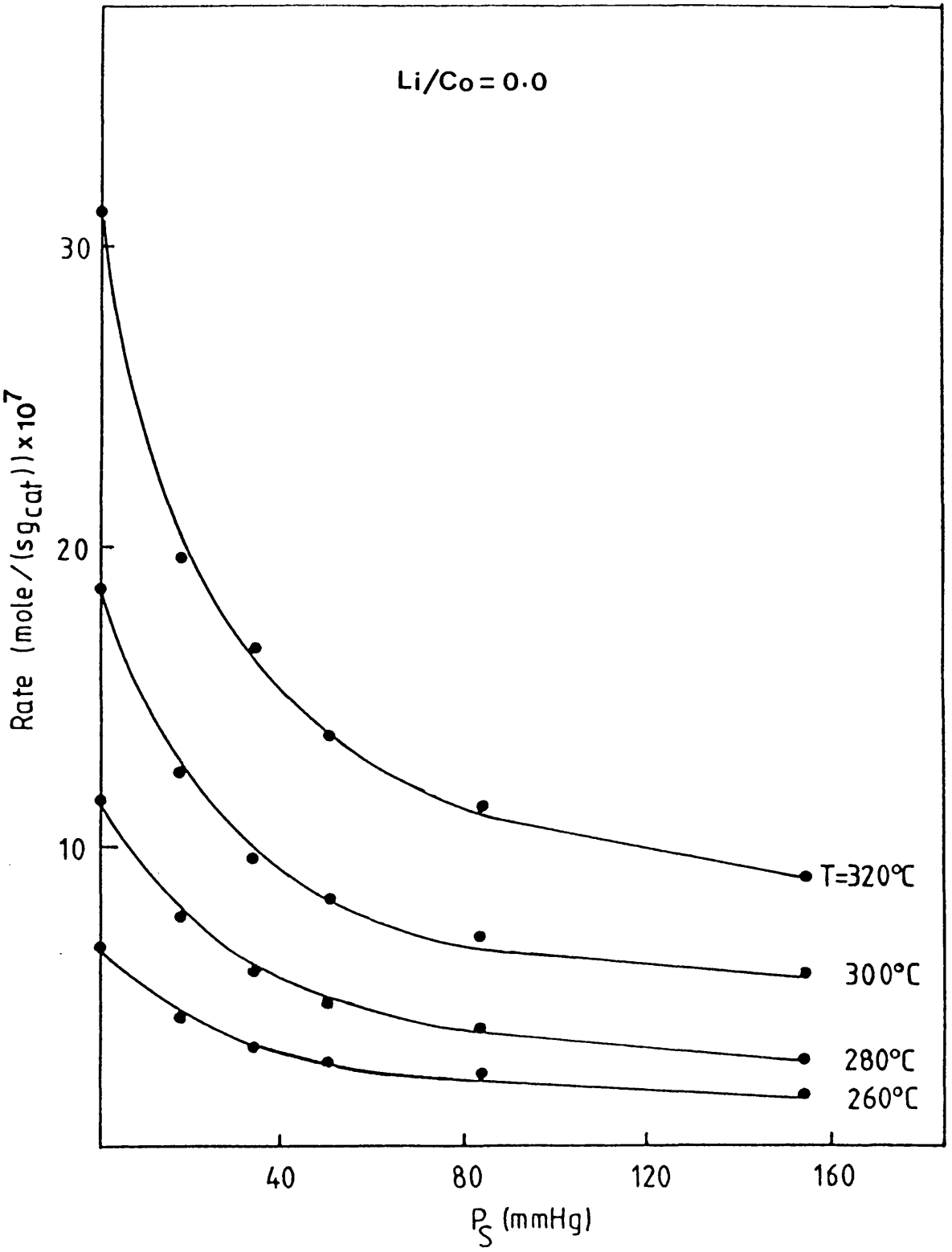

Figure 4.3 Variation of the reaction rate with the hydrogen sulphide partial pressure at various temperatures for the lithium free cobalt molybdate catalyst

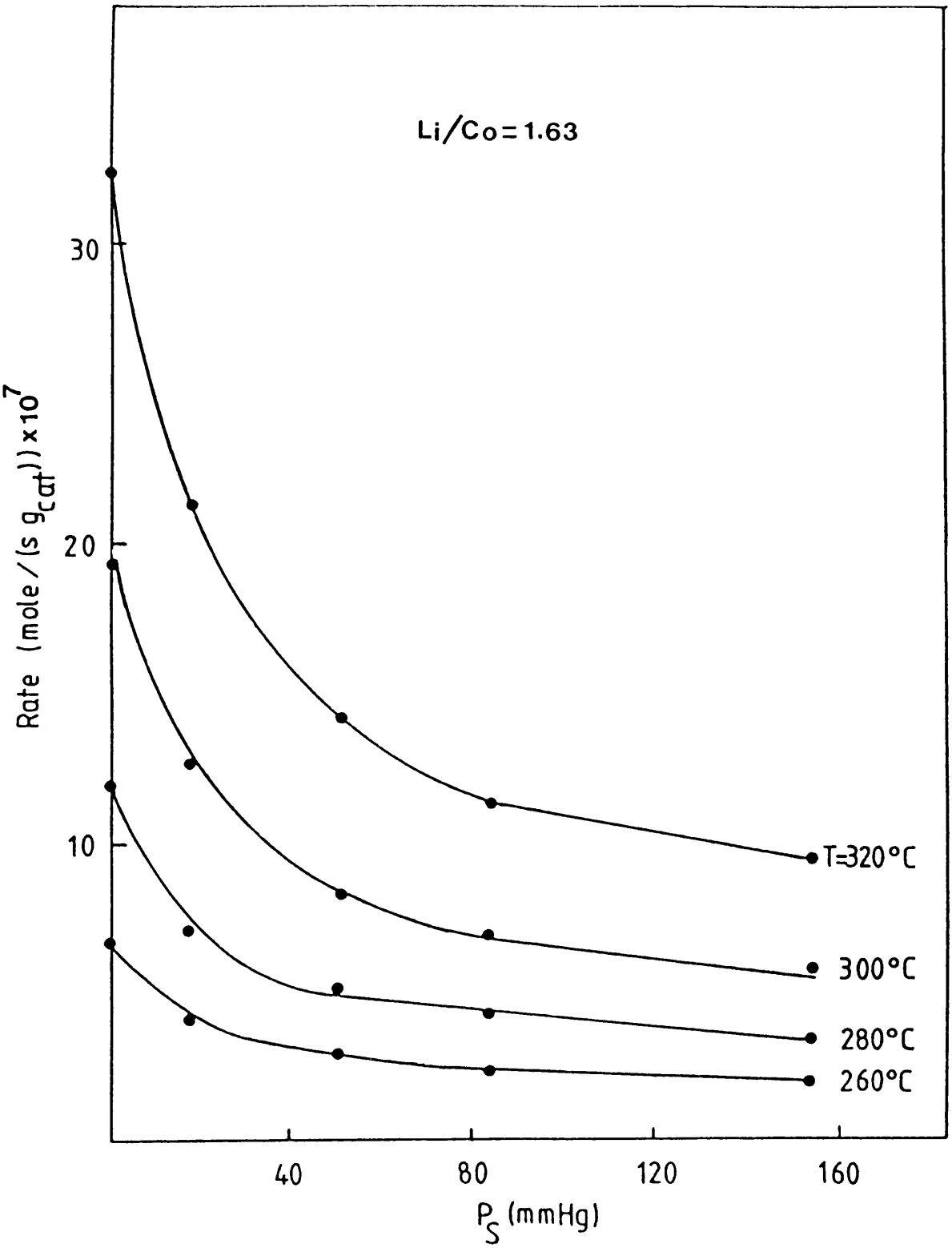

Figure 4.4 Variation of the reaction rate with hydrogen sulphide partial pressure at various temperatures for the cobalt molybdate catalyst containing 0.25% lithium

This suggests that the activation by lithium may depend on the temperature employed for hds. Other factors such as the small amount of catalyst used for kinetic studies could also account for these insignificant differences of rate between the two catalysts. It was, of course, necessary to choose conditions of low temperature and small amounts of catalyst for the kinetic studies to achieve conversion less than 3% (differential operating conditions). Attempts to model the kinetics of hds reaction will be based on the catalyst with Li/Co = 0.0 in view of the fact that there is no significant difference between the kinetic data for the two catalysts studied.

The effects of reactants and products on the rate of reaction of hydrodesulphurisation of thiophene have been reported by several investigators.[33,34,36] Their experiments were carried out using batch and external or internal recycle reactors. In such reactor types the reactants and products are always mixed together in appreciable amounts. Therefore the effects of thiophene and hydrogen sulphide on the rate of reaction are very difficult to evaluate. The use of a tubular differential reactor helped to overcome this problem since the reactor operates at very low conversions (*i.e.*, very little product is formed). This enables one to examine clearly the effect of thiophene on the reaction rate. On the other hand, by using a mixed feed of reactant with at least one of the products (thiophene + H_2S) and by keeping the thiophene concentration constant, the effect of hydrogen sulphide on the rate could be assessed with little difficulty.

4.6 Modelling of the Reaction Kinetics Data

(1) Numerical estimation of kinetic parameters

Two numerical estimation techniques were used to evaluate the unknown parameters in a particular kinetic rate expression. These techniques are described briefly below:

(i) Multivariable linear regression analysis

This technique was applied to the cases where the kinetic rate expression can be transformed into a linear expression such as:

$$y = \beta_o + B_1X_2 + \beta_2X_2 + ... \qquad (4.23)$$

where y is a function depending on the observed rate and often on the partial pressure of the reactants. The variables X_i are usually the partial pressures of reactants and products and β_i are the kinetic parameters to be determined. The technique minimises the sum of squares of residuals (SSR).

$$SSR = \sum_{i=1}^{n} (y_{ob\ i} - y_{pred\ i})^2 \qquad (4.24)$$

The estimated parameters which minimise the SSR are evaluated by solving the following matrix:

$$b = (X^TX)^{-1}X^TY \qquad (4.25)$$

where b is the matrix of the bi estimated values of β_i, X is the matrix of the independent variables at each observation (X_{ij}), Y is the matrix of the dependent variable at each observation (y_i) and X^T is the transpose of X. Details of the linear regression analysis can be found in Draper and Smith.[100]

It may be pointed out here that the dependent variable y in equation (4.24) contains the observed rate of reaction lumped with some other terms. The minimisation of the SSR is with respect to the lumped variable y and not based solely on the rate observed. Furthermore, the estimated parameters β_i are not the kinetic parameters, but a combination of them.

The advantage of this technique is its simplicity in application and also the low computing time required. The computer programme for linear regression analysis used in this study is part of a statistical programme package (Minitab) developed by the Statistics Department, Pennsylvania State University, U.S.A. Details of the programme package are given in reference 101.

(ii)Non-linear regression analysis

Kinetic rate expressions may be formulated in non-linear form. Non-linear regression analysis techniques provide a direct estimation of the unknown kinetic parameters by minimising the SSR based on the observed rate.

$$SSR = \sum_{i=1}^{n} (r_{obs\ i} - r_{pred\ i})^2 \qquad (4.26)$$

where r_{obs} and r_{pred} are observed and predicted rates respectively.

The non-linear regression analysis used in this investigation was a P3R subroutine from the Biomedical program package, Health Science Computing Faculty, University of California, U.S.A. The subroutine requires the non-linear function, the partial derivatives with respect to each of the unknown parameters and the initial values of the parameters.

The programme stops when a convergence criterion, c, is satisfied for 5 successive iterations, K.

$$\frac{SSR\ (K + 1) - SSR\ (K)}{SSR\ (K + 1)} < C$$

Details of the subroutine are given in reference 102.

The computer programmes for linear and non-linear regression analyses were made available through the South Western University Computer network, University of Bath.

(2) Adsorption of reactants and products

Studies on the adsorption of reactants (hydrogen, thiophene) and products (C_4-hydrocarbons, hydrogen sulphide) were carried out over cobalt-molybdate catalysts, using the catalyst as oxide, reduced, or reduced and sulphided forms.[11,19,58,103-108]

(a) Adsorption of reactants

The reversible adsorption of hydrogen has been reported by several workers[19,103,104] and the adsorption appears to be negligible at room temperature.[103]

The kinetics of adsorption of hydrogen were studied in the temperature range 150-280° C.[105] The activation energy was found to be about 50 kcal/mol, which was indicative of a dissociative type chemisorption. In their studies Owen and Amberg[11,13] found that there are two types of adsorbed hydrogen, one very strongly chemisorbed and the other weakly and reversibly adsorbed. Based on their experimental evidence they claimed that the weakly reversibly adsorbed (or perhaps even non adsorbed) hydrogen is necessary for the desulphurisation reaction to occur. The strongly adsorbed hydrogen was found to be almost inactive, although it was believed to play an important role in modifying the adsorption of thiophene.

Thiophene adsorption has been reported to be reversible,[11,58,106-108] although irreversible adsorption of thiophene has also been observed.[19] The temperature coefficient, which gives an idea of the order of magnitude of the heat of adsorption, was found to be 9.5 kcal/mol.[11]

(b) Adsorption of products

Adsorption of butanes in cobalt-molybdate catalysts was found to be 10 to 15 times weaker than thiophene adsorption.[11] A temperature coefficient of 8.5 kcal/mol was calculated for butene adsorption. The weak adsorption of butanes suggests that these products should not have any significant effect on the desulphurisation reaction rate.

In the case of hydrogen sulphide, a reversible adsorption has been observed experimentally.[11,58,107] The rate of desorption was found to be very slow and proportional to the surface coverage. On the other hand, it has also been found that hydrogen sulphide can adsorb and decompose on alumina,[109] which is commonly used as a support for cobalt-molybdate catalysts. The rate of thiophene desulphurisation is affected significantly by the presence of adsorbed hydrogen sulphide.[11,34-36]

(3) Power law rate expression

Kinetic data for the thiophene desulphurisation reaction given in Appendix B-2 was obtained in two ways: (i) by using a thiophene feed in hydrogen and (ii) by using a mixed feed (thiophene and hydrogen sulphide) in hydrogen.

In the former case, the effect of the hydrogen sulphide on the rate of reaction was considered to be negligible over the range of

partial pressures of thiophene studied because of the low conversion and hence very small amount of hydrogen sulphide found in the product. In the latter case the partial pressure of thiophene was held constant over the entire range of partial pressures of hydrogen sulphide studied and leads one to consider two power law rate expressions of the type given in equation (4.5) to describe the kinetic data.

$$r_1 = k_1 P_t^{n_t} \text{ for } P_S \sim 0,\ P_t \text{ VARIABLE} \tag{4.27}$$

where

$$k_1 = A_1 e^{-E/RT};\quad A_1 = A_{o1} P_h^{n_h} \tag{4.28}$$

and

$$r_2 = k_2 P_S^{n_S} \text{ for } P_S \text{ variable},\ P_t = 101 \text{ mmHg} \tag{4.29}$$

where

$$k_2 = A_2 e^{-E/RT};\quad A_2 = A_{o2} P_h^{n_h} P_t^{n_t} \tag{4.30}$$

These two rate expressions were assumed to be independent of the hydrogen partial pressure because the variation in the partial pressure of hydrogen (12%and 23%) in the two cases discussed above covers a narrow range to determine a meaningful rate of reaction with respect to hydrogen.

The term A_1 in equation (4.28) includes the partial pressure of hydrogen while the term A_2 in equation (4.30) contains the partial pressure of thiophene in addition to hydrogen. In other words, they are not proper pre-exponential factors independent of temperature and concentration. Equations (4.27) and (4.29) were linearised and treated, over a range of temperature, by a multivariable linear regression analysis technique using the kinetic data given in Appendix B-2. The results are given in Table 4.2.

$\ln A_i$*	E	n_t	n_s	R^2
(i = 1, 2)	(kJ/mole)			(%)
-3.78	56.4 (13.5)	0.52	-	98
1.12	64.4 (15.4)	-	-0.41	99

*$A_1 = A_{o1} P_h^{n_h}$; $A_2 = A_{o2} P_h^{n_h} P_t^{n_t}$ where P_t = 101 mmHg

The values in parentheses express the activation energy (E) in kcal/mole

Table 4.2 Result of analysis on Power Law Rate Expression

The order of reaction with respect to thiophene and hydrogen changes slightly with the reaction temperature. This can be seen by applying linear regression analysis to the kinetic data at each temperature level. The variation in the order of reaction with temperature is shown in Table 4.3.

T (° C)	n_t	n_s
260	0.43	-0.42
280	0.54	-0.38
300	0.52	-0.40
320	0.60	-0.46

Table 4.3 Variation of the order of reaction with temperature

Figures 4.5 and 4.6 show the graphs of the calculated reaction rate according to equations (4.27) and (4.28), and the results of Table 4.2 plotted against the observed rate. The error in the rate (e%), defined by the relation given below, lies between 0.6 and 19.3%.

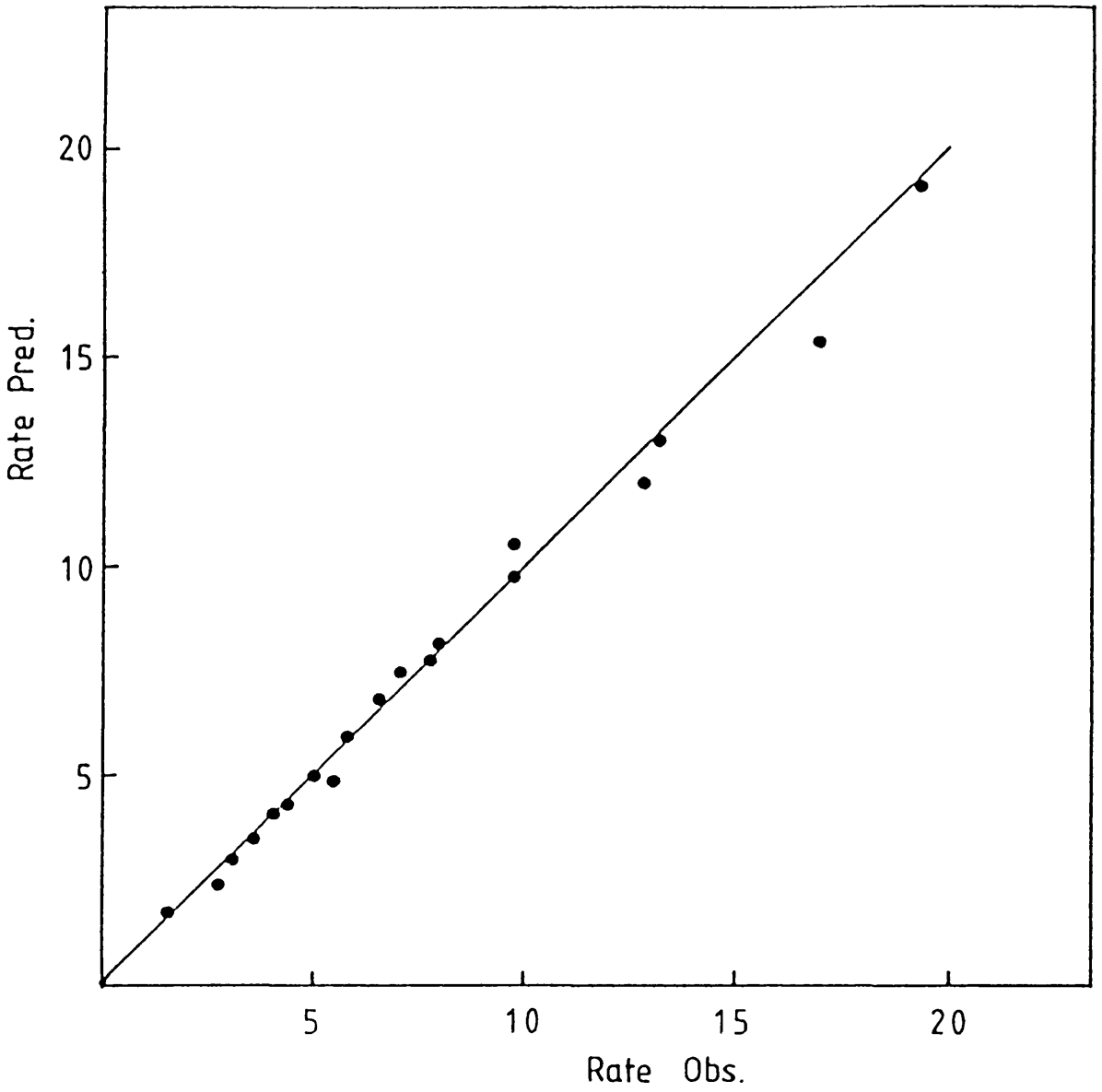

Figure 4.5 Power Law predicted rate against observed rate for case with hydrogen sulphide added to the feed

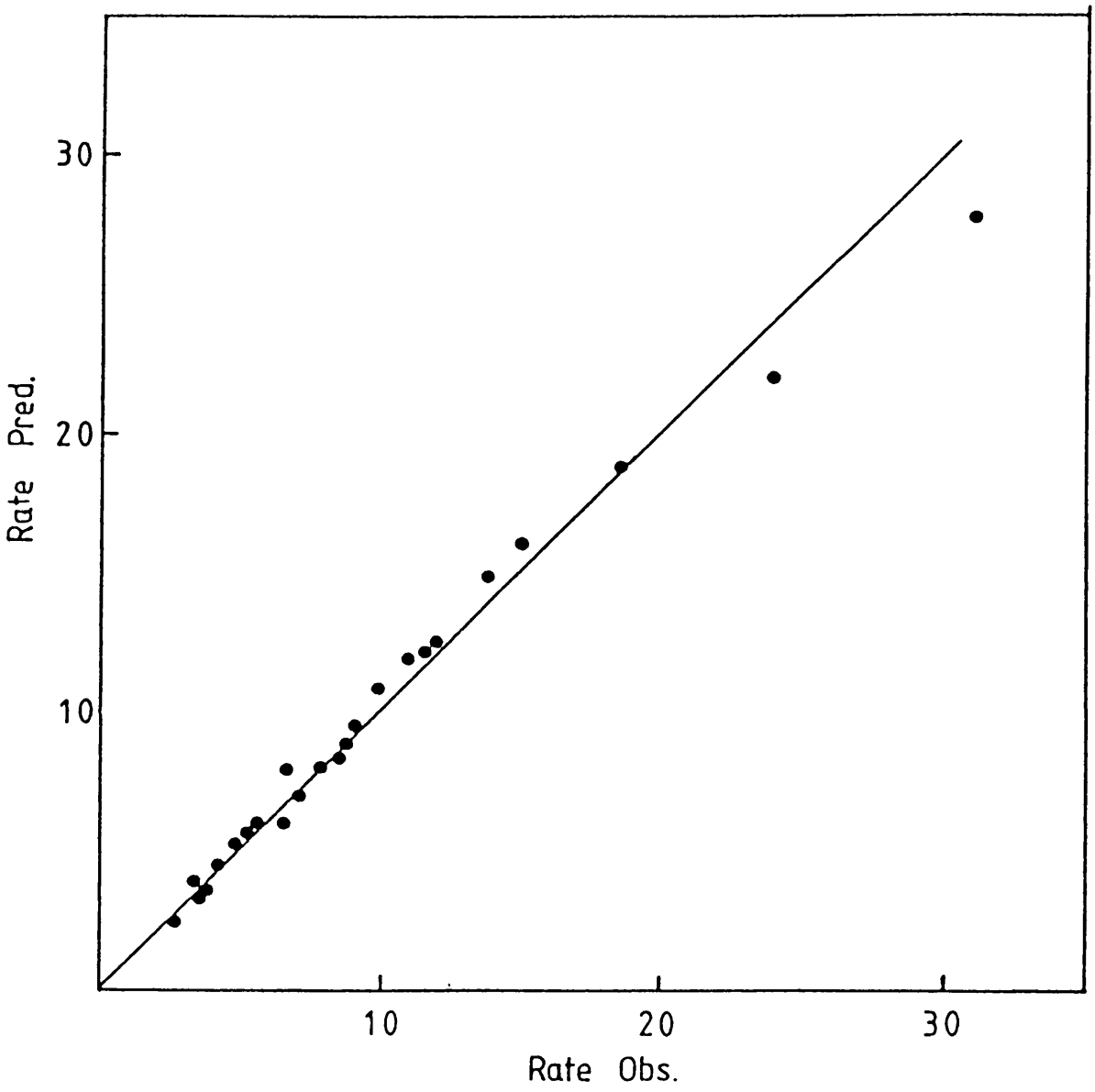

Figure 4.6 Rate predicted from Power Law against rate observed for case with no hydrogen sulphide in the feed

$$e\ \% = \left| \frac{r_{pred} - r_{obs}}{r_{obs}} \right| x\ 100 \qquad (4.31)$$

where r_{pred} and r_{obs} represent the predicted and observed rate respectively.

The kinetic data given in Appendix B-2 do not allow the formulation of a unique power law rate expression. Nevertheless, the results obtained give an indication of the value of the apparent activation energy and also suggest that hydrogen sulphide has an inhibiting effect.

(4) LH-HW rate expressions

Table 4.4 lists the most appropriate kinetic models found by applying the mechanistic information given in Chapter 1.1(2)(a) and Chapter 4.4(2). All the kinetic expressions (models 1, 2, 4-6) are of the LH-HW type, except model 3, which follows an Eley-Rideal mechanism in which surface reaction between adsorbed thiophene and gas phase hydrogen is assumed to be the rate limiting step.

Many aspects, from the conflicting literature presented in Chapter 1, have been considered in the rate expression proposed in Table 4.4. The following points were taken into account:

(i) Single and multipoint adsorption of thiophene

(ii) Homogeneous surface sites for adsorption for both hydrogen and thiophene.

(iii) Two different types of site for adsorption of hydrogen and thiophene.

(iv) No adsorption of hydrogen.

No adsorption term for butenes or butane were included in the kinetic rate models, the amount of those products formed during the reaction being very small (low conversions obtained in a differential reactor). Furthermore, the results of Owen and Amberg[11,13] indicated that the

No.	Model	R.L.S.[a]	Surface
1	$r = \frac{kP_t}{(1 + K_s P_s + K_h P_h)^n}$	Thiophene adsorption	homogeneous
2	$r = \frac{kP_t}{(1 + K_s P_s)^n}$	Thiophene adsorption	heterogeneous. Two types types of sites: thiophene and H_2S in one, H_2 on the other.
3	$r = \frac{kP_t P_h}{(1 + K_t P_t + K_s P_s)^n}$	Surface reaction	homogeneous
4	$r = \frac{kP_t P_h}{(1 + K_t P_t + K_s P_s + K_h P_h)^{n+1}}$	Surface reaction	homogeneous
5	$r = \frac{kP_t P_h}{(1 + K_t P_t + K_s P_s)^n (1 + K_h P_h)}$	Surface reaction	heterogeneous. Two types of sites: thiophene and H_2S in one, H_2 on the other.
6	$r = \frac{kP_h}{(1 + K_t P_t + K_s P_s)}$	Hydrogen adsorption	homogeneous

[a] R.L.S. = rate limiting step. [b] n = thiophene point of adsorption (n = 1, 2, 3).

Table 4.4 Most probable models to describe the kinetics of thiophene desulphurisation

presence of butenes do not retard the react of reaction significantly.

(a) Preliminary discrimination of kinetic model

An inspection of the kinetic data, illustrated in Figures 4.1 and 4.3, indicates that the rate of reaction is inhibited by thiophene and hydrogen sulphide. Therefore the inhibition term in the LH-HW rate expression term sould contain the partial pressure of thiophene and hydrogen sulphide. Models 1 and 2 are not consistent with the experimental data reported. Their inhibition terms only contain the term for hydrogen sulphide. The present results are in agreement with the result of Owen and Amberg[13] who concluded that thiophene adsorption was unlikely to be the rate determining step. Instead they suggested the possibility of either surface reaction or hydrogen adsorption as a rate limiting step.

Model 6 considers the possibility of hydrogen adsorption being the rate limiting step. However, some of the kinetic parameters obtained by a multivariable linear regression analysis were found to be negative. Negative values of adsorption constants have no physical meaning and therefore this model was also rejected (although several investigators[8,13] put forward the hypothesis that adsorption of hydrogen might control the reaction rate).

The remaining models proposed in Table 4.4 were analysed by using a non-linear regression technique. The number of points, n, required for thiophene adsorption was varied from 1 to 3. The initial parameter values required for the subroutine P3R were taken from the results of a linear-analysis of the models when linearisation of the kinetic expression was possible, otherwise (*e.g.*, model 5) these initial values were guessed

on the basis of the information obtained from other equations, such as that used to describe model 3.

A modification of model 5 was necessary due to a very poor estimation of the kinetic parameters. This was noticed by examining the sum of squares of residuals (SSR). A very small change in the SSR (at the fourth decimal place) produced a large variation in the estimated parameter value and this is an indication of poorly estimated values. The assumption of a large coverage by hydrogen ($K_h P_h >> 1$) was considered in the following modified form of model 5, which therefore results in the expression

$$r = \frac{kP_t}{(1 + K_t P_t + K_s P_s)^n} \qquad (4.32)$$

However, the assumption of a very small coverage by hydrogen ($K_h P_h << 1$) leads to a model similar to model 3 proposed earlier.

(b) Final correlation of the kinetic expression

The computed values of the kinetic parameters (k, K_t, K_s, K_h), at various temperatures, for the models which best fit the experimental data are shown in Table 4.5.

The values of K_h for model 4 (n = 1) were found to be very small and negative. However, on the basis of these results this model cannot be rejected as Froment[110] pointed out that the parameter K_h should be significantly negative before discarding any particular model. In the present study, uncertainty in the value of K_h may be due to the fact that the range of variation in the hydrogen partial pressure was small and that the partial pressure of hydrogen does not vary independently of the variation of thiophene and hydrogen sulphide.

Model No.	Rate expression	t (° C)	k x 10^{11}	K_t x 10^3 (mm^{-1} Hg)	K_s x 10^3 (mm^{-1} Hg)	K_h x 10^3 (mm^{-1} Hg)	SSR x 10^{14}
3 (n = 1)	$r = \frac{kP_tP_h}{(1 + K_tP_t + K_sP_s)}$	260	4.1	30.9	77.4		1.40
		280	4.9	19.4	62.0		2.84
		300	7.3	17.4	50.9		7.57
		320	9.9	11.3	49.0		15.73
3 (n = 2)	$r = \frac{kP_tP_h}{(1 + K_tP_t + K_sP_s)^2}$	260	3.5	9.2	13.0		1.82
		280	4.5	6.7	12.8		4.94
		300	6.7	6.1	11.3		12.68
		320	9.5	4.5	12.3		27.53
3 (n = 3)	$r = \frac{kP_tP_h}{(1 + K_tP_t + K_sP_s)^3}$	260	3.4	5.3	6.2		2.01
		280	4.4	4.1	6.4		5.81
		300	6.6	3.7	5.8		14.85
		320	9.4	2.8	6.5		32.87
4 (n = 1)	$r = \frac{kP_tP_h}{(1 + K_tP_t + K_sP_s + K_hP_h)^2}$	260	3.4	9.1	12.9	-0.9	1.82
		280	5.1	7.3	13.8	9.2	4.94
		300	6.7	6.1	11.3	0.10	12.68
		320	8.4	4.2	11.5	-8.1	27.53
5 (n = 1) $K_HP_H >> 1$	$r = \frac{kP_t}{(1 + K_tP_t + K_sP_s)}$	260	3330	40.11	117.0		1.21
		280	3920	25.35	89.3		1.71
		300	5880	23.16	73.8		4.51
		320	7790	15.60	67.1		9.39
5 (n = 2) $K_HP_H >> 1$	$r = \frac{kP_t}{(1 + K_tP_t + K_sP_s)^2}$	260	2710	10.72	16.9		1.6
		280	3480	8.10	16.2		3.96
		300	5200	7.39	14.3		10.03
		320	7310	5.72	15.1		20.95

Table 4.5 Result of the non linear analysis on models 3, 4 and 5

The final selection of the rate expression is based on two factors. (i) The examination of the kinetic data and (ii) the prediction of rates from the models in Table 4.5. Consider the prediction of rates for models 3, 4 and 5 by assuming either that one, two or three points are required for thiophene adsorption. The rate expression for models 3 and 5 predict a maximum in the reaction rate with respect to the thiophene partial pressure when thiophene adsorbs at two or more sites. The value of the thiophene partial pressure for which the rate is maximum is given by:

$$P_t = \frac{1 + K_s P_s}{(n-1)K_t} \qquad (4.33)$$

where n = 2, 3.

Similarly, model 4 also predicts a maximum in the rate for even a single point adsorption of thiophene. The partial pressure of thiophene for the maximum value of the rate (single point adsorption) is given by:

$$P_t = \frac{1 + K_s P_s + K_h P_h}{K_t} \qquad (4.34)$$

An examination of the experimental results shown in Figure 4.1 does not indicate a maximum in the rate of reaction over the entire range of thiophene partial pressure studied [which also includes the partial pressure predicted by equations (4.33) and (4.34)]. There are, therefore, good grounds for rejecting model 4.

Model 3 (n = 2) is similar to that proposed earlier by Satterfield and Roberts.[34] Although this model gave a fairly good fit to the experimental data it was rejected since our range of thiophene partial pressure was larger than theirs and no maximum in the rate was observed

contrary to their observations. This probably confirms that the simultaneous effect of thiophene and hydrogen sulphide masks any true trends in the data, as suggested earlier in Chapter 1(2)(a)(ii).

This analysis leads one to consider only those kinetic expressions which do not predict a maximum in the reaction rate. Assuming that thiophene is adsorbed at only one point (n = 1), Models 3 and 5 conform to general requirements. Their kinetic expressions are given below.

$$\text{Model 3 } (n = 1) \quad r = \frac{kP_tP_h}{(1 + K_tP_t + K_sP_s)} \tag{4.35}$$

$$\text{Model 5 } (n = 1) \quad r = \frac{kP_t}{(1 + K_tP_t + K_sP_s)} \tag{4.36}$$

(modification of the original model 5 by the assumption $K_hP_h >> 1$)

The sum of the square of residuals (SSR) for these two models was found to be of the same order of magnitude. Any small difference, however, may not be critical in order to discriminate between the two rival models. The parameter represented by k in the rate expressions [equations (4.35) and (4.36)] is a function of an intrinsic rate constant, k_i, and also the thiophene adsorption constant, K_t. This function arises because of the initial assumptions in the formulation of the rate expression for models 3 and 5. The assumptions were: (a) Eley-Rideal mechanism is operative in the case of model 3, (b) high coverage of hydrogen in the case of model 5, and (c) one point thiophene adsorption in the case of both the models. The relation between k_i

and K_t is similar for both models 3 and 5.

$$k = k_i \cdot K_t \qquad (4.37)$$

In order to determine the values of the apparent activation energies (E), enthalpies (ΔH_t, ΔH_s) and entropies (ΔS_t, ΔS_s) of adsorption, the temperature dependence of k_i and K_t and K_s, were linearised and plotted against 1/T (Figures 4.7 and 4.8).

$$k_i = ko \exp(-E/RT) \qquad (4.38)$$

$$K_t = \exp(-\Delta H_t/RT + \Delta S_t/R) \qquad (4.39)$$

$$K_s = \exp(-\Delta H_s/RT + \Delta S_t/R) \qquad (4.40)$$

Table 4.6 contains the final result of the analysis of the models 3 and 5 for the kinetics of thiophene hds reaction. In Figures 4.9 and 4.10 the predicted rates are plotted against the observed rate for models 3 and 5. The maximum errors (%) are 34.9 and 25.4 respectively. However, 92% of the data falls within a 20% error bound for both models 3 and 5.

4.7 Discussion of the Kinetic Modelling for Hds of Thiophene

The modelling of the reaction rate for thiophene desulphurisation shows that it is not possible to formulate a generalised power law rate expression from the kinetic data collected. A selection of a series of kinetic expressions (in the case of either LH-HM or ER models) was given in Table 4.4. Their discrimination was conducted mainly by an examination of the experimental data in conjunction with the information reported by earlier workers. Such discrimination leads to the selection of models 3 and 5 ,with n = 1) as the most appropriate models predicting rate measurements. The following discussion will be based on these two models only.

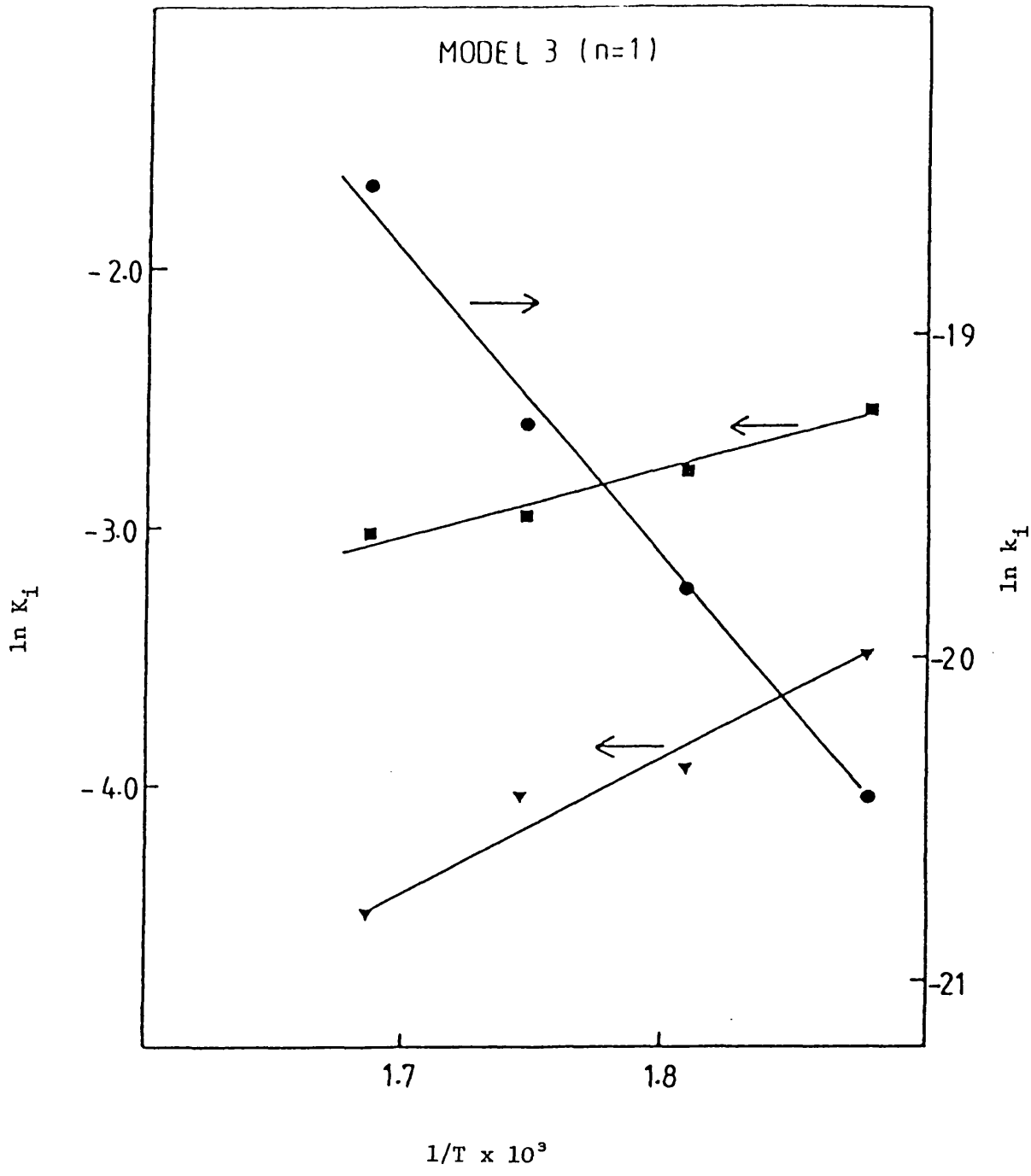

Figure 4.7 Temperature dependence of the rate constant and equilibrium adsorption constants [k_i (●), K_t (▼), K_s (■)]

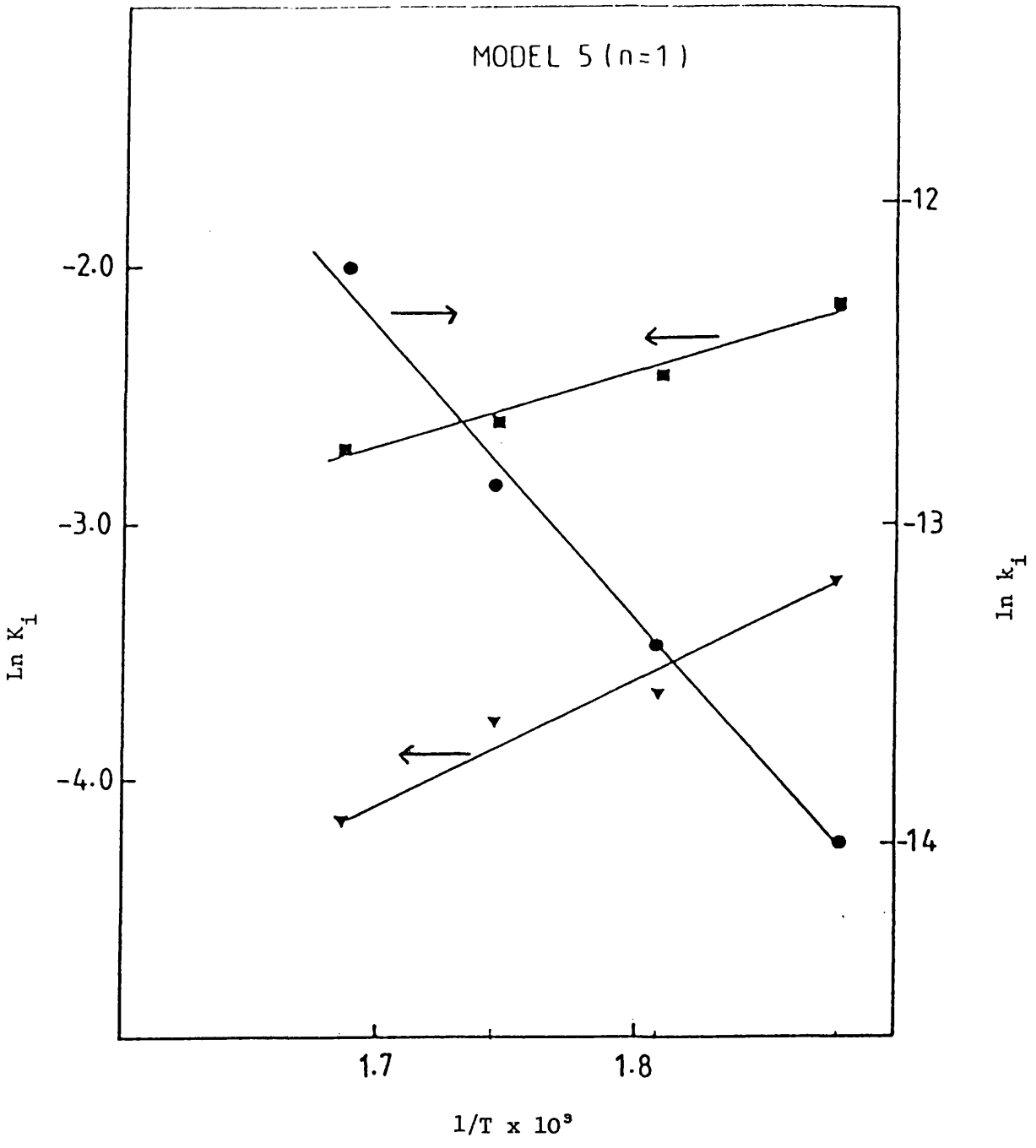

Figure 4.8 Temperature dependence of the rate constant and equilibrium adsorption constants [k_i (●), K_t (▼), K_s (■)]

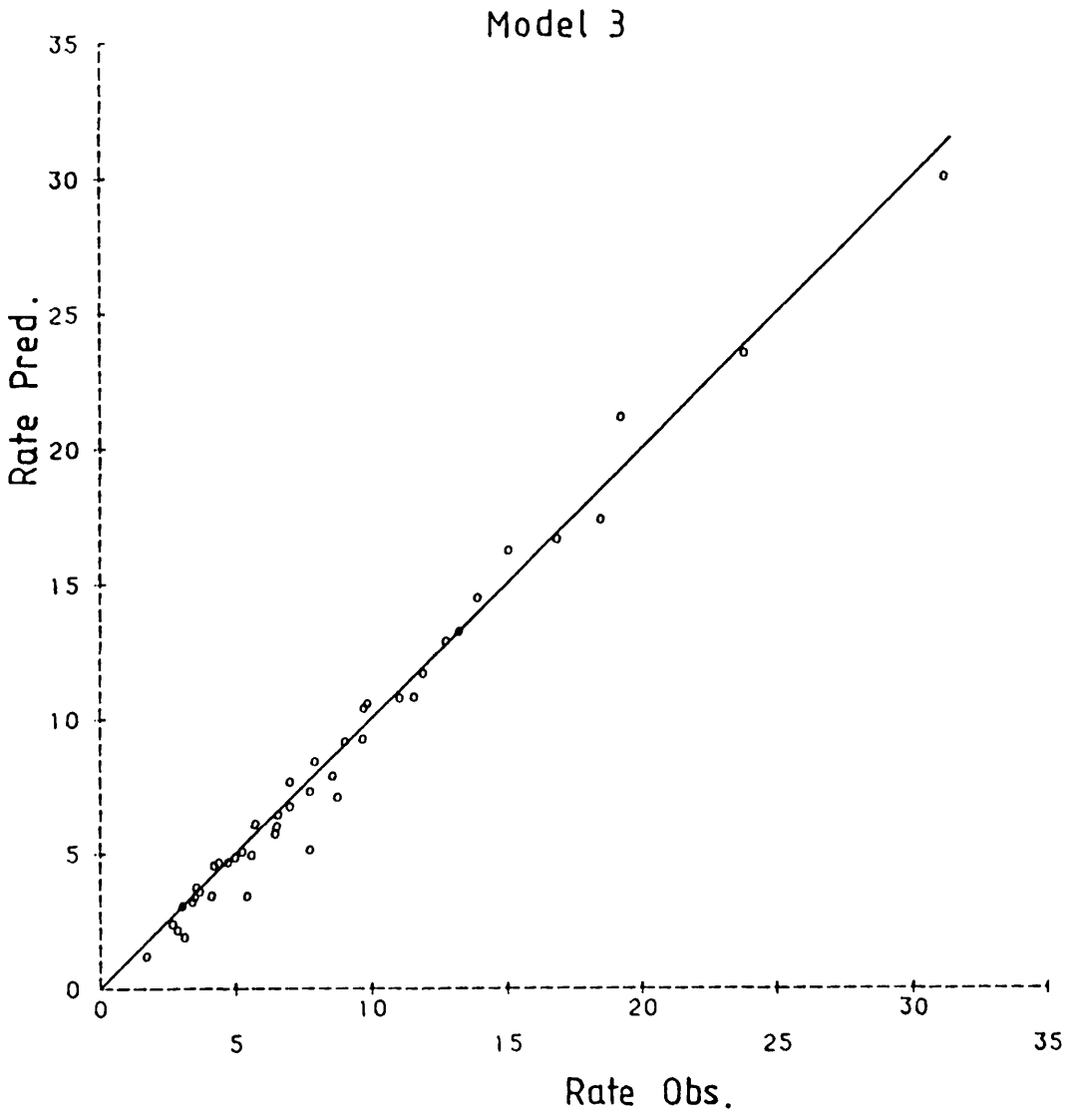

Figure 4.9 Plot of predicted rate against observed rate for model 3 (n = 1)

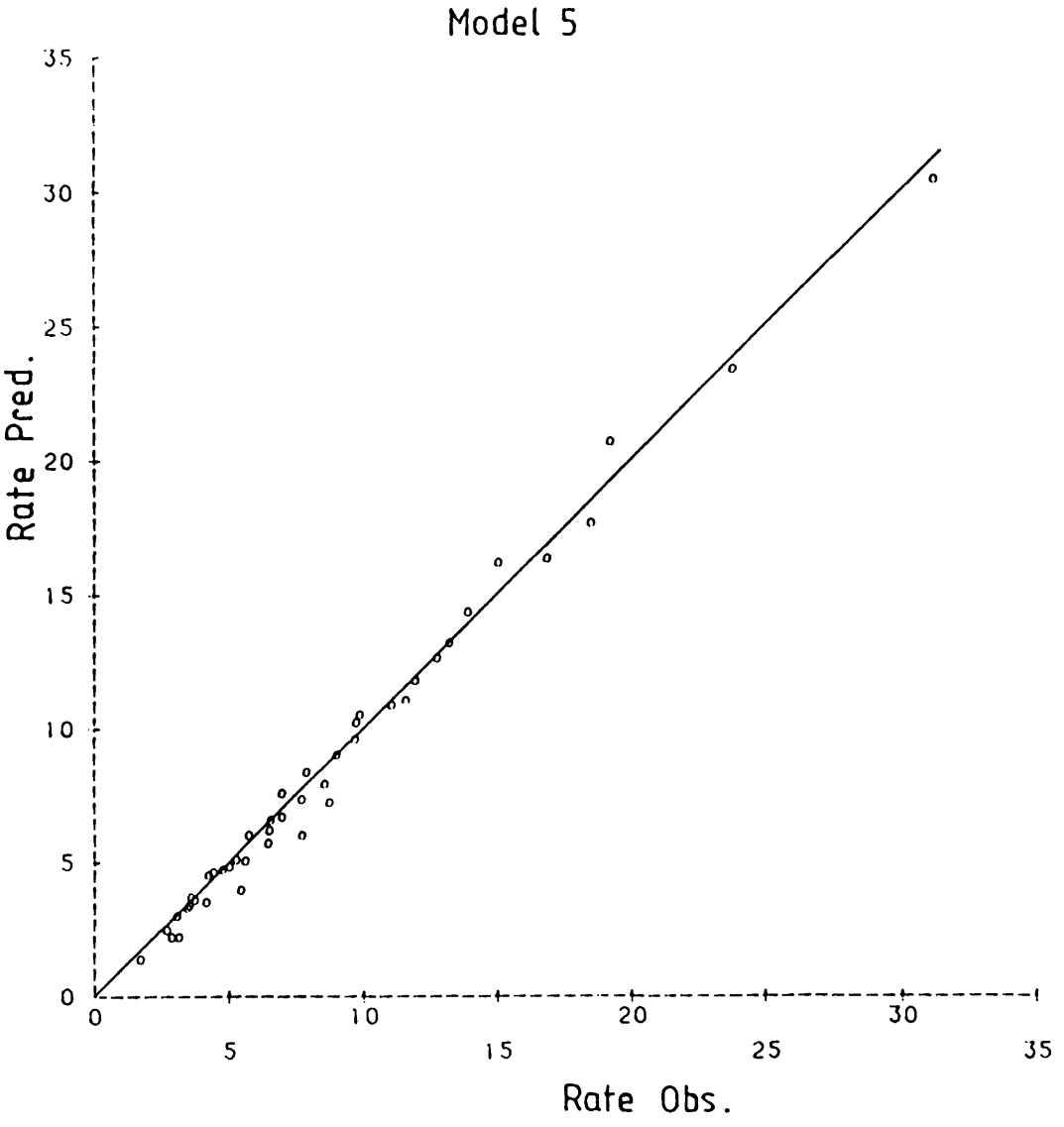

Figure 4.10 Plot of predicted rate against observed rate for model 5 (n = 1)

Parameter	Model 3	Model 5
k_o*	0.11	30.0
E (kJ/mole)	80.7 (19.3)	76.9 (18.4)
ΔH_t (kJ/mole)	-41.0 (-9.8)	-38.5 (-9.2)
ΔS_t (J/mole K)	-106.0 (-25.4)	-98.6 (-23.6)
ΔH_s (kJ/mole)	-20.9 (-5.0)	-24.7 (-5.9)
ΔS_s (J/mole K)	-60.6 (-14.5)	-64.0 (-15.3)

The values in parenthesis are express in kcal/mol, except those for ΔS_t and ΔS_s, which are expressed in cal/mole K.

*Unit for k_o Model 3 mole/(s.g_{cat} mm^2Hg)

Model 5 mole/(S.g_{cat} mmHg)

Table 4.6 Final analysis of the models 3 and 5 for the kinetics of thiophene desulphurisation

Discrimination between the two rival models 3 and 5 (with n = 1) cannot be discerned by statistical means because of insignificant differences in the SSR values. Furthermore, the kinetic information reported in the literature is conflicting. Model 5 (n = 1), which is independent of the hydrogen partial pressure, agrees very well with the findings of Pease and Keighton.[27] On the other hand, model 3 (n = 1), which assumes an Eley-Rideal mechanism, agrees with the results presented by Amberg *et al.*[11]

Roberts and Satterfield[34] have proposed a kinetic expression similar to that of model 3 (n = 1). This expression gave a reasonably good fit to their experimental data. However, they rejected such a model, presumably because it failed to predict a maximum in the rate of reaction *versus* thiophene partial pressure which they observed

experimentally. Nevertheless, one might presume that their observation of a rate maximum may well be caused by the simultaneous effect of thiophene and hydrogen sulphide on the reaction rate (as discussed earlier in Chapter 1). This is confirmed by the fact that, in this present work, a large range of thiophene partial pressure was employed and no maximum in the rate was observed. Neither is a maximum in the rate predicted by model 5 (n = 1). Furthermore, models 3 and 5 were tested by using the kinetic data reported by Lee and Butt.[36] Both models gave a reasonably good fit, model 3 proving better than model 5. Model 5 gave negative values of the parameters at the lowest temperature. However, the values of the parameters (k, K_t, K_s) in the rate expressions obtained in this way were different from the corresponding values obtained by analysis of the kinetic data obtained in this thesis.

The inhibition effect of thiophene and hydrogen sulphide for both models 3 and 5 are significant, especially at low temperature. This can be seen by examining the variation of the values of K_tP_t and K_sP_s of the adsorption term as a function of temperature. The values of K_tP_t and K_sP_s were larger than unity for the maximum values of partial pressure of thiophene and hydrogen sulphide used in this investigation. The inhibition effect of hydrogen sulphide was larger than that of thiophene. The adsorption constants for thiophene and hydrogen sulphide for models 3 and 5 may, in theory, be related to the heat and entropy changes of the chemisorption process. The enthalpy and entropy for both models are given in Table 4.5. The values of ΔH_T were -41.0 and -38.5 kJ/mole (-9.8 and -9.2 kcal/mol) for models 3 and 5 respectively.

These values may be compared with ΔH_T = -9.5 kcal/mol reported by Owen and Amberg[11] from chemisorption studies on a cobalt molybdate catalyst. No standard entropy values for the chemisorption of thiophene and hydrogen sulphide are available in the literature at present. However, the entropy values given in Table 4.6 follow the rules of entropy analysis proposed by Boudart[98], outlined in section 4.3(a).

A comparison of the enthalpy and entropy values given in Table 4.6 with those derived from kinetic models proposed by earlier workers and reviewed in Chapter 1, Table 1.4, is not very helpful, because the values depend mainly on the kinetic models employed.

A comparison between a power law model and models 3 and 5 with n = 1 was not possible in the present work because the kinetic data collected did not allow formulation of a general power law rate expression for the hds reaction. However, the average order of reaction, 0.52 and -0.41, obtained from the two separated power law equations for thiophene and hydrogen sulphide respectively, are within the range 0 to 1 for thiophene and -1 to 0 for hydrogen sulphide, as indeed predicted by models 3 and 5. The apparent activation energy of 56.4 and 64.4 kJ/mol derived from the power law models given in Table 4.2 are comparable to 80 and 77 kJ/mol obtained from models 3 and 5 respectively. To summarise, the kinetic expressions given by models 3 and 5 (with n = 1) are found to describe reasonably well the rate of reaction for thiophene hydrodesulphurisation.

Nevertheless, it should be pointed out that the form of kinetic expression may not be proof of the particular mechanism, since similar rate expressions can be formulated by assuming different mechanisms. For example, model 3 (n = 1) could be derived by assuming an Eley-Rideal mechanism or could be regarded as a special case of the original model 5 (Table 4.4) by assuming that hydrogen chemisorption occurs at a site different from that used by thiophene and that its coverage is very low ($K_H P_H << 1$). In spite of this, it is worth noting certain characteristics of models 3 and 5. Both models imply that one point is required for thiophene adsorption and this agrees with the suggestion put forward by Lipsch and Schuit[19] that adsorption of thiophene occurs *via* the heteroatom on an anion vacancy of reduced MoO_3. Nicholson,[111] however, observed that thiophene can adsorb by using either one or more points, but no information was provided as to which adsorbed species was active for hds reaction.

CHAPTER 5

CONCLUSIONS AND RECOMMENDATIONS

5.1 Conclusions

(1) Catalytic activity studies

(a) Lithium addition to a cobalt-molybdate catalyst was found to affect the reducibility of molybdenum. The catalytic activity towards thiophene desulphurisation correlates well with the reducibility of molybdenum. Hence the results presented in this investigation give further support to the idea that the desulphurisation reaction is associated with molybdenum. It was also found that the species Mo^{III} is an active species in the hds reaction. The results of physico-chemical characterisation were found to be useful in elucidating the effect of structural properties of the catalyst on its activity.

(b) Two types of isomerisation reaction of the hydrocarbon occurring simultaneously with the desulphurisation reaction of thiophene, may be associated with the strength of Lewis type acidic sites. The strong acidic sites are probably responsible for the isomerisation reaction between but-1-ene and but-2.ene, while the weak acidic sites are related to the *cis*-but-2-ene $\rightleftharpoons$ *trans*-but-2-ene isomerisation.

(2) Reaction kinetic studies

(a) Two rate expressions for the hydrodesulphurisation reaction of thiophene were found to describe the kinetic data over the range of experimental conditions investigated. These are:

$$r = \frac{kP_t P_h}{(1 + K_t P_t + K_s P_s)} \qquad (5.1)$$

and

$$r = \frac{kP_t}{(1 + K_t P_t + K_s P_s)} \qquad (5.2)$$

Thiophene and hydrogen sulphide were found to inhibit the rate of reaction significantly.

(b) Both models support the view that thiophene adsorbs *via* the heteroatom on a vacant site of reduced MoO_3. The nature of hydrogen adsorption is still not clear - whether it is chemisorbed (low or high coverage) or does not adsorb at all.

5.2 Recommendations

(1) Further physico-chemical studies might be undertaken in order to investigate whether the cobalt in the series of catalysts is affected by lithium addition. Such studies may indirectly lead to an understanding of the promoting role of cobalt in the cobalt-molybdate catalysts.

(2) In order to obtain a unique model for a kinetic expression for the hds of thiophene, the dependence of the rate on the hydrogen partial pressure should be studied more carefully. This could be achieved either by studying the dependence of the rate expression on the total pressure, or by varying the hydrogen pressure independently of thiophene and hydrogen sulphide partial pressure over a wide range of conditions.

APPENDIX A

RESULTS OF THE CHARACTERISATION STUDIES

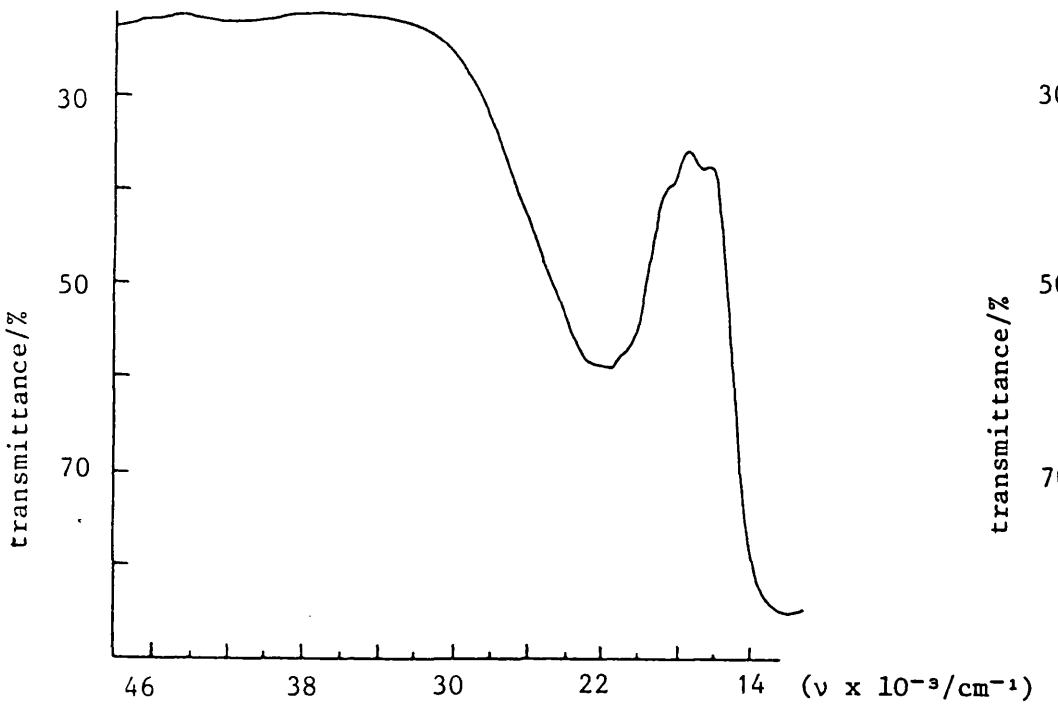

(a) Catalyst with Li/Co = 0.0

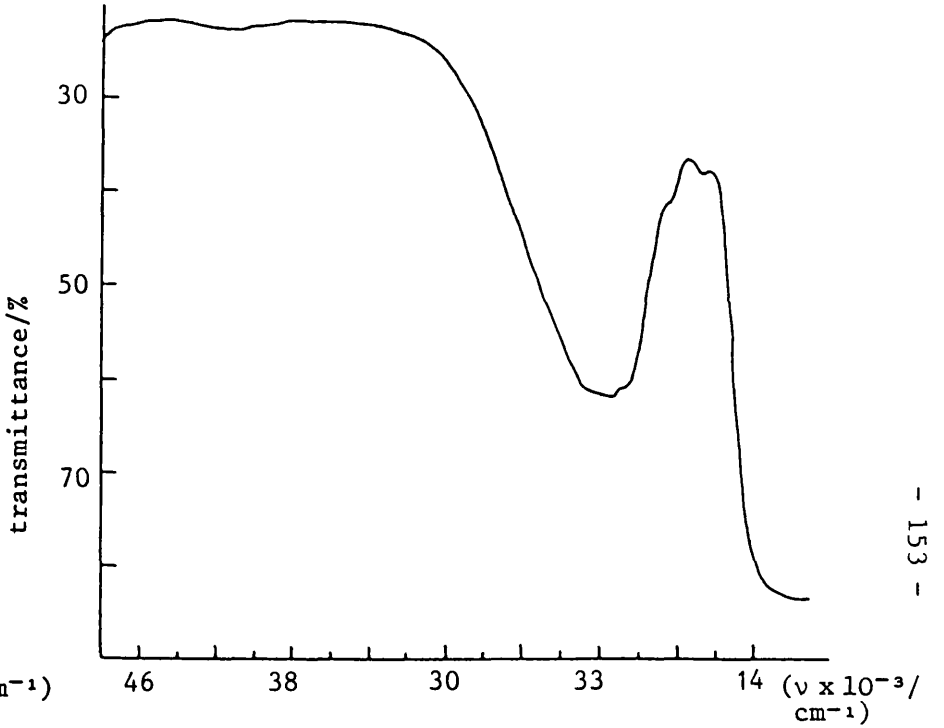

(b) Catalyst with Li/Co = 1.63

Appendix A-1 Reflectance spectra of the lithium containing catalyst series

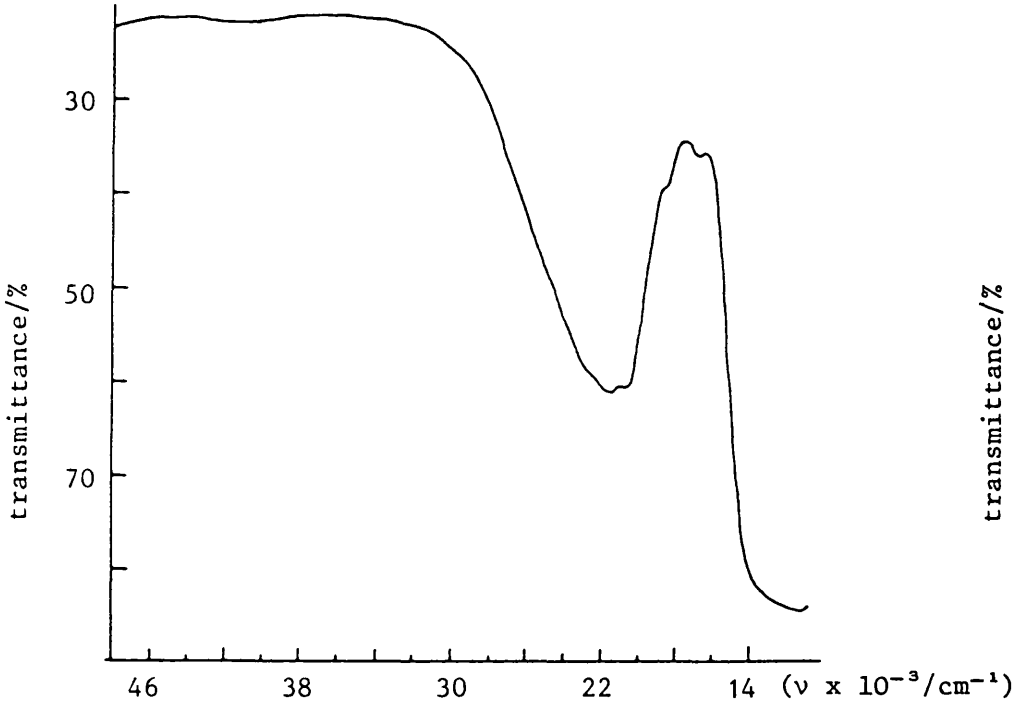

(c) Catalyst with Li/Co = 3.26

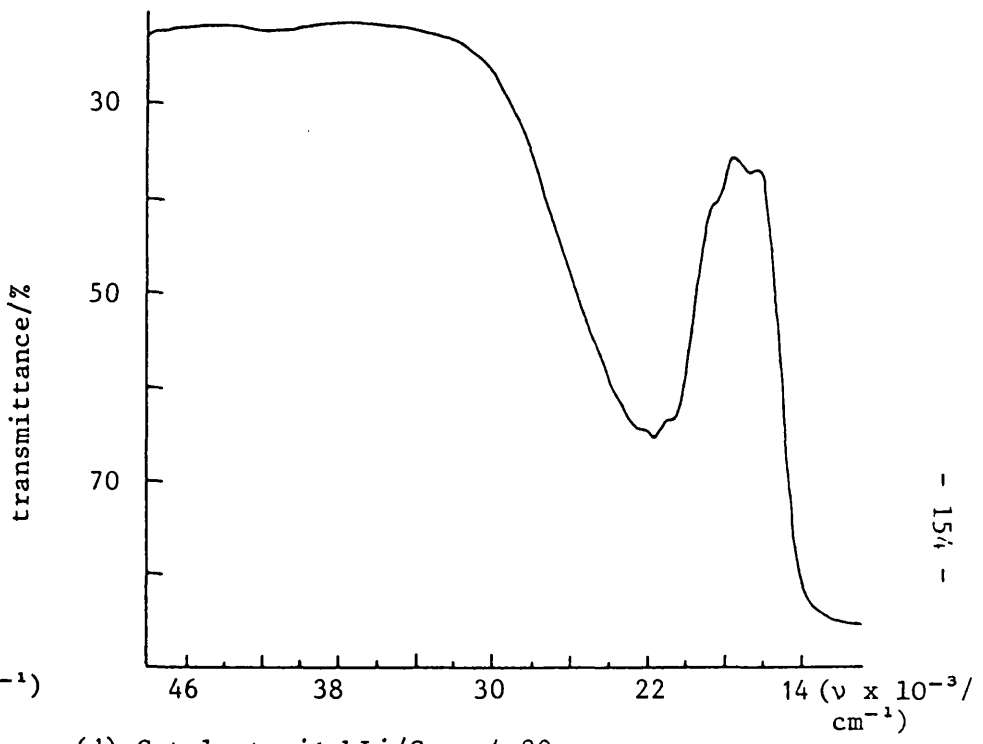

(d) Catalyst with Li/Co = 4.89

Appendix A-1 Reflectance spectra of the lithium containing catalyst series

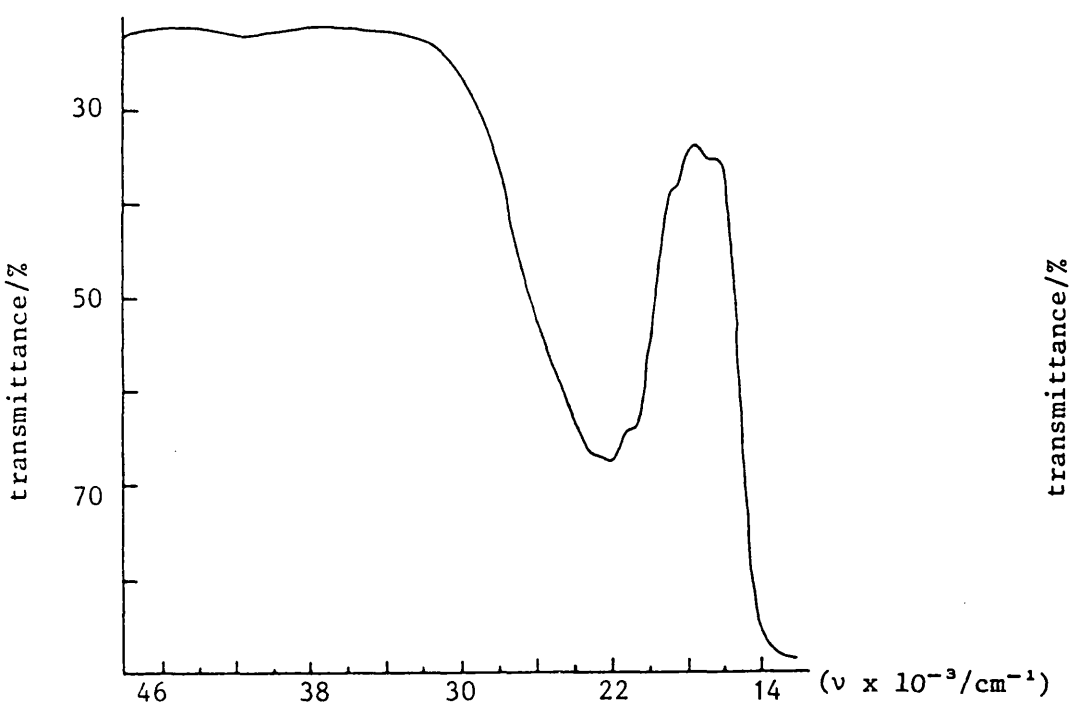

(e) Catalyst with Li/Co = 6.53

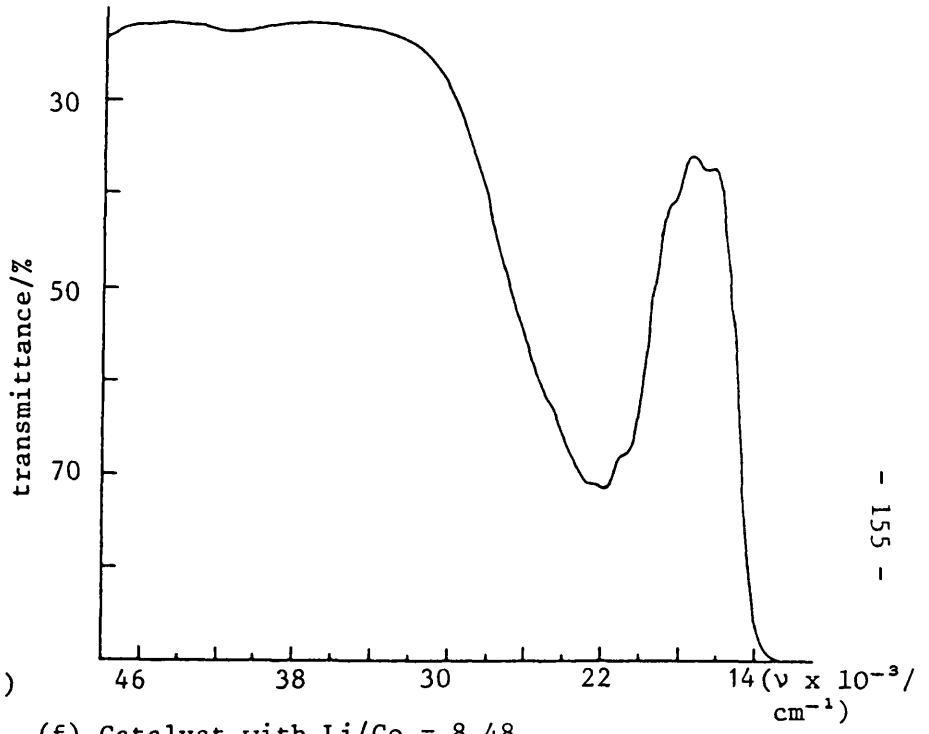

(f) Catalyst with Li/Co = 8.48

Appendix A-1 Reflectance spectra of the lithium containing catalyst series

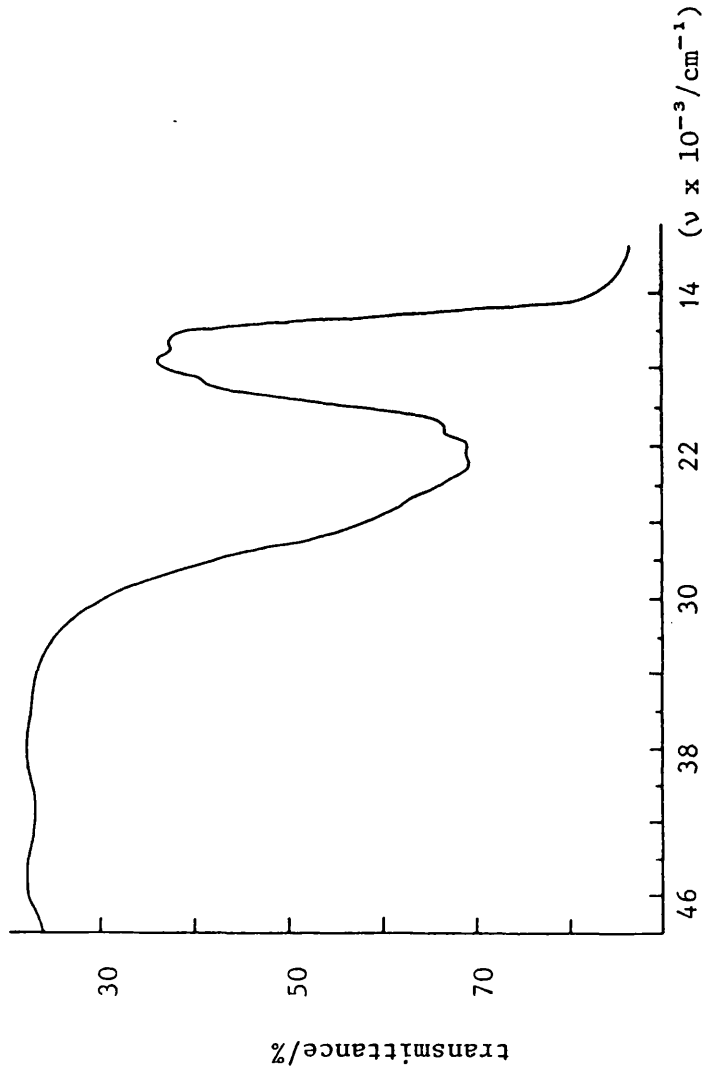

(g) Catalyst with Li/Co = 9.78

Appendix A-1 Relectance spectra of the lithium containing catalyst series

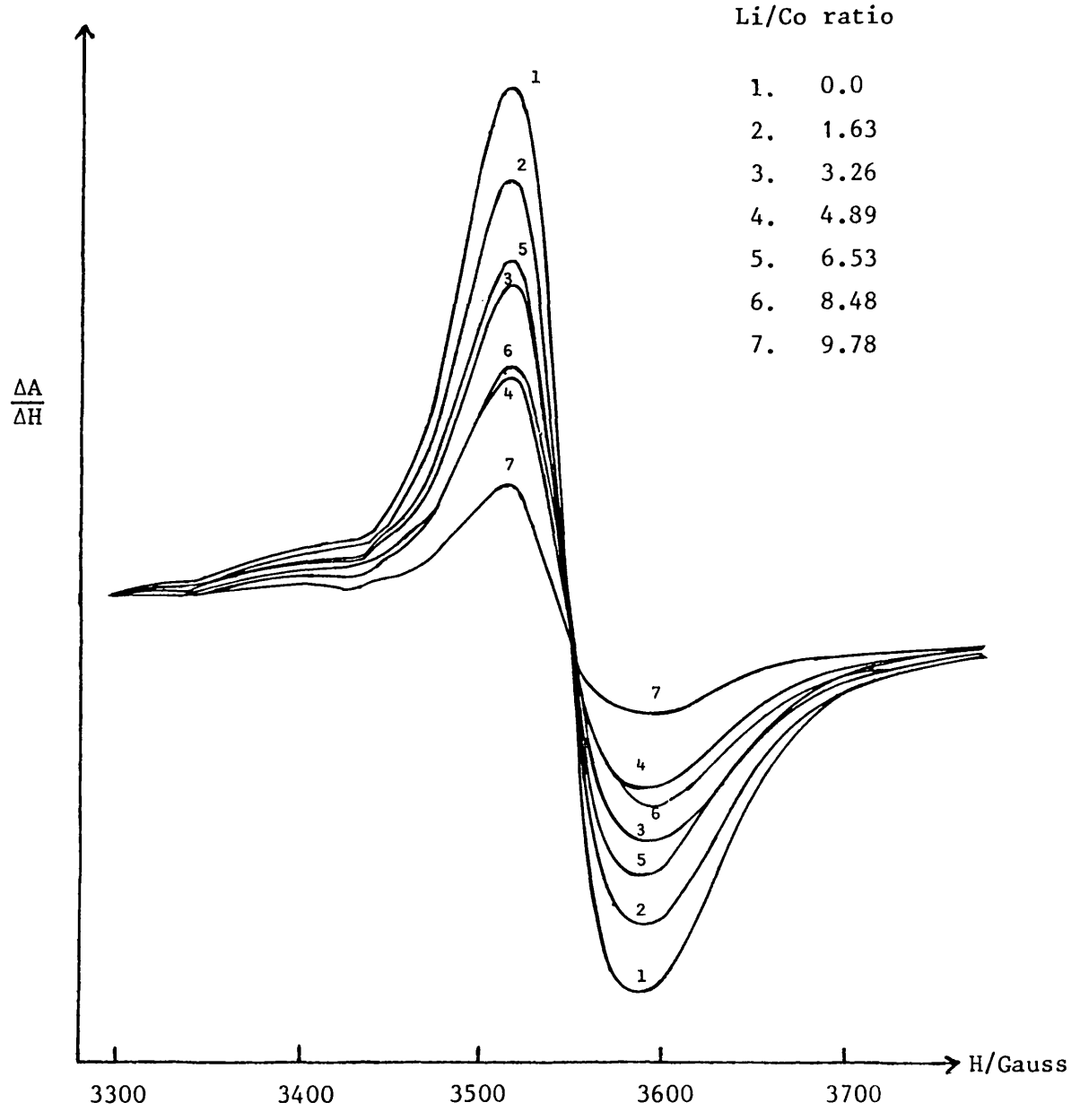

Appendix A-2 (i) E.s.r. spectra for catalysts treated with hydrogen

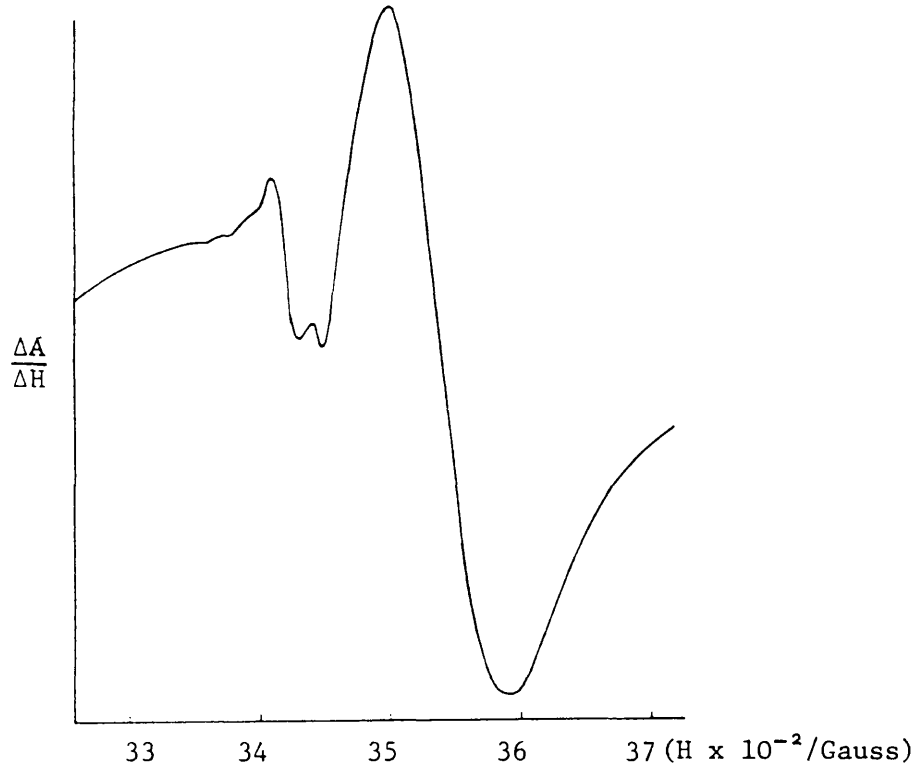

(a) Catalyst with Li/Co = 0.0

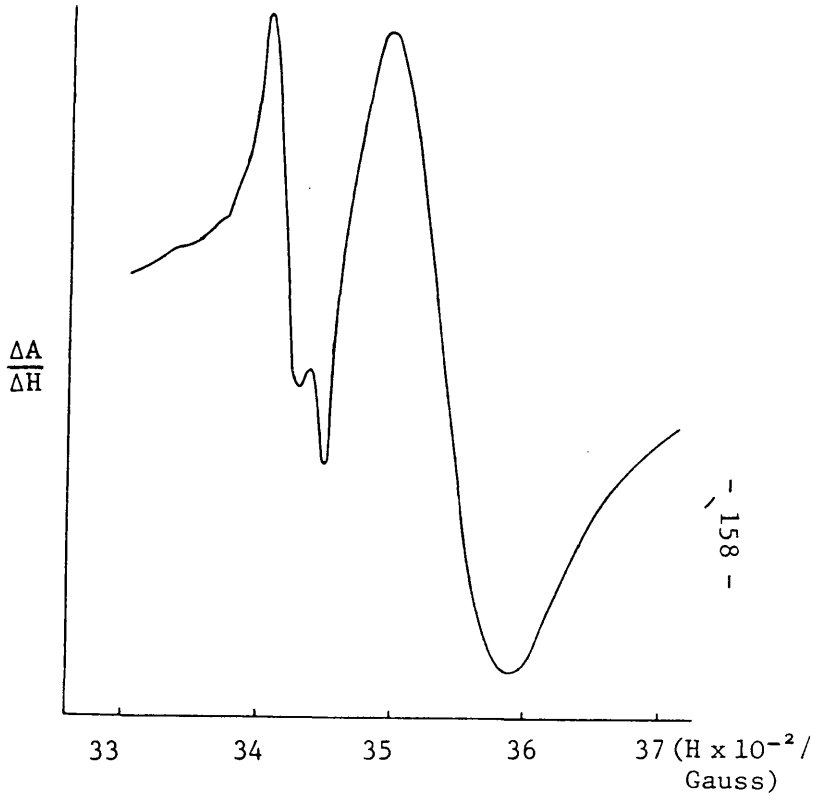

(b) Catalyst with Li/Co = 1.63

Appendix A-2 (ii) E.s.r. spectra for catalysts treated with a mixture of 10 volume % H_2S in hydrogen

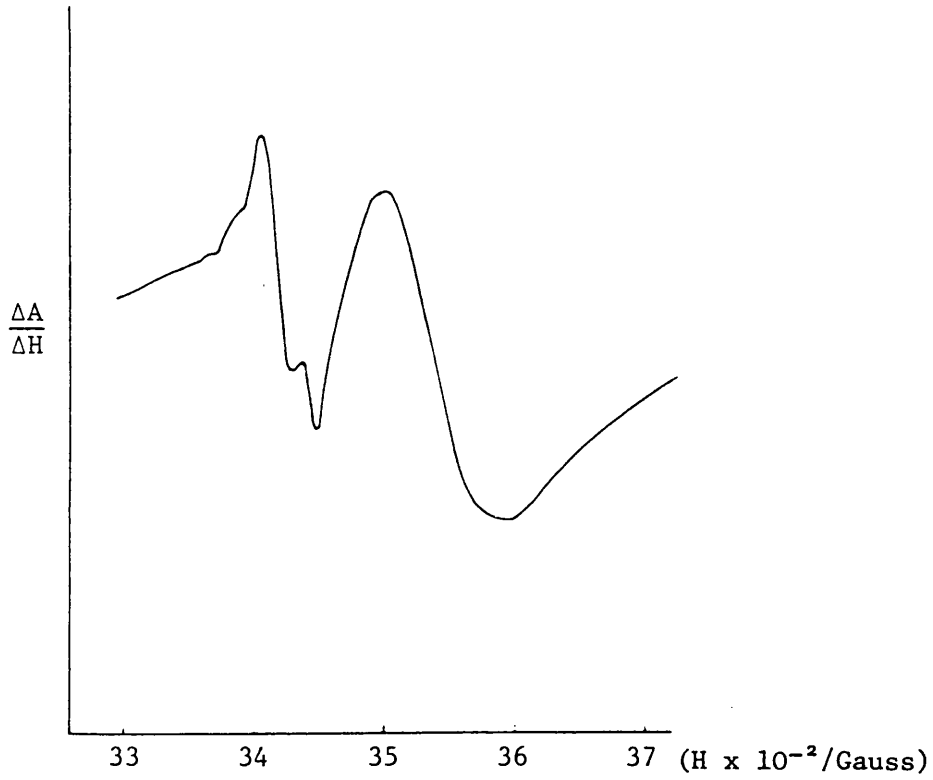

(c) Catalyst with Li/Co = 3.26

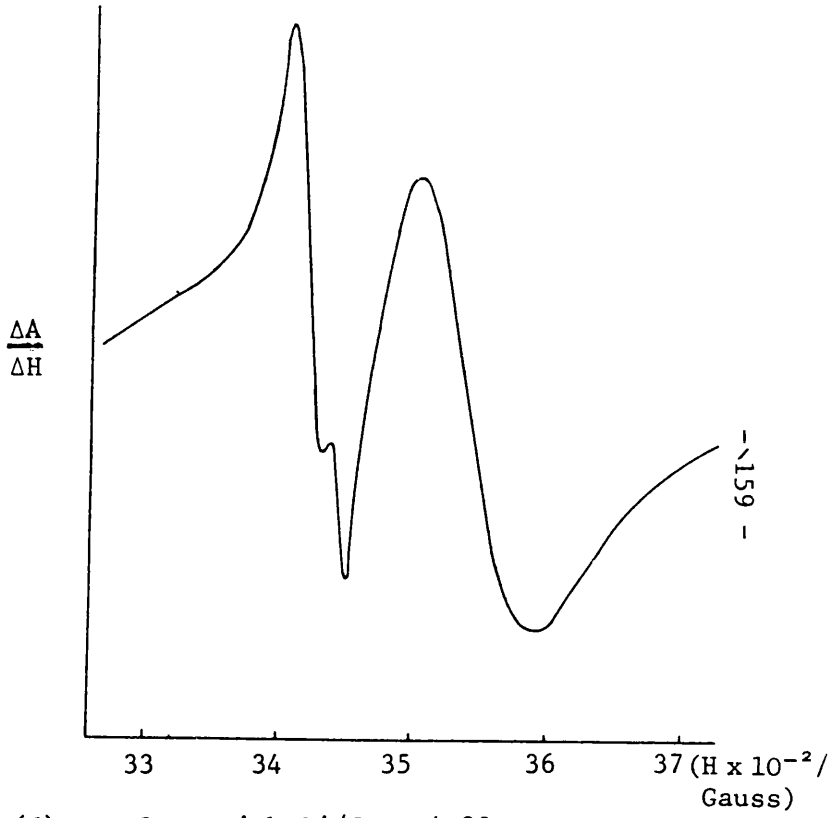

(d) Catalyst with Li/Co = 4.89

Appendix A-2(ii) E.s.r. spectra for catalysts treated with a mixture of 10 volume % H_2S in hydrogen

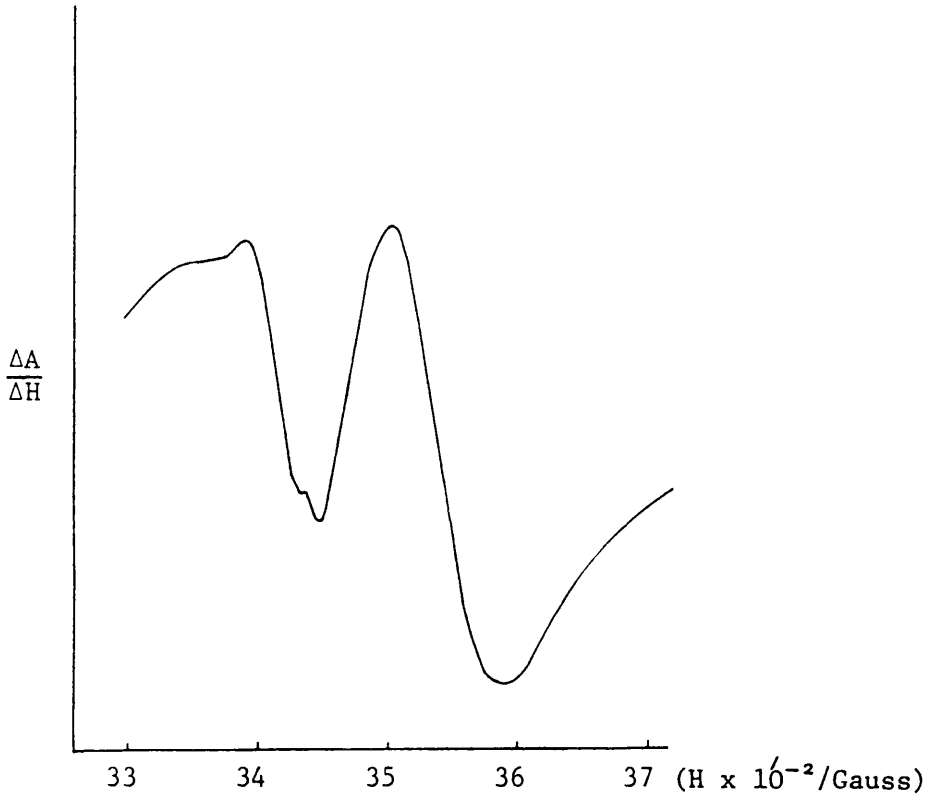

(e) Catalyst with Li/Co = 6.53

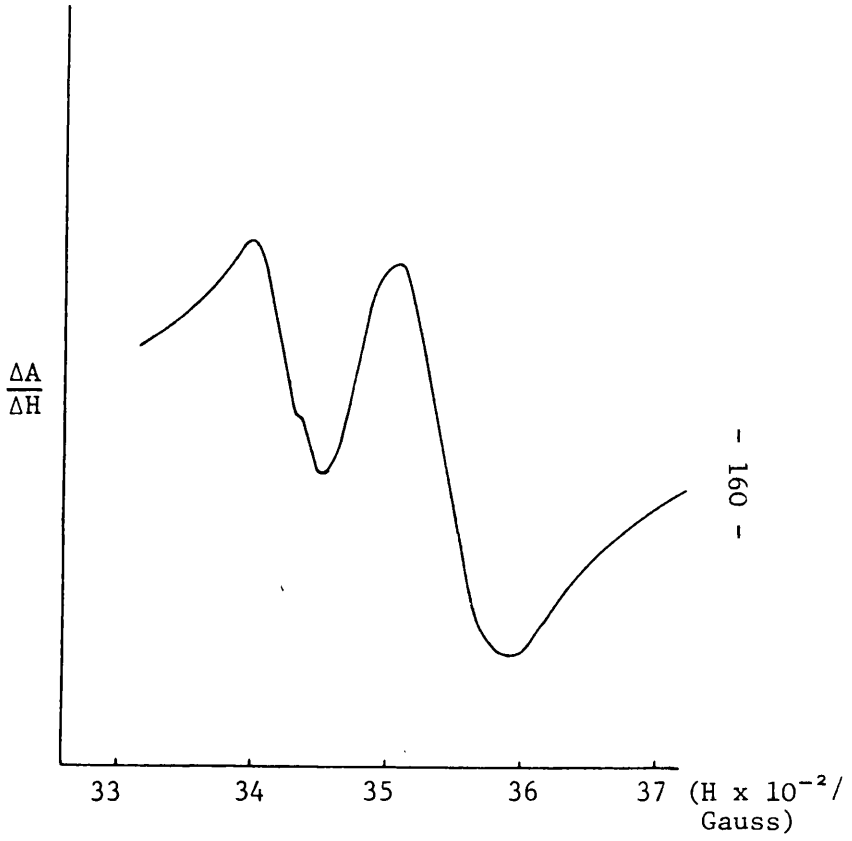

(f) Catalyst with Li/Co = 8.48

Appendix A-2 (ii) E.s.r. spectra for catalysts treated with a mixture of 10 volume % H_2S in hydrogen

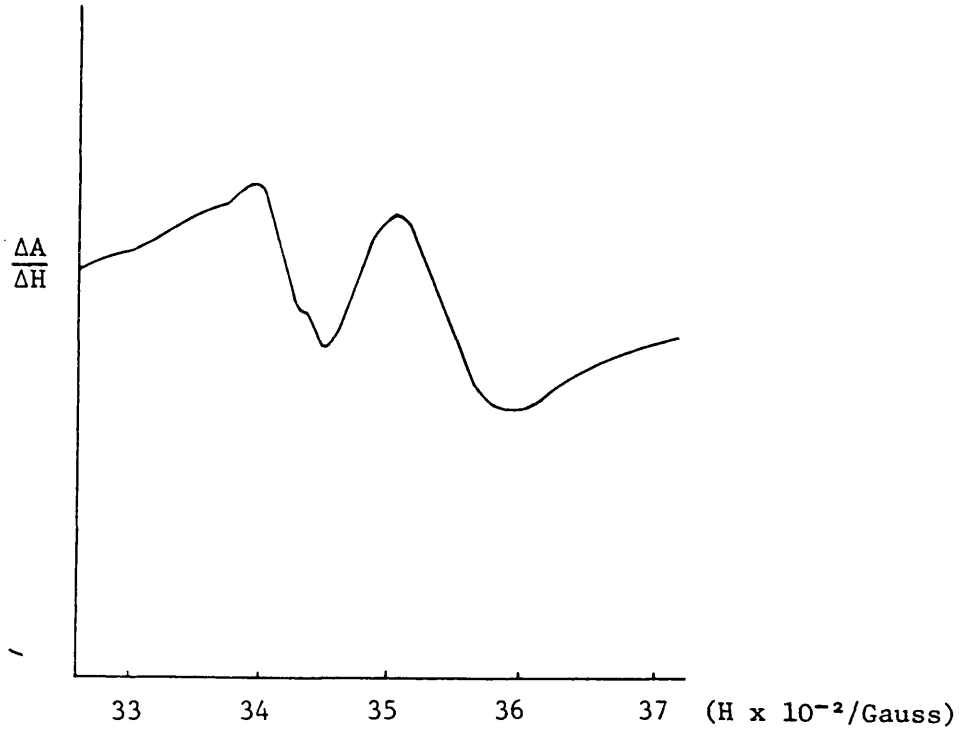

(g) Catalyst with Li/Co = 9.78

Appendix A-2 (ii) E.s.r. spectra for catalysts treated with a mixture of 10 volume % H_2S in hydrogen

ADSORPTION

P_a (mmHg)	V_a (cm^3/g)	ΣV_a (cm^3/g)	P_a/P_s
103.4	43.82	43.82	0.139
145.9	3.28	47.10	0.196
195.5	3.60	50.70	0.263
243.6	3.50	54.20	0.328
300.8	4.67	58.87	0.405
362.3	6.13	65.00	0.488
422.9	10.66	75.66	0.569
475.5	11.88	87.54	0.640
514.0	12.11	99.64	0.692
540.1	13.13	112.77	0.727
558.2	13.44	126.21	0.751
578.2	11.84	138.06	0.779
589.5	12.60	150.65	0.794
610.2	8.58	159.24	0.821
623.1	9.24	168.48	0.839
632.9	9.37	177.85	0.852
641.6	9.01	186.85	0.864
651.6	8.14	194.99	0.877
662.1	7.24	202.23	0.891

DESORPTION

P_a (mmHg)	V_a (cm^3/g)	ΣV_a (cm^3/g)	P_a/P_s
658.9	-0.25	201.99	0.887
643.5	-3.30	198.69	0.866
617.6	-6.89	191.80	0.831
592.3	-11.39	180.41	0.797
563.6	-15.96	164.45	0.758
528.4	-18.93	145.52	0.711
505.3	-21.35	124.18	0.680
475.2	-17.84	106.34	0.639
449.5	-16.94	89.40	0.605
417.2	-13.15	76.24	0.562
377.4	-8.89	67.35	0.508
336.9	-5.58	61.77	0.453
301.3	-3.72	58.06	0.405
278.8	-2.68	55.37	0.365
246.1	-1.97	53.41	0.331

(a) Catalyst with Li/Co = 0.0

Appendix A-3 Physisorption studies

ADSORPTION

P_a (mmHg)	V_a (cm^3/g)	ΣV_a (cm^3/g)	P_a/P_s
112.8	41.55	41.55	0.152
154.0	2.84	44.39	0.207
199.7	2.98	47.37	0.269
247.2	3.07	50.44	0.333
291.6	2.95	53.39	0.393
347.2	4.20	57.59	0.467
411.8	3.74	61.33	0.554
474.1	9.66	70.99	0.638
512.3	12.08	83.07	0.690
542.0	12.28	95.35	0.730
565.3	11.90	107.25	0.761
582.5	11.91	119.16	0.784
596.4	11.57	130.73	0.803
608.8	11.22	141.95	0.820
622.3	10.02	152.67	0.838
630.4	10.56	163.23	0.849
641.2	9.46	172.69	0.863
648.3	9.71	182.40	0.873
659.4	8.47	190.87	0.888
666.2	8.36	199.23	0.897

DESORPTION

P_a (mmHg)	V_a (cm^3/g)	ΣV_a (cm^3/g)	P_a/P_s
662.8	-0.30	198.93	0.883
640.3	-4.33	194.60	0.862
616.4	-7.66	186.94	0.830
595.6	-14.20	172.74	0.802
578.2	-20.19	152.55	0.778
545.1	-21.84	130.71	0.734
512.7	-20.14	110.57	0.690
484.2	-18.96	91.61	0.652
451.3	-15.64	75.96	0.608
418.5	-13.26	69.70	0.563
369.1	-5.88	56.82	0.497
325.6	-4.00	52.82	0.438
289.8	-2.90	49.92	0.390
260.1	-2.18	47.74	0.350
236.1	-1.60	46.15	0.318

(b) Catalyst with Li/Co = 1.63

Appendix A-3 Physisorption studies

ADSORPTION

P_a (mmHg)	V_a (cm^3/g)	ΣV_a (cm^3/g)	P_a/P_s
113.6	40.10	40.10	0.149
156.3	2.80	42.90	0.205
203.7	2.93	45.83	0.267
254.2	3.25	49.08	0.333
317.9	4.37	53.45	0.416
392.5	6.52	59.97	0.514
461.5	9.93	69.90	0.604
508.9	11.27	81.17	0.666
542.2	11.91	93.08	0.710
571.7	10.51	103.59	0.749
588.4	11.64	115.23	0.771
602.1	11.16	126.39	0.789
620.6	9.13	135.52	0.813
631.0	9.44	144.96	0.826
644.0	8.66	153.61	0.843
654.3	7.34	160.95	0.857
663.6	7.09	168.04	0.869

DESORPTION

P_a (mmHg)	V_a (cm^3/g)	ΣV_a (cm^3/g)	P_a/P_s
656.4	-0.63	167.41	0.853
636.8	-4.03	163.38	0.834
611.2	-7.09	156.29	0.801
588.2	-12.91	143.38	0.770
556.8	-15.20	128.18	0.729
537.2	-16.54	111.64	0.704
503.3	-11.50	100.14	0.659
473.6	-16.41	83.73	0.620
438.2	-13.28	70.45	0.574
399.3	-9.85	60.60	0.523
354.2	-5.41	55.19	0.464
312.7	-3.49	51.70	0.409
279.1	-2.52	49.18	0.365
251.4	-1.87	47.31	0.329

(c) Catalyst with Li/Co = 3.26

Appendix A-3 Physisorption studies

ADSORPTION

P_a (mmHg)	V_a (cm^3/g)	ΣV_a (cm^3/g)	P_a/P_s
111.9	39.19	39.19	0.146
156.9	2.89	42.08	0.205
203.3	3.53	45.61	0.266
259.6	3.42	49.03	0.400
322.4	4.09	53.12	0.422
389.5	4.71	57.83	0.510
451.5	9.57	67.40	0.591
500.0	11.18	78.58	0.655
538.0	10.54	89.12	0.705
565.5	10.90	100.02	0.741
590.4	9.57	109.59	0.773
607.9	9.95	119.54	0.796
620.1	10.05	129.59	0.812
632.9	9.15	138.74	0.830
643.1	8.77	147.51	0.842
648.9	9.33	156.84	0.850
659.7	7.74	164.58	0.864
669.2	7.30	171.87	0.876
669.1	9.22	181.09	0.876

DESORPTION

P_a (mmHg)	V_a (cm^3/g)	ΣV_a (cm^3/g)	P_a/P_s
665.1	-1.07	180.02	0.871
652.2	-3.50	176.52	0.854
631.1	-6.89	169.63	0.826
609.2	-12.39	157.24	0.798
583.4	-16.82	140.42	0.764
545.8	-18.64	121.78	0.715
509.7	-18.74	103.04	0.667
476.6	-16.66	86.38	0.624
450.3	-16.36	70.02	0.589
403.7	-8.76	61.26	0.528
356.7	-5.45	55.81	0.467
315.3	-3.49	52.32	0.413
280.2	-2.48	49.84	0.367

(d) Catalyst with Li/Co = 4.89

Appendix A-3 Physisorption studies

ADSORPTION

P_a (mmHg)	V_a (cm^3/g)	ΣV_a (cm^3/g)	P_a/P_s
123.0	42.06	42.06	0.163
167.8	3.04	45.10	0.222
215.3	3.14	48.23	0.285
261.3	3.14	51.37	0.345
324.9	4.74	56.11	0.430
394.5	5.86	61.97	0.522
466.1	8.72	70.69	0.616
513.0	10.89	81.58	0.678
545.7	11.64	93.22	0.722
569.1	10.93	104.15	0.752
595.4	9.29	113.44	0.787
608.1	11.22	124.66	0.804
637.0	5.58	130.24	0.842

DESORPTION

P_a (mmHg)	V_a (cm^3/g)	ΣV_a (cm^3/g)	P_a/P_s
628.3	-0.16	.130.08	0.831
617.9	-2.81	127.27	0.817
563.5	-4.97	122.30	0.745
542.1	-7.49	114.81	0.716
523.5	-11.24	103.57	0.692
484.1	-17.37	86.20	0.640
447.2	-15.73	70.47	0.591
402.3	-7.33	63.14	0.532
356.7	-5.23	57.91	0.472
315.6	-3.63	54.28	0.417
280.8	-2.67	51.61	0.371

(e) Catalyst with Li/Co = 6.53

Appendix A-3 Physisorption studies

ADSORPTION

P_a (mmHg)	V_a (cm^3/g)	ΣV_a (cm^3/g)	P_a/P_s
121.7	33.32	33.32	0.163
163.5	2.35	35.37	0.219
208.7	2.47	38.14	0.280
255.8	2.80	40.94	0.343
317.9	3.79	44.73	0.426
393.1	5.53	50.26	0.527
467.3	7.84	58.10	0.627
518.2	9.47	67.57	0.695
556.1	9.56	77.13	0.746
578.0	11.37	88.50	0.775
597.7	10.52	99.02	0.802
607.5	12.10	111.12	0.815
622.9	9.55	120.67	0.835
632.1	10.34	131.01	0.848
641.7	9.59	170.60	0.861
650.2	9.23	149.83	0.872
652.1	10.66	160.49	0.875

DESORPTION

P_a (mmHg)	V_a (cm^3/g)	ΣV_a (cm^3/g)	P_a/P_s
648.1	-0.20	160.29	0.869
635.2	-5.23	155.06	0.852
609.4	-8.11	146.95	0.817
587.3	-16.81	130.12	0.788
563.7	-18.81	111.31	0.756
529.5	-20.76	90.55	0.710
499.4	-20.31	70.24	0.670
448.8	-12.04	58.20	0.602
394.9	-7.35	50.84	0.530
344.5	-4.42	46.42	0.462
303.1	-3.13	43.29	0.407
269.2	-2.21	41.08	0.361
242.4	-1.61	39.47	0.325

(f) Catalyst with Li/Co = 8.48

Appendix A-3 Physisorption studies

ADSORPTION

P_a (mmHg)	V_a (cm^3/g)	ΣV_a (cm^3/g)	P_a/P_s
16.68	15.18	15.18	0.022
78.72	3.56	18.74	0.105
137.1	2.21	20.95	0.183
193.6	1.92	22.87	0.257
245.1	1.81	24.68	0.327
300.8	2.01	26.69	0.401
366.5	2.48	29.17	0.489
436.7	2.95	32.12	0.582
510.9	4.30	36.42	0.681
560.3	6.23	42.65	0.747
601.6	4.64	47.29	0.802
626.2	6.67	53.96	0.835
641.6	7.73	61.69	0.855
652.6	8.01	69.70	0.870
662.9	7.29	76.99	0.884
670.7	7.42	84.41	0.894
675.4	7.82	92.23	0.901
680.2	7.30	99.53	0.907
685.5	6.91	106.44	0.914
688.3	7.51	113.95	0.917

DESORPTION

P_a (mmHg)	V_a (cm^3/g)	ΣV_a (cn^3/g)	P_a/P_s
670.6	-0.57	113.38	0.889
662.2	-4.29	109.09	0.878
649.6	-7.76	101.33	0.861
634.8	-11.19	90.14	0.841
612.8	-15.54	74.60	0.812
576.3	-22.78	51.82	0.763
519.4	-12.24	39.58	0.688
447.7	-7.62	31.96	0.593
378.6	-1.82	30.14	0.501

(g) Catalyst with Li/Co = 9.78

Appendix A-3 Physisorption studies

ADSORPTION				DESORPTION			
P_a (mmHg)	V_a (cm^3/g)	ΣV_a (cm^3/g)	P_a/P_s	P_a (mmHg)	V_a (cm^3/g)	ΣV_a (cm^3/g)	P_a/P_s
23.32	12.29	12.29	0.031	685.1	-0.96	51.77	0.882
91.24	1.97	14.26	0.120	663.4	-2.95	48.82	0.869
162.0	1.33	15.59	0.212	640.1	-5.87	42.95	0.383
230.3	1.22	16.81	0.302	612.5	-9.96	32.99	0.802
299.4	1.28	18.09	0.392	546.8	-9.34	23.65	0.716
383.2	1.68	19.77	0.502	459.1	-5.00	18.65	0.601
464.5	1.92	21.69	0.608	390.3	-2.50	16.14	0.511
539.7	2.61	24.30	0.707	334.4	-1.09	15.05	0.438
589.2	2.46	26.76	0.772	288.4	-0.85	14.20	0.377
623.5	3.49	30.25	0.817	248.5	-0.59	13.60	0.325
648.5	3.47	33.72	0.849	225.4	-0.33	13.28	0.295
665.5	4.36	38.08	0.872				
672.1	6.60	44.68	0.880				
680.4	3.76	48.44	0.891				
496.2	4.28	52.73	0.909				

(h) Catalyst with Li/Co = 11.43

Appendix A-3 Physisorption studies

ADSORPTION

P_a (mmHg)	V_a (cm^3/g)	ΣV_a (cm^3/g)	P_a/P_s
17.31	14.36	14.36	0.023
97.42	3.80	18.16	0.129
177.9	2.63	20.79	0.236
262.6	2.69	23.48	0.318
345.0	2.83	26.31	0.457
434.2	3.65	29.96	0.575
512.7	3.87	33.83	0.679
565.2	5.36	39.19	0.749
603.2	5.66	44.85	0.799
627.6	8.04	52.89	0.832
641.9	8.03	60.92	0.851
656.5	7.24	68.16	0.870
671.9	5.79	73.95	0.890
678.5	7.03	80.98	0.899
674.4	9.75	90.73	0.894
681.4	6.54	97.27	0.903
685.2	7.21	104.48	0.908

DESORPTION

P_a (mmHg)	V_a (cm^3/g)	ΣV_a (cm^3/g)	P_a/P_s
677.3	-0.82	103.66	0.888
662.7	-3.60	100.06	0.878
646.8	-8.00	92.06	0.857
633.6	-13.46	78.60	0.840
614.2	-13.33	65.27	0.814
581.4	-13.96	51.31	0.771
536.3	-15.09	36.21	0.711
461.3	-6.48	29.73	0.611
393.7	-3.18	26.55	0.522
338.2	-1.93	24.62	0.448
292.8	-1.55	23.07	0.388
257.6	-1.05	22.20	0.341

(i) Catalyst with Li/Co = 13.06

Appendix A-3 Physisorption studies

Li/Co ratio	C	V_m	BET surface area (m^2/g)
0.0	525	38.1	166
1.63	569	35.1	153
3.26	586	34.1	149
4.89	296	33.8	147
6.53	284	35.2	153
8.48	358	27.9	122
9.78	289	17.3	75
11.43	401	12.5	54
13.06	311	16.1	70

Appendix A-4 Result of the BET equation for the lithium containing cobalt molybdate catalyst series.

P/P_s	$\Sigma V/W$ ml/g STP	r_c Å	t Å	ΣS m^2/g	% Pore volume associated with radii less than r_c
0.887	201.99	92.8	12.31	0.11	99.85
0.866	198.69	78.3	11.57	1.92	97.70
0.831	191.90	62.72	10.64	6.81	93.06
0.797	180.41	52.23	9.94	16.91	85.10
0.758	164.45	43.78	9.29	34.43	73.50
0.711	145.52	36.74	8.67	59.98	59.30
0.680	124.18	33.20	8.33	93.51	42.50
0.639	106.34	29.29	7.92	124.30	28.83
0.605	89.40	26.75	7.63	157.67	15.32
0.562	76.24	23.97	7.29	183.79	5.84
0.508	67.35	21.11	6.90	198.21	1.24
0.453	61.77	18.77	6.56	202.69	0

(a) Catalyst with Li/Co = 0

0.883	189.93	89.85	12.15	0.14	99.82
0.862	194.60	76.53	11.47	2.58	96.97
0.830	186.94	62.27	10.62	8.06	91.78
0.802	172.74	53.62	10.03	20.29	81.75
0.778	152.55	47.69	9.60	40.42	67.11
0.734	130.71	39.79	8.95	66.74	51.13
0.690	110.57	34.21	8.43	95.51	36.09
0.652	91.61	30.35	8.04	127.02	21.51
0.608	75.96	26.98	7.65	155.11	9.96
0.563	62.70	24.02	7.29	181.06	0.46
0.497	56.82	20.53	6.82	182.54	0

(b) Catalyst with Li/Co = 1.63

Appendix A-5 Pore size distribution

P/P_s	$\Sigma V/W$ ml/g STP	r_c Å	t Å	ΣS m^2/g	% Pore volume associated with radii less than r_c
0.853	167.41	72.52	11.23	0.38	99.48
0.834	163.38	64.05	10.72	3.20	96.13
0.801	156.29	53.34	10.02	9.36	90.02
0.770	143,38	46.01	9.47	22.89	78.45
0.729	128.18	39.13	8.89	42.04	64.53
0.704	111.64	35.82	8.59	65.75	48.75
0.659	100.14	31.06	8.11	83.18	38.70
0.620	83.73	27.87	7.75	114.43	22.51
0.574	70.45	24.60	7.37	141.57	10.11
0.523	60.60	21.91	7.01	161.58	1.96
0.464	55.19	19.17	6.62	166.81	0.10
0.409	51.70	17.18	6.30	167.12	0
(c) Catalyst with Li/Co = 3.26					
0.871	180.03	81.0	11.72	0.56	99.22
0.854	176.53	72.96	11.25	2.65	96.62
0.826	189.63	60.49	10.48	7.75	91.33
0.798	157.25	52.51	9.96	18.72	81.46
0.764	140.42	44.80	9.38	36.68	67.68
0.715	121,79	37.28	8.72	61.07	52.11
0.667	103.05	31.88	8.19	90.64	35.11
0.624	86.39	28.17	7.79	120.93	21.35
0.589	70.03	25.56	7.49	155.4	6.35
0.528	61.27	22.17	7.05	168.38	1.35
0.467	55.82	19.28	6.64	172.37	0.027
0.413	52.34	17.32	6.32	172.47	0
(d) Catalyst with Li/Co = 4.89					

Appendic A-5 Pore size distribution

P/P_s	$\Sigma V/W$ ml/g STP	r_c Å	t Å	ΣS m^2/g	% Pore volume associated with radii less than r_c
0.831	130.08	62.7	10.64	0.12	99.81
0.817	127,27	57,8	10.33	2.37	96.40
0.745	122.30	41.6	9.10	8.25	89.93
0.716	114.81	37.4	8.73	18.61	79.70
0.692	103.57	35.0	8.51	35.69	63.85
0.640	86.20	29.0	7.97	68.70	38.51
0.591	70.47	26.0	7.52	101.36	16.03
0.532	63.14	22.4	7.07	114.47	8.24
0.472	57.91	19.5	6.67	122.70	4.0
0.417	54.28	17.3	6.45	131.42	0

(e) Catalyst with Li/Co = 6.53

0.869	160.29	79.6	11.65	0.11	99.84
0.852	155.06	72.1	11.20	3.28	95.35
0.817	146.94	57.8	10.33	9.63	88.16
0.788	130.12	49.6	9.75	25.68	72.56
0.756	111.31	43.4	9.26	46.57	54.76
0.710	90.55	36.6	8.66	74.30	34.86
0.670	70.24	32.1	8.21	106.24	14.76
0.602	58.20	26.5	7.60	124.42	5.31
0.530	50.85	22.2	7.05	133.46	1.37
0.462	46.42	19.1	6.61	135.93	0.45
0.407	43.29	17.1	6.28	137.27	0

(f) Catalyst with Li/Co = 8.48

Appendix A-5 Pore size distribution

P/P_s	$\Sigma V/W$ ml/g STP	r_c Å	t Å	ΣS m^2/g	% Pore volume associated with radii less than r_c
0.889	113.38	94.1	12.35	6.25	99.31
0.878	109.09	86.1	11.98	2.34	94.17
0.861	101.33	76.1	11.46	6.70	84.69
0.841	94.14	67.0	10.89	13.97	70.81
0.812	74.60	57.7	10.32	26.02	50.99
0.763	51.82	44.8	9.38	49.66	20.77
0.688	39.58	34.87	8.51	64.50	6.03
0.593	31.96	25.75	7.49	72.72	0
(g) Catalyst with Li/Co = 9.78					
0.882	51.76	89.1	12.12	0.45	97.46
0.869	48.82	80.0	11.67	2.01	89.58
0.838	42.95	65.8	10.83	5.92	73.32
0.802	32.99	53.6	10.04	14.43	44.35
0.716	23.65	37.4	8.73	25.97	16.91
0.601	18.65	26.4	7.59	33.15	4.84
0.511	15.14	21.3	6.92	36.66	0.14
0.438	15.05	18.2	6.47	36.78	0
(h) Catalyst with Li/Co = 11.43					
0.888	103.66	93.6	12.35	0.36	98.94
0.878	100.06	86.1	11.98	2.12	94.25
0.857	92.06	72.3	11.33	6.62	84.13
0.840	78.60	66.7	10.88	15.48	65.71
0.814	65.27	57.0	19.27	25.86	47.28
0.771	51.31	46.2	9.49	39.40	27.79
0.711	36.21	36.7	8.67	58.34	6.11
0.611	29.73	27.2	7.68	64.54	0.87
0.522	26.55	21.8	7.00	65.8	0
(i) Catalyst with Li/Co = 13.06					

Appendix A-5 Pore size distribution

APPENDIX B

CATALYTIC ACTIVITY AND KINETIC DATA

Lithium content (wt %)	Li/Co ratio	Thiophene conversion (%)	C_4 hydrocarbon distribution (%)				$\frac{IB^a}{(TB + CB)}$	$\frac{CB^b}{TB}$	$\frac{NB^c}{IB}$
			NB	IB	TB[d]	CB			
0.00	0.00	15.45	24.85	20.55	32.83	21.77	0.38	0.66	1.21
0.10	0.65	18.25	26.39	19.84	31.78	21.99	0.37	0.69	1.40
0.25	1.63	19.43	24.48	20.53	32.47	22.52	0.37	0.69	1.19
0.50	3.26	17.60	21.47	22.87	33.10	22.56	0.41	0.68	0.94
0.75	4.89	15.67	25.57	20.72	31.88	21.83	0.39	0.69	1.23
1.00	6.53	14.13	25.43	20.95	32.30	21.32	0.39	0.66	1.21
1.30	8.48	11.60	18.97	25.31	32.84	22.88	0.45	0.70	0.75
1.50	9.78	8.64	21.74	25.64	31.31	21.31	0.49	0.68	0.85
1.75	11.43	5.30	16.38	29.63	31.72	22.72	0.55	0.70	0.55
2.00	13.06	3.78	11.77	32.07	32.78	23.38	0.57	0.71	0.37

[a] IB = but-1-ene. [b] CB = *cis*-but-2-ene. [c] NB = *n*-butane. [d] TB = *trans*-but-2-ene.

Appendix B-1 Results of catalytic activity studies

Estimation of errors involved in measurements of the rate of reaction

Consider the observation y to lie within the range $y' = y \pm \delta y$, where y' is the worst determination and δy is the absolute error. Let us now consider y as a function of dependent variables $X_1, X_2, .., X_n$

$$y = f(X_1, X_2, ... X_n) \qquad B-1$$

In general the differential of the function y can be written as:

$$dy = \sum_{i=1}^{n} \frac{\partial y}{\partial x_i} dx_i \qquad B-2$$

Now the worst possible value of dy will occur when all the terms on the right-hand side of equation B-2 are either positive or negative. Therefore equation B-2 can be rewritten as

$$\delta y = \sum_{i=1}^{n} \left|\frac{\partial y}{\partial x_i}\right| \delta x_i \qquad B-3$$

Usually the experimental errors are reported as a percentage of relative error and defined as:

$$\%e = \frac{\delta y}{y} \times 100 = \left[\frac{1}{y} \sum_{i=1}^{n} \left|\frac{\partial y}{\partial x_i}\right| \delta x_i\right] \times 100 \qquad B-4$$

where the term $\frac{\delta y}{y}$ is the relative error in the observation y.

Example: In this research the rate of reaction was computed by using equation 4-22 written as:

$$r = F_t \frac{X}{W}$$

where F_t is the molar flowrate of thiophene, X is the conversion measured in a differential reactor and W is the mass of catalyst used. By applying equation B-4, the error involved on the rate r can be assessed as:

$$\frac{\delta r}{r} \times 100 = \left[\frac{\delta F_t}{F_t} + \frac{\delta X}{X} + \frac{\delta W}{W}\right] \times 100$$

The errors in $\frac{F_t}{F_t}$, $\frac{\delta X}{X}$ and $\frac{\delta W}{W}$ were assessed from the equipment used. They are weighed values of 0.03, 0.03 and 2×10^{-4} respectively. The latter value was much smaller than the other two values and therefore was neglected. Hence the overall error involved in measurement of the rate of reaction is:

$$\frac{\delta r}{r} \times 100 = 6\%$$

NB The rates of reaction reported in Appendix B-2 are not consistent with the error involved on the rate of reaction. Therefore care should be taken in reading these rates from pages 179-186. For example, a rate $r = 18.49 \times 10^{-7} \frac{mol}{s\,g}$ should be read as $r = (18 \pm 1) \times 10^{-7} \frac{mol}{s\,g}$.

(a) T = 260° C

F_t ml/min	F_h ml/min	F_S ml/min	P_t mmHg	P_S mmHg	% Conversion	10^7 rate mole/g_{cat} s
23.1	150	-	101	-	0.21	6.54
13.0	160	-	57	-	0.36	6.47
7.1	166	-	31	-	0.43	4.16
4.4	170	-	20	-	0.59	3.64
4.0	170	-	18	-	0.63	3.49
2.5	170	-	11	-	0.76	2.65
23.1	145	4.0	101	18	0.14	4.37
23.1	140	7.5	101	33	0.11	3.51
23.1	140	11.5	101	50	0.09	3.00
23.1	130	19.0	101	83	0.07	2.28
23.1	115	35.0	101	154	0.05	1.67

Appendix B-2 Result of kinetic studies (Cobalt molybdate catalyst with no lithium)

(b) T = 280 °C

F_t ml/min	F_h ml/min	F_S ml/min	P_t mmHg	P_S mmHg	% Conversion	10^7 rate mole/g_{cat} s
23.1	150	-	101	-	0.36	11.5
13.0	160	-	57	-	0.50	8.98
7.1	166	-	31	-	0.72	6.98
4.4	170	-	20	-	0.86	5.24
4.0	170	-	18	-	0.85	4.71
2.5	170	-	11	-	0.98	3.40
23.1	145	4.0	101	18	0.22	6.97
23.1	140	7.5	101	33	0.18	5.72
23.1	140	11.5	101	50	0.15	4.95
23.1	130	19.0	101	83	0.13	4.10
23.1	115	35.0	101	154	0.10	3.07

Appendix B-2 Result of kinetic studies (Cobalt molybdate catalyst with no lithium)

(c) T = 300° C

F_t ml/min	F_h ml/min	F_S ml/min	P_t mmHg	P_S mmHg	% Conversion	10^7 rate mole/g_{cat} s
23.1	150	-	101	-	0.58	18.49
13.0	160	-	57	-	0.78	13.90
7.1	166	-	31	-	1.01	9.82
4.0	170	-	20	-	1.40	8.57
4.0	170	-	18	-	1.39	7.73
2.5	170	-	11	-	1.60	5.56
23.1	145	4.0	101	18	0.40	12.72
23.1	140	7.5	101	33	0.31	9.71
23.1	140	11.5	101	50	0.25	7.88
23.1	130	19.0	101	83	0.20	6.49
23.1	115	35.0	101	154	0.17	5.41

Appendix B-2 Result of kinetic studies (Cobalt molybdate catalyst with no lithium)

(d) T = 320° C

F_t ml/min	F_h ml/min	F_S ml/min	P_t mmHg	P_S mmHg	% Conversion	10^7 rate mole/g_{cat} s
23.1	150	-	101	-	0.98	31.22
13.0	160	-	57	-	1.33	23.83
7.1	166	-	31	-	1.54	15.01
4.4	170	-	20	-	1.94	11.86
4.0	170	-	18	-	1.94	11.02
2.5	170	-	11	-	2.50	8.71
23.1	145	4.0	101	18	0.60	19.23
23.1	140	7.5	101	33	0.53	16.88
23.1	140	11.5	101	50	0.41	13.20
23.1	130	19.0	101	83	0.30	9.64
23.1	115	35.0	101	154	0.24	7.71

Appendix B-2 Result of kinetic studies (Cobalt molybdate catalyst with no lithium)

(a) T = 260° C

F_t ml/min	F_h ml/min	F_S ml/min	P_t mmHg	P_S mmHg	% Conversion	10^7 rate mole/g_{cat} s
23.1	150	-	101	-	0.21	6.63
13.0	160	-	57	-	0.36	6.45
7.1	166	-	31	-	0.46	4.50
4.4	170	-	20	-	0.63	3.88
4.0	170	-	18	-	0.59	3.26
2.5	170	-	11	-	0.77	2.68
23.1	145	4.0	101	18	0.14	4.50
23.1	140	7.5	101	33	0.11	3.53
23.1	140	11.5	101	50	0.09	2.89
23.1	130	19.0	101	83	0.07	2.33
23.1	115	35.0	101	154	0.05	1.62

Appendix B-3 Result of kinetic studies (Cobalt molybdate catalyst with Li/Co = 1.63)

(b) T = 280° C

F_t ml/min	F_h ml/min	F_S ml/min	P_t mmHg	P_S mmHg	% Conversion	10^7 rate mole/g_{cat} s
23.1	150	-	101	-	0.37	11.78
13.0	160	-	57	-	0.52	9.29
7.1	166	-	31	-	0.69	6.73
4.4	170	-	20	-	0.95	5.80
4.0	170	-	18	-	0.95	5.26
2.5	170	-	11	-	1.0	3.50
23.1	145	4.0	101	18	0.22	6.91
23.1	140	7.5	101	33	0.18	5.78
23.1	140	11.5	101	50	0.16	5.10
23.1	130	19.0	101	83	0.13	4.19
23.1	115	35.0	101	154	0.10	3.16

Appendix B-3 Result of kinetic studies (Cobalt molybdate catalyst with Li/Co = 1.63)

(c) T = 300° C

F_t ml/min	F_h ml/min	F_S ml/min	P_t mmHg	P_S mmHg	% Conversion	10^7 rate mole/g_{cat} s
23.1	150	-	101	-	0.59	18.76
13.0	160	-	57	-	0.79	14.09
7.1	166	-	31	-	1.14	11.10
4.4	170	-	20	-	1.51	9.25
4.0	170	-	18	-	1.52	8.45
2.5	170	-	11	-	1.67	5.80
23.1	145	4.0	101	18	0.41	13.10
23.1	140	7.5	101	33	0.32	10.04
23.1	140	11.5	101	50	0.25	7.89
23.1	130	19.0	101	83	0.20	6.49
23.1	115	35.0	101	154	0.17	5.42

Appendix B-3 Result of kinetic studies (Cobalt molybdate catalyst with Li/Co = 1.63)

(d) T = 320° C

F_t ml/min	F_h ml/min	F_S ml/min	P_t mmHg	P_S mmHg	% Conversion	10^7 rate mole/g_{cat}s
23.1	150	-	101	-	1.01	32.03
13.0	160	-	57	-	1.35	24.15
7.1	166	-	31	-	1.57	15.29
4.4	170	-	20	-	2.06	12.63
4.0	170	-	18	-	2.06	11.47
2.5	170	-	11	-	2.58	8.98
23.1	145	4.0	101	18	0.62	19.70
23.1	140	7.5	101	33	0.53	17.02
23.1	140	11.5	101	50	0.42	13.43
23.1	130	19.0	101	83	0.29	9.21
23.1	115	35.0	101	154	0.23	7.30

Appendix B-3 Result of kinetic studies (Cobalt molybdate catalyst with Li/Co = 1.63)

APPENDIX C

R E F E R E N C E S

[1]J.B. McKinley, 'Catalysis', (Ed) P.H. Emmett, Vol.5, Reinhold, New York, 1957, p.405.

[2]S.C. Schuman and H. Shalit, *Cat. Rev.*, 1971, 4, 245.

[3]G.C.A. Schuit and B.C. Gates, *A.I.Ch.E.J.*, 1973, 19, 417.

[4]A.C. Cope and E. Farkas, *J. Org. Chem.*, 1954, 19, 385.

[5]H. Hoog, *Rec. Trav. Chim.*, 1950, 69, 1289.

[6]R.N. McCoy and F.T. Weiss, *Anal. Chem.*, 1954, 26, 1928.

[7]C.M. Cawley and C.C. Hall, *J.Soc.Chem. Ind.*, 1943, 62, 116.

[8]R.H. Griffith, J.D.F. Marsh and W.B.S. Newling, *Proc. Roy. Soc. (London)*, 1949, 197A, 194.

[9]V.I. Komarewki and E.A. Knaggs, *Ind. Eng. Chem.*, 1951, 43, 1414.

[10]C.H. Amberg, Proc. of the Climax First Int. Conf. on the Chemistry and Uses of Molybdenum, (Ed.) P.C.H. Mitchell, Climax Molybdenum Co. Ltd., London, 1974.

[11]P.J. Owen and C.H. Amberg, 'Adv. Chem. Series', Vol.33, *American Chemical Society*, 1961, p.182.

[12]P.J. Owen and C.H. Amberg, *Canad. J. Chem.*, 1962, 40, 941.

[13]P.J. Owen and C.H. Amberg, *Canad. J. Chem.*, 1962, 40, 947.

[14]P. Desikan and C.H. Amberg, *Canad. J. Chem.*, 1963, 41, 1966.

[15]P. Desikan and C.H. Amberg, *Canad. J. Chem.*, 1964, 42, 843.

[16]S. Kolboe and C.H. Amberg, *Canad. J. Chem.*, 1966, 44, 2623.

[17]S. Kolboe, *Canad. J. Chem.*, 1969, 47, 352.

[18]R.J. Mikovsky, A.J. Silvestry and H. Heinemann, *J. Catal.*, 1974, 34, 352.

[19]J.M.J.G. Lipsch and G.C.A. Schuit, *J. Catal.*, 1969, 15, 163, 174 and 179.

[20]G.V. Smith, C.C. Hinckley and F. Behbahany, *J. Catal.*, 1973, 30, 218.

[21]P. Kieran and C. Kemball, *J. Catal.*, 1965, 4, 394.

[22]M. Zdrazil, *Coll. Czech. Chem. Comm.*, 1975, 40, 3491.

[23]J. Kraus and M. Zdrazil, *React. Kinet. Catal. Lett.*, 1977, 6, 475.

[24]R. Lopez, R. Peter and M. Zdrazil, *J. Catal.*, 1982, 73, 406.

[25]O. Weisser and S. Landa, 'Sulphide Catalysts. Their Properties and Applications', Pergamon Press, Oxford, 1973.

[26]H. Kwart, G.C. Schuit and B.C. Gates, *J. Catal.*, 1980, 61, 128.

[27]R.N. Pease and W.B. Keighton, *Ind. Eng. Chem.*, 1933, 25, 1012.

[28]S.R. Ghosal, S.C. Ghosh and M.M. Majumdar, *Technology*, 1966, 3, 3.

[29]J. Phillipson, 68th National Meeting, A.I.Ch.E., 1971, 31B.

[30]P. Chakraborty, B. Bhattacharjee and A.K. Kar, *Indian Chem. Manuf.*, 1977, 15, 25.

[31]N. Sharma, P. Chakravarty and A.K. Kar, *J. Chem. Tech. Biotechnol.*, 1981, 31, 273.

[32]C.G.B. Hammar, Third World Petroleum Congress, Section IV, 1951, 295.

[33]M. Van Looy and G. Limido, *Ind. Chim. Belge*, Supp.1, 1959, 645.

[34]C.N. Satterfield and G.W. Roberts, *A.I.Ch.E. J.*, 1968, 14, 159.

[35]S. Morooka and C.E. Hamrin Jr., *Chem. Eng. Sci.*, 1977, 32, 125.

[36]H.C. Lee and J.B. Butt, J. Catal., 1977, 49, 320

[37]T.B. Metcalfe, 64th National Meeting A.I.Ch.E. J., 1969, 20B.

[38]P.C.H. Mitchell, 'The Chemistry of some Hydrodesulphurisation Catalysts containing Molybdenum', Climax Molybdenum Co., 1967.

[39]P. Grange and B. Delmon, *J. Less Comm. Met.*, 1974, 36, 353.

[40]V.H.J. de Beer and G.C.A. Schuit, 'Preparation of Catalyst', (Eds) B. Delmon, P.A. Jacobs and G. Poncelet, Elsevier Scientific Publishing Co., Amsterdam, 1976.

[41]F.E. Massoth, *Adv. Catal.*, 1978, 27, 265.

[42]P. Grange, *Catal. Rev. Sci. Eng.*, 1980, 21, 135.

[43]E. Furimsky, *Catal. Rev. Sci.Eng.*, 1980, 22, 371.

[44]P. Ratnasamy and S. Sivasanker, *Catal. Rev. Sci.Eng.*, 1980, 22, 401.

[45]J.T. Richardson, *Ind. Eng. Chem. Fund.*, 1964, 3, 154.

[46]J.H. Ashley and P.C.H. Mitchell, *J.Chem.Soc., (A)*, 1968, 2821.

[47]P.C.H. Mitchell and F. Trifiro, *J. Catal.*, 1974, 33, 350.

[48]N. Giordano, A. Castellan, J.C.J. Bart, A. Vaghi and F. Campadelli, *J. Catal.*, 1975, 37, 204.

[49]H. Beuther, R.A. Flinn and J.B. McKinley, *Ind. Eng. Chem.*, 1959, 51, 1349.

[50]R.S. Mann, *J. Chem. Soc.*, 1964, 1531.

[51]E.B. Andrews, Proc. Symp. Catalysis in Practice, 1963, p.18.

[52]S.P. Ahuja, M.L. Derrien and J.F. Le Page, *Ind. Eng. Chem. Prod. Res.Dev.*, 1970, 9, 272.

[53]A.E. Hargreaves and J.R.H. Ross, 6th Int. Cong. Catal., 1977, Vol.2, p.937.

[54]V.H.J. de Beer, T.H.M. Van sintFielt, J.F. Engelen, A.C. Van Haandel, M.W.J. Wolfs, C.H. Amberg and G.C.A. Schuit, *J. Catal.*, 1972, 27, 357.

[55]M.W. Ranney, 'Desulphurisation of Petroleum', Noyes Data Corporation, London, 1975.

[56]P.C.H. Mitchell, 'Catalysis', (Ed.) C. Kemball, The Chemical Society, London, 1977, Vol.1, p.204.

[57]N.P. Martinez and P.C.H. Mitchell, 'Proc. 3rd Int. Conf. the Chemistry and Uses of Molybdenum', Climax Molybdenum Co., 1980, p.105.

[58]P. Ratnasamy, A.V. Ramaswamy, K. Banerjee, D.K. Sharma and N. Ray, *J. Catal.*, 1975, 38, 19.

[59]A. Lycourghiotis, C. Defosse, F. Delannay, J. Lemaitre and B. Delmon, *J.C.S. Faraday I*, 1980, 76, 1677.

[60]A. Lycourghiotis, C. Defosse, F. Delannay and B. Delmon, *J.C.S. Faraday I*, 1980, 76, 2052.

[61]J.F. Kelly and M. Ternan, *Canad. J. Chem. Eng.*, 1979, 57, 726.

[62]W.K. Hall and P.H. Emmett, *J. Am. Chem. Soc.*, 1957, 79, 2091.

[63]J.B. Galeski and J.W. Hightower, *Can. J. Chem. Eng.*, 1970, 48, 151.

[64]C.N. Satterfield, 'Heterogeneous Catalysis in Practice', McGraw Hill, 1980, p.82.

[65]R. Kaiser, 'Gas Phase Chromatography', Butterworths, 1963, Vol.1, p.179 and Vol.3, p.86.

[66]J.H. Ashley and P.C.H. Mitchell, *J. Chem. Soc.*, 1969, 2730.

[67]M.Lo Jacono, A. Cimino and G.C.A. Schuit, *Gazz. Chim. Ital.*, 1973, 103, 1281.

[68]M.J.M. Van der Aalst and V.H.J. de Beer, *J. Catal.*, 1977, 49, 247.

[69]W.W. Wendlandt and H.G. Hecht, 'Reflectance Spectroscopy', Interscience, London, 1966.

[70]L.G. Dent Glasser, 'Crystallography and Its Applications', Van Nostrand Reinhold, 1977, p.135.

[71]K.W. Sing, 'Characterisation of Power Surface', (Eds) G.D. Parffitt and K.W. Sing, Academic Press (London), 1976.

[72]C. Orr and J.M. Dalla Valle, 'Fine Particle Measurement', MacMillan, London, 1959.

[73]J.M. Thomas and W.J. Thomas, 'Introduction to the Principles of Heterogeneous Catalysis', Academic Press, 1967.

[74]A.L. McClellan and H.F. Harnsberger, *J. Colloid and Interface Sci.*, 1967, 23, 577.

[75]J.H. de Boer, B.G. Linsen and Th.J. Osinga, *J. Catal.*, 1965, 4, 643.

[76]C. Pierce, *J. Phys. Chem.*, 1953, 57, 149.

[77]R.S. Drago, 'Physical Methods in Inorganic Chemistry', Reinhold Publishing Corporation, 1965.

[78]N.P. Martinez, P.C.H. Mitchell and P. Chiplunker, *J. Less-Common Met.*, 1977, 54, 333.

[79]J.C.P. Broekhoff, 'Preparation of Catalysts', Vol.III, (Eds) B. Delmon, P. Grange, P. Jacobs and G. Poncelet, Elsevier, Amsterdam, 1979.

[80]K.S. Seshadri, F.E. Massoth and L. Petrakis, *J. Catal.*, 1970, 19, 95.

[81]S. Ramaseshan and G. Suryan, *Phys. Rev.*, 1951, 84, 593.

[82]M. Bhaduri and P.C.H. Mitchell, *J. Catal.*, 1982, 77, 132.

[83]R. Thomas, E.M. Van Oers, V.H.J. de Beer, J. Medema and J.A. Moulijn, *J. Catal.*, 1982, 76, 241.

[84]V.H.J. de Beer, M.J.M. van der Aalst, C.J. Machiels and G.C.A. Schuit, *J. Catal.*, 1976, 43, 78.

[85]H. Pines and W. Haag, *J. Am. Chem. Soc.*, 1960, 82, 2471.

[86]R.T. Lewis, *J. Vac. Sci. Technol.*, 1974, 11, 404.

[87]D. German and E. Pollitzer, U.S.P., (a) 3,898,179 1975; (b) 3,962,367 1976; C.A. 83: 163 609h.

[88]O.A. Hougen and K.M. Watson, 'Chemical Process Principles', Part III, John Wiley and Sons, New York, 1953.

[89]C.N. Hinshelwood, 'The Kinetics of Chemical Change', Oxford University Press, 1947.

[90]J.M. Coulson and J.F. Richardson, 'Chemical Engineering', Vol.3, Pergamon Press, 1979.

[91]J.J. Carberry, 'Chemical and Catalytic Reaction Engineering', McGraw Hill, New York, 1976.

[92]J.R. Kittrell, *Adv. Chem. Eng.*, 1970, 8, 97.

[93]S.W. Weller, *Adv. Chem. Ser.*, 1975, 148, 26.

[94]M. Boudart, *A.I.Ch.E. J.*, 1956, 2, 62.

[95]S.W. Weller, *A.I.Ch.E. J.*, 1956, 2, 59.

[96]L.H. Thaller and G. Thodos, *A.I.Ch.E. J.*, 1960, 6, 369.

[97]R. Mezaki and J. Happel, *Catal. Rev. Sci. Eng.*, 1969, 3, 241.

[98]M. Boudart, D.E. Mears and M.A. Vannice, *Ind. Chim. Belge*, 32nd special issue, 1967, Part I, 281.

[99]T.E. Corrigan, *Chem. Eng.*, 1955, 62, 199.

[100]N.R. Draper and H. Smith, 'Applied Regression Analysis', John Wiley and Sons, 1966.

[101]T.A. Ryan Jr., B.L. Joiner and B.F. Ryan, 'Minitab Reference Manual', Duxbury Press, 1981.

[102]W.J. Dixon and M.B. Brown, 'Biomedical Computer Programs', University of California Press, 1979.

[103]G.C. Stevens and T. Edmonds, *J. Less-Common Met.*, 1977, 54, 321.

[104]M. Lo Jacono and W.K. Hall, *J. Colloid Interface Sci.*, 1977, 58, 76.

[105]P. Samuel and L.M. Yeddenapalli, *J. Appl. Chem. and Biotech.*, 1974, 24, 777.

[106]D. Dollimore, A. Galwey and G. Rickett, *J. Chim. Phys.*, 1975, 72, 1059.

[107]F.E. Massoth, *J. Catal.*, 1975, 36, 164.

[108]F.E. Massoth, *J. Catal.*, 1977, 47, 316.

[109]T.L. Slager and C.H. Amberg, *Canad. J. Chem.*, 1972, 50, 3416.

[110]F.G. Froment and K.B. Bischoff, 'Chemical Reactor Analysis and Design', John Wiley and Sons, New York, 1980.

[111]D.E. Nicholson, *Anal. Chem.*, 1962, 34, 370.